Dissertation

submitted to the
Combined Faculty of Natural Sciences and Mathematics of the Ruperto Carola
University Heidelberg, Germany for the degree of
Doctor of Natural Sciences

Presented by

M.Sc.: Paulina Fischer

born in: Nisko (Poland)

Oral examination: ……

Krr1 is a coordinating ribosome assembly factor spanning distant regions on the 90S pre-ribosome

Referees: Prof. Dr. Ed Hurt

Dr. Mandy Jeske

“In God we trust, all others must bring data.”

W. Edwards Deming

This PhD thesis was conducted at the Biochemistry Institute Heidelberg of the Ruperto Carola University Heidelberg under the supervision of Prof. Dr. Ed Hurt. I herewith declare that I wrote this Thesis independently, under supervision, and that I used no other sources and aids than those indicated throughout the thesis. All Figures in this Thesis were either adapted from publications as indicated or created by myself. Cryo-EM models were created by myself using Chimera and the indicated published PDB files.

Parts of this thesis were published in the article: “Thermophile 90S Pre-ribosome Structures Reveal the Reverse Order of Co-transcriptional 18S rRNA Subdomain Integration” Paulina Fischer*, Jingdong Cheng*, Jochen Baßler*, Benjamin Lau, Nikola Kellner, Ruth Kunze, Sabine Griesel, Martina Kallas, Otto Berninghausen, Daniela Strauss, Roland Beckmann, Ed Hurt. Molecular Cell 2019. September 19 75(6) doi: 10.1016/j.molcel.2019.06.032. * Co-First Authorship. As author I retain the right to include the Figures in my thesis without explicit permission or license.

Following Journals kindly permitted reuse of the listed Figures under the indicated licenses:

License No.	Date	Publisher	Journal	Reference	Figure taken
5011931253490	18.2.2021	Elsevier	Cell	(Kornprobst et al., 2016)	1, 7
5012370384868	19.2.2021	Elsevier	Molecular Cell	(Osheim et al., 2004)	2, 6
5012380680301	19.2.2021	Elsevier	Trends in Biochemical Science	(Klinge, Voigts-Hoffmann, Leibundgut, & Ban, 2012)	1
1098369-1 1098382-1	18.2.2021 19.2.2021	Annual Reviews, Inc.	Annual Review of Biochemistry	(Bassler & Hurt, 2018)	1, 3, S1c, S1d 6
5046970108251	13.4.2021	Springer	Nature Reviews Molecular Cell Biology	(Klinge & Woolford, 2018)	2, 6a

I herewith declare that I have not used the presented thesis for application, submission or examination at any other institution or faculty nor have I applied at any other institution or faculty for examination.

Thank you!!!

Prof. Dr. Ed Hurt – Thank you for patiently supervising my work and giving me the opportunity to fail and succeed, while pursuing my curiosity in a creative, scientific and sometimes artsy way. Thank you for giving me so much support in the past years, not only by always having time to discuss ideas, but also by pushing me with new suggestions. I learned many valuable lessons while working for you and with you and I feel prepared to take on any new adventures for the time after the Hurt Lab.

Dr. Mandy Jeske – thank you for taking the time and making the effort to be my TAC member and second evaluator of my work. I especially appreciated your comments during our seminars.

Prof. Dr. Michael Brunner – thank you for investing your time in being the chair of my oral examination.

Dr. Jirka Peschek – thank you for making the effort and taking part in the oral examination as my 4th examiner.

I want to thank all the members of the Hurt lab. In many cases I made friendships, experiences and lessons that will outlast my time in the Hurt lab and keep enriching my daily life in the future. As exhausting as the scientific work can be sometimes, having a good company kept me going when the science wouldn't! I want to thank PD Dr. Jochen Baßler especially. You helped open the door for an exhausting and very successful and rewarding time for me, culminating in this work.

Lastly, I want to thank my loves - family and friends and friends who are family: life's most golden, yet underrated pleasures. You make my life as rich and colorful and enjoyable as it can get. The most frustrating times of my PhD were endurable knowing that you guys always have my back. I want to mention Möni, Melis and Marcin, who supported me in all the ways I needed. Thank you!

Summary

Ribosomes are the cellular machines that are built from proteins and rRNA and are responsible for *de novo* protein production. Given the essentiality of this process and the need to be tightly controlled and regulated, the production of ribosomes, or ribosome biogenesis, has to be executed flawlessly. Among cellular processes conserved from prokaryotes and eukaryotes, ribosome biogenesis stands out as herculean task: in eukaryotes, over 200 assembly factors (AFs) help navigating the 18S, 25S and 5.8S rRNA species along their unique pathway from one common precursor to mature rRNA molecules, which are complexed with ribosomal proteins and ready to engage in efficient and faultless *de novo* production of proteins. Despite genetic, biochemical and structural research over several decades, the precise role of most eukaryotic AFs remained unknown.

In my PhD thesis, I have investigated the role of the KH domain containing assembly factor Krr1 during maturation of the first biochemically accessible ribosomal pre-cursor, the 90S pre-ribosome. One key feature of the 90S particle is that its AFs function as a scaffold, which allows for the maturation of the 35S pre-rRNA organized in subdomains. These subdomains are positioned in different regions of the 90S particle (head, body and base). I generated cryo-EM structure-based mutations of different AFs with the focus on Krr1 and performed biochemical analysis of 90S particles isolated from such mutant yeast cells. Following this approach, I was able to uncover and dissect the genetic and functional network between Krr1 and several AFs, reaching from the head through the body to the base region of the 90S. Disruption of Krr1's contact site in the base region is genetically and functionally connected to its interaction site in the head of the 90S pre-ribosome. Both are important at later stages of 90S particle maturation, before the huge precursor transitions into an early pre-40S particle. Together with the finding that maturation of the different 90S rRNA subdomains does not follow the direction of transcription (5'>3'), this places Krr1 in a special position as an assembly factor that bridges the three different regions of the 90S pre-ribosome. Thus, Krr1 is not only a placeholder for the essential 90S/pre-40S factor Pno1/Dim2, but also can act as a sensor of the coordinated assembly and maturation processes in the 90S particle "from head to toe".

Zusammenfassung

Ribosomen sind zelluläre Maschinen bestehend aus Proteinen und rRNA und verantwortlich für die *de novo* Produktion von Proteinen. Angesichts der Essentialität dieses Prozesses und der Notwendigkeit, ihn engmaschig zu kontrollieren und regulieren, muss die Ribosomenproduktion, oder Ribosomenbiogenese, fehlerfrei durchgeführt werden. Ribosomenbiogenese sticht unter den Prozessen, die von Prokaryoten zu Eukaryoten konserviert sind, als Herkulesaufgabe heraus: In Eukaryoten helfen über 200 Assemblierungsfaktoren (AF) die 18S, 25S und 5.8S rRNAs von einem gemeinsamen Vorläufermolekül auf ihren individuellen Wegen zu lenken zu reifen rRNA Molekülen, die mit ribosomalen Proteinen verflochten und bereit sind, effizient und fehlerlos Proteine *de novo* herzustellen. Trotz jahrzehntelanger genetischer, biochemischer und strukturbiologischer Forschung sind die genauen Aufgaben der meisten AFs unbekannt. In meiner Dissertation habe ich untersucht, was die Rolle von Krr1, einem AF der KH Domänen enthält, in der Reifung des ersten biochemisch zugänglichen ribosomalen Vorläufers ist, dem 90S Prä-Ribosom. Ein Hauptmerkmal des 90S ist, dass die AFs ein Gerüst bilden, das die weitere Reifung der in Subdomänen organisierten 35S Prä-rRNA erleichtert. Diese Subdomänen befinden sich innerhalb des 90S Partikels in verschiedenen Bereichen (Kopf, Körper und Fuß). Ich habe auf cryo-EM Strukturen basierende Mutationen von verschiedenen AFs mit dem Focus auf Krr1 hergestellt und biochemische Analysen der 90S Partikel aus solchen mutierten Hefezellen durchgeführt. Mit diesem Ansatz ist es mir gelungen, das genetische und funktionelle Netzwerk zu enthüllen zwischen Krr1 und mehreren AFs, die sich in ihrer Reichweite vom Kopf über den Körper bis hin zum Fuß des 90S Prä-Ribosoms erstrecken. Der Bruch der Kontaktstelle von Krr1 im Fuß des 90S Partikels ist genetisch und funktionell zur Wechselwirkung von Krr1 mit der Kopfregion des 90S Prä-Ribosom gekoppelt. Beides ist später von Bedeutung für die Reifung des 90S Partikels, wenn der nächste Vorläufer aus dem 90S Prä-Ribosom freigelegt wird, das frühe pre-40S Partikel. In Kombination mit der Erkenntnis, dass die Reifung der verschiedenen 90S rRNA Subdomänen nicht der Richtung der Transkitpion folgt (5‘>3‘), stellt sich für Krr1 eine besondere Rolle heraus als AF, der eine Brücke schlägt zwischen den drei Bereichen des 90S Partikels. Damit ist Krr1 nicht nur der Platzhalter für den essentiellen AF Pno1, sondern ein Sensor, der die koordinierten Reifungsprozesse des 90S Partikels von Kopf bis Fuß wahrnimmt.

Table of contents

1. Introduction 1

1.1 Ribosomes: Evolutionary conserved protein production machines 1

1.2 Ribosome biogenesis 4

1.2.1 Major milestones in eukaryotic ribosome biogenesis research 9

1.2.2 rRNA transcription, modification and cleavage are driving ribosome assembly 12

1.3 Assembly factors, snoRNPs and ribosomal proteins cooperatively produce translation competent ribosomes 17

1.3.1 Role of snoRNPs during pre-rRNA maturation 20

1.3.2 DExD/H-box helicases involved in ribosome biogenesis 24

1.3.3 Structural roles of assembly factors and modules during ribosome biogenesis 26

1.4 The 90S pre-ribosome is the earliest ribosomal precursor 27

1.4.1 Co-transcriptional assembly of protein modules and AFs with newly synthesized rRNA leads to the 90S pre-ribosome 28

1.4.2 Shedding of 90S AFs liberates early 40S pre-ribosomes 33

1.5 Aims of this study 36

2. Results 37

2.1 Krr1 contacts different regions within the 90S particle 37

2.2 Krr1 has a genetic link to the Kre33 module through its ß-propeller containing protein Enp2 40

2.2.1 Structure based mutational analysis of the Kre33 module members Enp2 and Bfr2 40

2.2.2 Genetic relationship analysis of Kre33 module mutants reveals connection to Krr1 via Enp2 45

2.2.3 Anchoring of Krr1's C-helix to the Kre33 module is crucial for cell growth when the C-terminus of Enp2 is missing 46

2.3 Krr1 C-terminus has an important role in contributing to the organization of the central domain in the 90S particle 50

2.4 Krr1's KH domains have functions beyond acting as placeholder for Pno1 53

3. Discussion 60

3.1 Krr1 contacts the 5' domain in the head region with its C-helix via the Kre33 module 61

3.2 Krr1's unstructured C-terminal extension contributes to maturation of the central region of the 90S particle 64

3.3 A_1 cleavage is accompanied by crucial structural rearrangements of the 90S pre-ribosome leading to Krr1 realease 66

3.4 Conclusion and outlook 69

4. Materials and Methods 71

4.1 Molecular biology and genetic methods 71

4.1.1 Construction of plasmids 71

4.1.2 Introduction of point mutations through site-directed mutagenesis 71

4.1.3 Yeast growth and construction of yeast strains 73

4.1.4 Generation of yeast double shuffle strains 73

4.1.5 GAL-promoter regulated overexpression of ribosome assembly factors 75

4.2 Biochemical methods 75

4.2.1 Tandem-affinity purification of 90S pre-ribosomes 75

4.2.2 Protein identification and quantification with mass spectrometry (MALDI and SemiQ-MS) 76

4.2.3 rRNA extraction and analysis by Northern blot 77

4.3 Computational methods and programs used for *in silico* analysis of proteins, semiQ MS data and cryo-EM maps 77

5. Supplemental Information 79

5.1 Multiple Sequence Alignment Krr1 79

5.2 Multiple Sequence Alignment Enp2 80

5.3 Multiple Sequence Alignment Bfr2 81

5.4 Affinity-purification of pre-ribosomal particles from cells expressing different Bfr2 truncation mutants. 82

5.5 Semi-quantitative mass spectrometry of 90S particles isolated via different TAP-tagged AFs from cells overexpressing *krr1*∆Pro or expressing *krr1*∆C2. 83

5.6 Semi-quantitative mass spectrometry of 90S particles isolated via Noc4-FTpA in cells where the contact site of Krr1 and Utp7 is disturbed. 84

6. Appendix 85

6.1 List of Abbreviations 85

6.2 List of Figures 88

6.3 Own Publications 90

7. References 91

1. Introduction

1.1 Ribosomes: Evolutionary conserved protein production machines

From simple, single cellular organisms to multicellular, complex living systems, all cells contain ribosomes, which are very sophisticated and essential macromolecular complexes essential for synthesizing the polypeptides of all cells. They are conserved in biochemical composition and structure and responsible for *de novo* protein synthesis. Proteins account for a large portion of biomass and they fulfill various functions inside and outside the cells. As versatile biological macromolecules, they catalyze most reactions in any living cell, but also provide essential regulatory, structural and transport roles. Consequently, protein production is an essential cellular function for which cells invest a considerable amount of their energy and resources, biochemically and genetically (J.R. Warner, 1999).

Two subunits, the large ribosomal subunit (LSU) and the small ribosomal subunit (SSU), form the mature ribosome (Figure 1.1), a design principle that is conserved among all living cells (Ben-Shem et al., 2011; Klinge et al., 2012; Schuwirth et al., 2005). Both subunits consist of ribosomal RNA (rRNA) and ribosomal proteins (r-proteins) and both subunits and their rRNA molecules have unique functions. The SSU deciphers the genetic information intermediary stored in messenger RNA (mRNA) molecules. The genetic information is read as a string of three nucleotides, or codons: a codon of the mRNA molecule is paired with an appropriate amino acid via base pairing of the codon sequence to the anticodon of an aminoacyl-transfer RNA (tRNA). The LSU translates the sequential pairing of codon and aminoacyl-tRNA into a functional protein by connecting individual amino acids through the formation of a peptide bond. Thus, ribosomes build the equipment with which a cell senses and reacts to its intra- and extracellular environment: the proteome.

Genetic analyses of r-protein genes reveal that on average the coding sequences of human, *Drosophila melanogaster*, *Caenorhabiditis elegans* and *Saccharomyces cerevisiae* (*S. cerevisiae*, further referred to as yeast) show a remarkable homology of 63% (Jenner et al., 2012; Yoshihama et al., 2002). Nevertheless, while their general design of ribosomes is similar in all cells, they vary in sizes and composition. Eukaryotic rRNA and r-proteins have expansion segments and extensions, respectively, and there are additional r-proteins in eukaryotes (Figure 1.1).

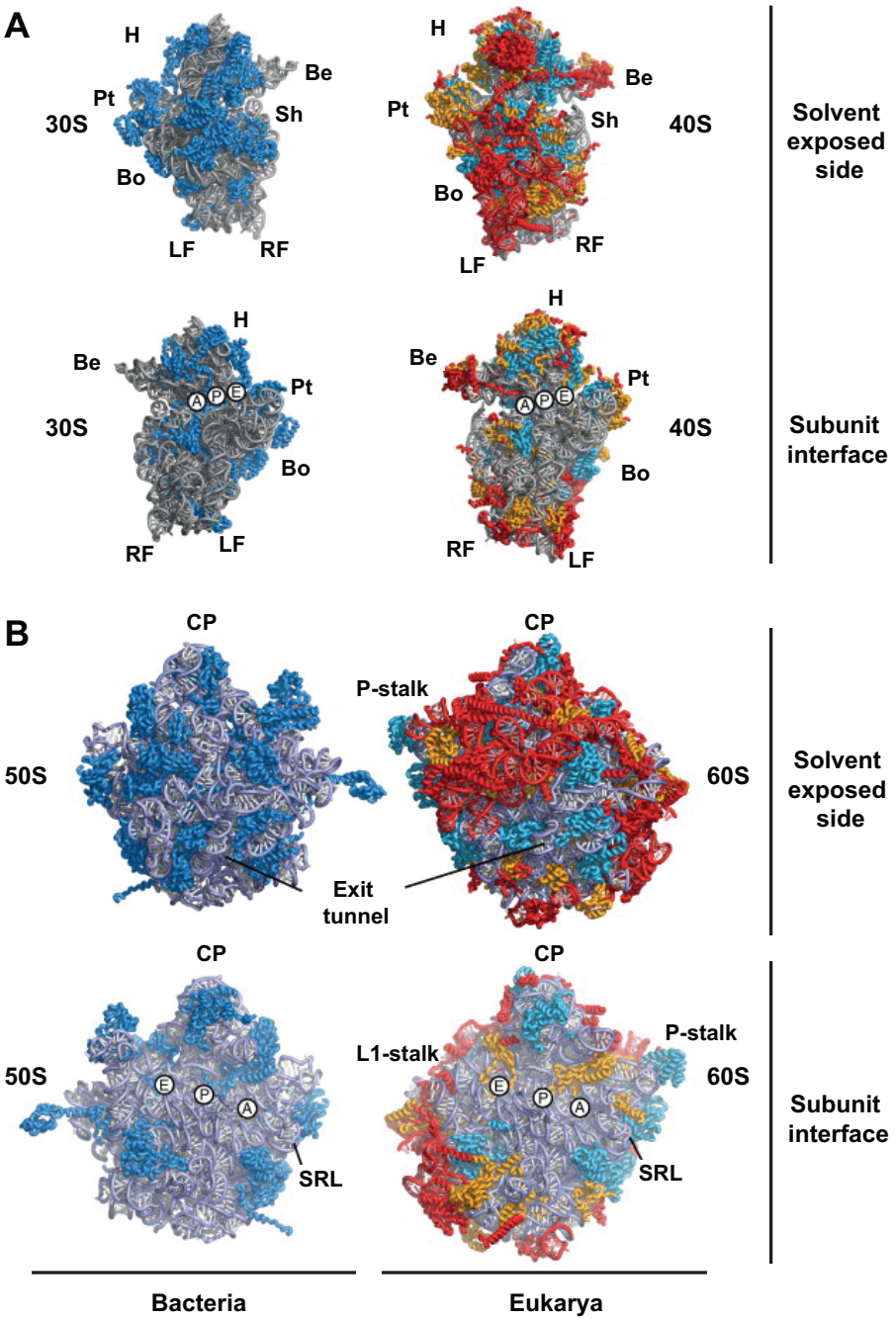


Figure 1.1 Structural comparison of the ribosomal subunits from a prokaryote and eukaryote. (A) and (B): Views of the solvent exposed side and subunit interface of the small ribosomal subunit (A) and large ribosomal subunit (B) are shown from *T. Thermophilus* (Bacteria) and *T. Thermophila* (Eukarya). Structural landmarks are labeled in each subunit: H: head, Be: beak, Pt: platform, Sh: shoulder, Bo: body, LF: left foot, RF: right foot, A: aminoacyl site, P: peptidyl site, E: exit site, CP: central protuberance, SRL: sarcin-ricin loop. Bacterial subunits are colored in shades of grey (rRNA) and blue (r-proteins). Structural models of the eukaryotic ribosomal subunits are colored according to the following scheme: rRNA: grey, prokaryotic proteins: dark blue, universally conserved proteins: light blue, proteins found in archaea and eukaryotes: orange, eukaryotic proteins: red. Figure adapted from (Klinge et al., 2012).

The increase in size (2.5 MDa in *Escherichia coli* (*E. coli*) vs 3.3 MDa in yeast and 4.3 MDa in human) is thought to reflect the higher complexity of cells and is likely linked to more complex translational regulation as well as the involvement of the ribosome in processes specific for eukaryotic cells (Ben-Shem, Jenner, Yusupova, & Yusupov, 2010; N. Fischer et al., 2015; Khatter, Myasnikov, Natchiar, & Klaholz, 2015).

The prokaryotic 70S ribosome (S for Svedberg unit, the apparent sedimentation rate) consists of the 50S LSU and the 30S SSU. In *E. coli*, the SSU is formed by the 16S rRNA and 21 r-proteins. The LSU consists of two rRNA molecules (5S and 23S) and 36 r-proteins. In contrast, eukaryotes have 80S ribosomes, that are formed by the 60S LSU and 40S SSU. In yeast, the LSU contains three rRNA molecules (25S, 5.8S and 5S) and 46 r-proteins while the SSU contains the 18S rRNA and 33 r-proteins. Both subunits have characteristic structural landmarks. Key structural features in the small subunit are the left and right foot, shoulder, platform, beak and head region (Figure 1.1A), while the large subunit shows prominent structural features as the central protuberance and the two stalks (acidic stalk, L1 stalk). Comparison of ribosomes from prokaryotes and eukaryotes shows that additional ribosomal proteins can be found on the surface of the ribosomal subunits, while functionally important sites like the exit tunnel, the subunit interface site or the mRNA entrance are conserved (Klinge et al., 2012). Moreover, conserved ribosomal proteins have been equipped with eukaryotic-specific extensions (Lecompte, Ripp, Thierry, Moras, & Poch, 2002). This concept is paralleled in the addition of eukaryotic-specific expansions in the sequences of mature rRNAs, which are mostly found on the solvent-exposed sides of the ribosomal subunits. A prominent example is the expansion segment 6 (ES6) region of the small subunit 18S rRNA, around 200nt long, changing the left foot area considerably (Jenner et al., 2012).

Human ribosomes are larger in size and contain additional ribosomal proteins, as well as additional rRNA segments. The mature rRNA in human cells is similar to yeast with the exception of the 28S rRNA, which is roughly 1.5-fold bigger than the yeast counterpart. Since human nucleoli are described to be more complex in terms of sub-compartments and protein content, it is reasonable to assume that ribosome biogenesis, even though conserved and similar to budding yeast, shows a higher level of complexity (Ahmad, Boisvert, Gregor, Cobley, & Lamond, 2009; Lamaye, Galliot, Alibardi, Lafontaine, & Thiry, 2011; Thiry & Lafontaine, 2005).

Ribosomes are ribozymes, which means that a specific RNA mediates the catalytic function of peptide formation. In contrast, protein enzymes catalyze the chemical reaction with the help of the side chains of their amino acids and/or additional co-factors. This makes RNA a special biochemical molecule: not only can it carry genetic information like DNA, it can act as biochemical catalyst similar to protein enzymes, thus combining two biochemically speaking very separate functions in one molecule (Root-Bernstein & Root-Bernstein, 2015). With that unique feature, RNA is an attractive candidate as the key player in very ancient, self-organizing and replicating chemical systems which can qualify as the beginning of all life (reviewed in (Bowman, Petrov, Frenkel-Pinter, Penev, & Williams, 2020; Fox, 2010)). The main enzymatic functional role of rRNA within the ribosome was confirmed by the crystal structure of the prokaryotic and eukaryotic ribosome: the rRNA molecules build the core of the ribosome and determine its overall structure, they are responsible for decoding the messenger RNA (mRNA) at the so called A-site and for the catalytic activity that leads to peptide bond formation at the so called P-site (Ben-Shem et al., 2010). The high-resolution crystal structures also revealed that r-proteins are located on the surface of the ribosome. They fill in gaps and sometimes reach into the core of the ribosome and hence complement the rRNA's fold (Figure 1.1) (Ben-Shem et al., 2011).

The fundamental task of ribosomes within the cell is the transfer of genetic information stored in mRNA molecules into a sequence of amino acids forming the polypeptide chain. The sequence of amino acids is specific for each protein's function. Therefore, correct translation of the nucleotide sequence of an mRNA molecule into a sequence of amino acids is of utmost importance for all cellular processes. Misreading even one nucleotide can lead to a protein that loses its function or gains a new function and both scenarios can have dramatic effects on a cell's life. Since ribosomes are the only machines capable of bulk protein production, their abundancy, efficiency, accuracy, functionality and accessibility for regulatory interference are equally important over the course of a cell's life span.

1.2 Ribosome biogenesis

To enable cells to grow and proliferate through the *de novo* synthesis of proteins, the translation apparatus comprises ribosomal proteins, rRNA, translation initiation factors and elongation factors as well as many factors involved in the *de novo* synthesis and biogenesis of ribosomes. Normally, the synthesis of components making up the

translation apparatus is well adjusted to cellular demands. Moreover, stress-inducing conditions force cells to redirect their energy and resources from growth supporting processes like translation to mechanisms that help them deal with or resolve stress-induced cellular damage. Thus, the production of ribosomes needs to be fine-tuned with whatever internal and external circumstances the cell, tissue, organ or organism is dealing with. It is important to point out that conditions causing imbalances in a subset of critical players involved in ribosome production influence ribosome biogenesis and transcription activity globally. For example, changes in the levels of pre-rRNA molecules caused by mutations affecting RNA polymerase I (Pol I) also affect pre-rRNA processing, ribosome assembly and the activities of the other two RNA polymerases, RNA polymerase II (Pol II) and RNA polymerase III (Pol III) (Laferte et al., 2006; Schneider et al., 2007). Likewise, changes in the components needed for ribosome assembly as well as ribosomal proteins influence downstream and upstream processes in the ribosome production pathway (Albert et al., 2019; J. E. Gallagher et al., 2004).

A high protein synthesis rate is a crucial requirement the cell needs to fulfill, if it wants to keep up rapid exponential growth. Therefore, cell growth physiology is mirrored by the number of ribosomes and the rate of protein synthesis (Kafri, Metzl-Raz, Jona, & Barkai, 2016). Moreover, ribosomes are not only the production site of all proteins in the cell, but translation was described to be a greater determinant of protein abundance than any of the other three processes contributing to protein levels (transcription rates, mRNA stability and protein stability) (Schwanhausser et al., 2011; Vogel et al., 2010). Several cell types like bacteria, yeast cells and cancer cells are characterized by their property to grow and divide within short time frames (bacteria <1h, yeast 90min) or shorter than their non-cancerous cell type. These fast-growing cells must adapt their growth rate quickly and adequately to nutrient-availability and stress factors, such as changes in temperature, exposure to UV light or oxidative stress. Consequently, ribosome biogenesis is subject to close regulation at the transcriptional and post-transcriptional level (reviewed in (de la Cruz et al., 2018)).

In *E. coli*, over 60% of the cell's biomass are proteins and more than two-thirds of the cell's ATP energy budget are invested in protein synthesis (G. W. Li, Burkhardt, Gross, & Weissman, 2014; Russell & Cook, 1995). Moreover, during exponential growth, about half of the cells dry mass is attributed to ribosome content (Dennis,

Ehrenberg, & Bremer, 2004). These numbers in the bacterium *E. coli* showcase the central role that ribosomes play in establishing and maintaining fast cell growth. In yeast, the numbers are just as dramatic. Around 2000 ribosomes are produced per minute in a rapidly dividing yeast cell, occupying 60% of all Pol I transcripts with rRNA genes, around 50% of mRNA transcripts by Pol II as well as 90% of splicing events for r-proteins (J.R. Warner, 1999). With an assumed translation efficiency of 9-10 aa/sec (P. Shah, Ding, Niemczyk, Kudla, & Plotkin, 2013), 40 000-50 000 ribosomes are needed alone just to produce the r-proteins required for ribosome assembly per minute. Given these extraordinary numbers, each cell needs to tightly regulate the production of ribosomes. Integration of various information about intra- and extracellular conditions with distinct cellular processes is needed to enable a rapid adjustment or switch whenever growth conditions turn from favorable to unfavorable or vice versa. Even though distant from bacteria, yeast cells and cancer cells share a conserved phenomenon regarding their energy metabolism, known as overflow metabolism: rapidly dividing cells tend to generate their energy with glycolytic fermentation instead of the respiration pathway based on the tricarboxylic acid cycle (TCA). In case of cancer cells, this phenomenon is known as the Warburg effect named after the scientist Otto Warburg, who first discovered it (Warburg, Wind, & Negelein, 1927). It is not surprising that upregulation of ribosome production is an important feature of cancerous cells due to their demand for ribosomes, which are at the base of ensuring short division cycles (for review see (Drygin, Rice, & Grummt, 2010; Gaviraghi, Vivori, & Tonon, 2019)).

Mediating a crucial step in the transfer of genetic information into a functional protein and building the base for rapid cell division, biogenesis of ribosomes is of pivotal role for every living cell. Considering the level of conservation of ribosomes, it does not surprise that the production of ribosomes is a conserved process among eukaryotes as well: the majority of presently known *trans*-acting factors or ribosome assembly factors (AFs; molecules that interact transiently with pre-ribosomes and facilitate necessary biogenesis steps as the maturation from pre-ribosome to ribosome progresses) was already present in the last universal cellular ancestor of all eukaryotic cells (Ebersberger et al., 2014). In bacterial cells, ribosome assembly takes around 3min and requires more than 20 ribosome assembly factors (Champney, 1977; Kaczanowska & Ryden-Aulin, 2007). The capacity to fold independently in the presence of Mg^{2+} ions or r-proteins was demonstrated for bacterial rRNAs with *in vitro*

experiments, explaining the reduced number of AF involved in the production of functional ribosomes (Nierhaus, 2014; Rohl & Nierhaus, 1982; Traub & Nomura, 1969; Woodson, 2011). However, the role of many assembly factors in bacterial cells has not been clarified yet. Moreover, AFs are still being identified because not all necessary steps, such as rRNA processing or modification, have been connected to a protein yet. For other AFs, such as GTPases, roles in ribosome assembly continue to emerge (Britton, 2009; Brown, 2005; Connolly & Culver, 2009).

Overall, more than 200 AFs are involved in the production of ribosomes in eukaryotes. They comprise individual proteins or protein complexes and small nucleolar ribonucleoproteins (snoRNPs with around 80 different snoRNAs), which make sure that the rRNA is folded, modified and processed into its mature form and correctly complexed with r-proteins (for review see (Bassler & Hurt, 2018; Thomson, Ferreira-Cerca, & Hurt, 2013; Woolford & Baserga, 2013)). The maturation of rRNA and its assembly with r-proteins is a highly dynamic process, which happens while the pre-ribosomes travel across different sub-compartments of the nucleus. The final maturation steps occur in the cytoplasm (Figure 1.2). Due to the high conservation and ribosomes' central role in a cell's life, there is not much room for mutations which ultimately affect the ribosomes function. Virtually all disturbances in ribosome biogenesis described so far in human cells lead to cell cycle arrest or apoptosis via tumor suppressor p53 (reviewed in (Golomb, Volarevic, & Oren, 2014; James, Wang, Raje, Rosby, & DiMario, 2014; Yang, Yang, & Yi, 2018)). Nevertheless, a growing number of diseases known as "ribosomopathies" are being described (for review see (Mills & Green, 2017)). These congenital disorders include diseases based on mutations in genes playing a role in ribosome biogenesis. In most cases, ribosomopathies share clinical symptoms like skeletal and skin abnormalities, bone marrow failure and a higher risk for the occurrence of cancer. Classical examples are Diamond-Blackfan Anemia, X-linked Dyskeratosis Congenita, Swachman-Diamond Syndrome, Cartilage-Hair Hypoplasia and Treacher-Collins Syndrome.

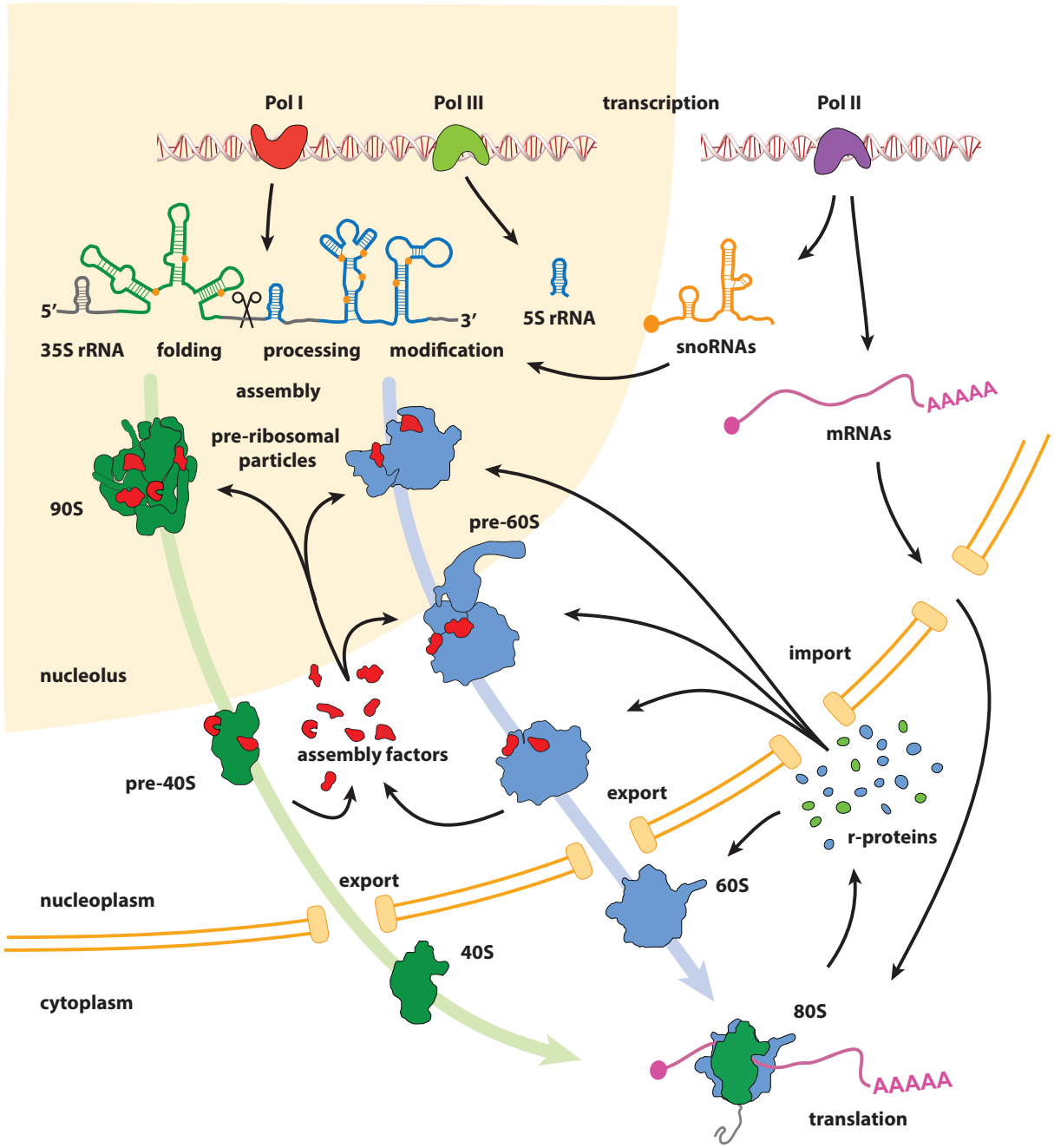


Figure 1.2 Overview of ribosome biogenesis in eukaryotic cells. rDNA repeats in the nucleolus are the birth place of ribosomes where Pol I transcribes the initial 35S rRNA precursor. Pol III transcribes the 5S rRNA and Pol II transcribes snoRNAs and mRNAs encoding for the proteins involved in ribosome biogenesis as well as r-proteins. Pre-rRNA molecules are co-transcriptionally folded, chemically modified and nucleolytically processed while also at the same time complexed with AFs and r-proteins, forming pre-ribosomal particles which travel across the nucleolus as they reach more mature stages with final maturation steps occurring in the cytoplasm after nuclear export. There, mature 40S and 60S subunits engage in translation forming the 80S ribosome. Figure taken from Figure 1 (Bassler & Hurt, 2018).

1.2.1 Major milestones in eukaryotic ribosome biogenesis research

Ribosomes were discovered in 1955 as part of a study analyzing the morphology of mammalian cells with electron microscopy (EM) and described as “particulate in nature and small in size” and often associated with the endoplasmatic reticulum (Palade, 1955). The first precursor rRNA were identified around a decade later and it was established in mammalian cells that the giant precursor leads to the large and the small ribosomal subunit (Scherrer, Latham, & Darnell, 1963). Another decade later, it was proposed that the proteins associated with the pre-rRNAs, which are more than the r-proteins found in mature subunits, function in producing mature ribosomes as they travel across the nucleolus (Kumar & Warner, 1972). Radioactive pulse-labeling of RNAs in human cells showed that a giant 45S pre-rRNA is transcribed, biochemically modified and cleaved into the rRNA components of the mature ribosome: 18S, 5.8S and 28S rRNA. The application of sucrose gradient centrifugation revealed that the rRNA precursor species are associated with different pre-ribosomal particles which had a higher protein to RNA ratio than expected from the mature ribosomal subunits (Tamaoki, 1966; Trapman, Retèl, & Planta, 1975; J. R. Warner & Soeiro, 1967). These studies already identified 90S pre-ribosomes, pre-60S particles (also known as 66S particle) and pre-40S particles (also known as 43S particle), which subsequently mature into the large and small ribosomal subunit, respectively. However, more than three decades should pass until these particles could be characterized in terms of protein composition and detailed structural features.

The first glimpse of the maturing ribosome was offered around 50 years ago through the technique known as Miller spreads, where chromatin spreads are visualized with EM (Figure 1.3A upper panel) (Miller & Beatty, 1969). Miller spreads depict several Pol I molecules sequentially synthesizing pre-rRNAs from a single rDNA repeat. The growing pre-rRNAs give the characteristic Christmas tree like shape and the blobs at the end of each RNA transcript correspond to the earliest pre-ribosomal assembly stages (Mougey et al., 1993). Later, it was shown that depletion of U3 snoRNA in mouse cells inhibited formation of these terminal knobs (Kass & Sollner-Webb, 1990; Kass, Tyc, Steitz, & Sollner-Webb, 1990; Mougey et al., 1993). Analyzing the length of the transcript as well as the size of the terminal knobs made it possible to assign different ribosomal maturation stages as Pol I progressively transcribes an rDNA gene cassette (Figure 1.3A lower panel) (Osheim et al., 2004).

The use of yeast dramatically improved the ribosome biogenesis research field because genetic manipulation, pulse-chase labeling and biochemical assays could be combined to identify r-proteins and also successfully investigate the progression of rRNA transcription, modification and processing. Initially, depletion or knockout experiments in the model organism yeast led to the identification of key players. Progression of ribosome biogenesis was monitored via pre-rRNA processing intermediates, abnormal polysome profiles and nuclear export defects of GFP-tagged reporter proteins. Moreover, distinct pre-ribosomal stages were defined by the pre-rRNA processing intermediate. However, the protein composition and structure of the pre-ribosomal particles carrying the different pre-rRNA species was elusive with the initial methods used. More importantly, the discovery of many ribosome assembly factors in combination with the powerful tandem-affinity purification method developed in 2001 marked another major methodological improvement in the field: several distinct stages in the ribosome assembly pipeline could be isolated via tandem-affinity purification (TAP)-tagged AFs and further analyzed biochemically and structurally (Bassler et al., 2001; Harnpicharnchai et al., 2001; Kressler, Linder, & De La Cruz, 1999; Puig et al., 2001; Venema & Tollervey, 1999). Since ribosome biogenesis is best understood in yeast and because I extensively used yeast in my doctoral research, all proteins and mechanisms described refer to the model organism yeast unless otherwise stated.

Finally, in recent years improvements in single-particle cryo-electron microscopy (cryo-EM) technology helped to uncover structural changes along the route of ribosome assembly. Structural rearrangements are difficult to address with conventional biochemical methods due to the complexity and dynamics of ribosome assembly intermediates (Figure 1.3B upper panel). Experimental limitations of classical structural biology techniques, such as requirements for large sample amounts, crystallization and size constraints, have for a long time prevented researchers from obtaining three-dimensional (3D) structures of big macromolecular assemblies with atomic detail. Improvements in detector technology and software propelled cryo-EM into the mainstream of structural biology, giving challenging systems such as low sample sized, huge macromolecular complexes a chance to be structurally investigated (for review see (Y. F. Cheng, 2015; Nogales, 2016)). The use of *Chaetomium thermophilum*, a eukaryotic thermophile with excellent properties for biochemical studies, further advanced our understanding of how ribosomes are

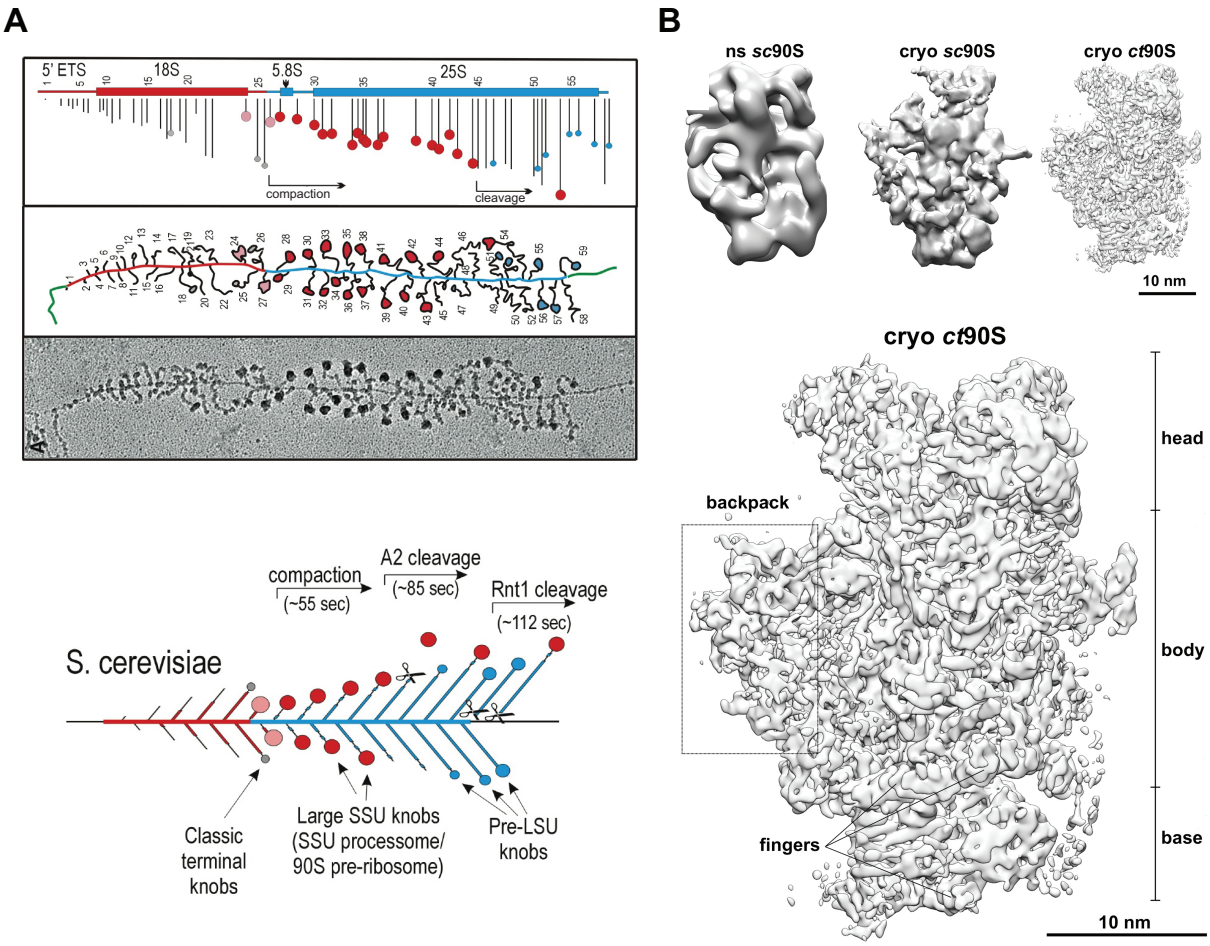


Figure 1.3 Visualization of pre-ribosomal 90S particles over the course of half a century. (A) Upper panel: Chromatin or "Miller" spreads with characteristic terminal knobs emerging from the pre-rRNA transcript along with graphic representation of the interpretation of EM images. Lower panel: Model of terminal knob formation as rDNA gene transcription progresses in yeast. Taken from (Osheim et al., 2004) Figure 2A and Figure 6. (B) Upper panel: Increased resolution gained through improvements in EM technology as well as model organism selection. Lower panel: First detailed structural visualization of the 90S pre-ribosome from *Chaetomium thermophilum* with the key features labeled for better orientation. Taken from (Kornprobst et al., 2016) Figure 3A and 3B.

assembled. Thermostable proteins show better biochemical properties and allow for a greater detail when analyzed by cryo-EM (Figure 1.3B lower panel) (Kornprobst et al., 2016). The improvement and application of cryo-EM in combination with adequate experimental approaches is likely to further uncover new ribosome biogenesis states as well as molecular functions of the AFs involved.

1.2.2 rRNA transcription, modification and cleavage are driving ribosome assembly

The birthplace of ribosomes is in the nucleolus at the tandem repeats of rDNA sequences, which also organize the structure of the nucleolus. The nucleolus contains distinct substructures across which the assembly line of ribosome production stretches (for review see (Correll, Bartek, & Dundr, 2019; Moss, Langlois, Gagnon-Kugler, & Stefanovsky, 2007; Strom & Brangwynne, 2019) and references within). Transcription of rDNA genes is located at the boundary of the dense fibrillar compartment (DFC) and the nucleolar fibrillar center (FC) (Cheutin et al., 2002). In the DFC, the nascent pre-rRNA molecule associates with r-proteins and AFs. Upon translocation to the granular component (GC), pre-rRNA maturation progresses and proceeds into the nucleoplasm and, upon export from the nucleus, final maturation steps take place in the cytoplasm (Milkereit et al., 2001). The principles of rRNA maturation are similar in all eukaryotes: One large polycistronic precursor rRNA molecule is transcribed by Pol I. It contains two external transcribed spacers (5'- and 3'-ETS) and two internal transcribed spacers (ITS1 and ITS2). These spacer sequences separate the mature rRNA molecules and are specifically targeted and eliminated by endo- and exonucleases. Cleavage in the ITS1 releases pre-rRNAs destined for the large ribosomal subunit from the pre-18S rRNA and cleavage in ITS2 separates 5.8S and 25S rRNAs (Figure 1.4A). While rRNA processing shows general similarities, the details vary between species and taxonomic groups (for review see (Tomecki, Sikorski, & Zakrzewska-Placzek, 2017)). The differences involve swapped cleavage sites as well as the order and timing of pre-rRNA processing in the pre-rRNA maturation pathway.

In yeast, transcription of rDNA genes is performed by Pol I, which synthesizes the 35S pre-rRNA molecule. Initiation-competent Pol I interacting with the Pol I-specific initiation factor Rrn3 is recruited to the rDNA gene promoter, which is associated with a Pol I initiation complex. The Pol I initiation complex contains the UAS upstream activity factor (UAF, constituting of Rrn5, Rrn9, Rrn10), histones H3 and H4 associated with the TATA-box binding protein (TBP) and the core factor (CF, a complex of Rrn6, Rrn7 and Rrn11) (for review see (Moss et al., 2007)). The upstream element (UE) is bound by UAF and CF is recruited to the core promoter of rDNA genes, both located in the 5'end of the 35S rRNA. Around 50% of the 150 rDNA genes are actively transcribed (Toussaint, Levasseur, Tremblay, Paquette, & Conconi, 2005) and Pol I

transcription is regulated at the level of transcription initiation, transcription elongation and by the ratio of active to inactive rDNA repeats. In 40-80% of transcripts, the earliest modification and cleavage reactions can occur co-transcriptionally as the nascent pre-rRNA molecule is synthesized (Kos & Tollervey, 2010; Osheim et al., 2004). rRNA modifications are catalyzed by two classes of snoRNPs: in yeast, box H/ACA snoRNPs mediate 44 pseudouridylation reactions and box C/D snoRNPs catalyze 67 2'-O-ribose methylation reactions (see section 1.2.3.1). These modifications involve around 80 snoRNAs and often occur at rRNA sequences important for optimal assembly and functionality of the ribosome. Many of these modifications have been shown to be dispensable for growth leaving their exact functional role a mystery, while some have been implicated in translation efficiency (Ojha, Malla, & Lyons, 2020).

rRNA molecules have the property to fold into secondary and tertiary structures by themselves (for 2D folding model of mature 18S and 25S with domain classification see Figure 1.4B). The spacer sequence ITS1 in the precursor rRNA can help mediate correct cleavage reactions by preventing either premature folding or misfolding (J. M. X. Hughes, 1996; Lamanna & Karbstein, 2011; R.W. Van Nues et al., 1994; R. W. van Nues, Venema, Rientjes, Dirks-Mulder, & Raue, 1995). In the 40S maturation pathway, base pairing of the ITS1 sequence 3' of the cleavage site A_2 with H44 of the 18S rRNA can prevent formation of the top of H44. After A_2 cleavage has occurred and the ITS1 sequence has dissociated, the helix formation is no longer blocked (Lamanna & Karbstein, 2011). Similarly, In the 60S pathway, sequences in ITS1 are important for pre-rRNA processing (R. W. van Nues, Rientjes, et al., 1995). Binding of AFs as well as r-proteins likely stabilizes favorable conformations of the pre-rRNA segments and therefore enables and times subsequent processing steps (Cote, Greer, & Peculis, 2002; Granneman, Petfalski, & Tollervey, 2011). Assuming this perspective, ribosome biogenesis is the transcription, modification, folding, assembly with r-proteins and processing of rRNA, the catalytically active agent in the ribosomes.

Processing of the 35S pre-rRNA molecule occurs at several sites and results in the removal of the two ETS and the two ITS sequences. Both spatial and temporal dynamic of ribosome biogenesis was defined by the order in which the sequential cleavage reactions occur. Similarly, many AFs and r-proteins as well as their role during ribosome biogenesis were identified via rRNA processing defects observed when AFs and r-proteins are mutated (reviewed in (Granneman & Baserga, 2004; Kressler et al., 1999)). The 3' end of the 35S rRNA can be co-transcriptionally released

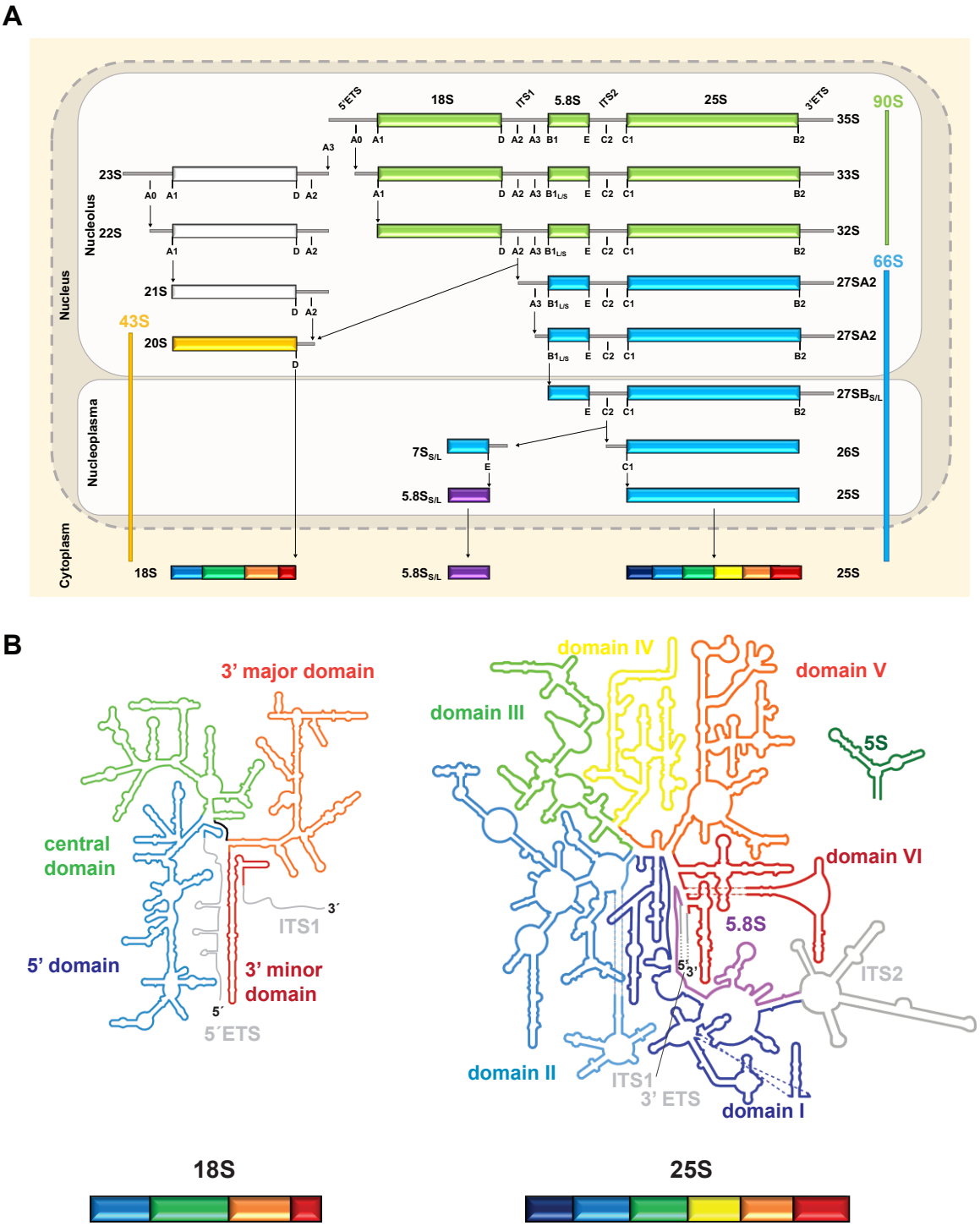


Figure 1.4 rRNA processing and folding during ribosome biogenesis in yeast. (A) The primary Pol I transcript, 35S pre-rRNA, is depicted with external and internal transcribed spacers (5'ETS, 3'ETS and ITS1, ITS2, respectively), mature rRNA species as well as cleavage sites. Pre-rRNA species are colored according to the pre-ribosomal particles they are predominantly associated with (light green for 90S, light blue for pre-60S, light orange for pre-40S) and white for species which are mainly considered to result from A3 cleavage and grouped according to the cellular compartment they occur in. (B) Mature 18S and 25S rRNAs are depicted in their 2D folding with rRNA segments colored according to their domain classification, which is also used in (A). Length of rectangles is not a proportional depiction of domain size or nt length. (B) is adapted from (Bassler & Hurt, 2018) Supplemental Figure 1b.

by the RNase III endonuclease Rnt1 (Henras, Bertrand, & Chanfreau, 2004; Kufel, Dichtl, & Tollervey, 1999). At the other end, the 5'ETS is removed by two subsequent cleavage reactions at the A_0 and A_1 site, producing the 33S and 32S pre-rRNA, respectively (Beltrame, Henry, & Tollervey, 1994). No enzyme has been clearly identified as nuclease responsible for A_0 cleavage yet. Utp24 was shown to cleave the pre-rRNA at A_1 and possibly A_2 in human and yeast cells (Bleichert, Granneman, Osheim, Beyer, & Baserga, 2006; Wells et al., 2016). Cleavage at the A_2 site separates the biogenesis of the SSU and LSU by generating the 20S pre-rRNA (part of the 43S pre-ribosomal particle and precursor to the 18S rRNA) and the $27SA_2$ pre-rRNA molecule (part of the 66S pre-ribosomal particle and precursor to the 5.8S and 25S rRNA) (Figure 1.4A). After separation of the two ribosomal subunit precursors at the A_2 cleavage site, the final pre-rRNA maturation step of the small ribosomal subunit precursor occurs after export from the nucleus to the cytoplasm. The 20S pre-rRNA is then cleaved endonucleolytically by Nob1 at site D, generating the mature 18S rRNA and marking the end point of the 18S pre-rRNA maturation pathway (Fatica, Oeffinger, Dlakic, & Tollervey, 2003; Pertschy et al., 2009; Vanrobays et al., 2001).

In plants and higher eukaryotes, both A_2 and A_3 cleavage sites in ITS1 can be processed without a strict order but with preference for cleavage at A_3 (Preti et al., 2013; Sloan et al., 2013; Zakrzewska-Placzek, Souret, Sobczyk, Green, & Kufel, 2010). In yeast, when cleavage at site A_3 occurs via RNase MRP prior to 5'ETS processing, the 23S pre-rRNA precursor is generated. The 23S pre-rRNA was proposed to be targeted by the RNA surveillance machinery (Allmang, Mitchell, Petfalski, & Tollervey, 2000; Houseley & Tollervey, 2006; Lygerou, Allmang, Tollervey, & Seraphin, 1996). Its role or importance within the cell is not clear, since it was also proposed to be the predominant processing intermediate in starving cells (Kos-Braun, Jung, & Kos, 2017). However, the 23S pre-rRNA precursor was described by other scientists to be a functional, i.e. productive, intermediate of post-transcriptionally cleaved 35S pre-rRNA and accordingly competent to finally yield mature 18S rRNA. This observation was made in cells, where processing of 27SA pre-rRNA was blocked by depletion of pre-60S AF Drs1 and as a consequence, co-transcriptional pre-rRNA processing and separation of pre-60S subunit appeared to be affected (Talkish et al., 2016).

Maturation of the LSU pre-rRNA is more complex than its SSU counterpart. The $27SA_2$ pre-rRNA molecule is processed in the nucleolus via two alternative and

mutually exclusive pathways. For the majority of pre-rRNA transcripts (around 85%), MRP RNase catalyzes the cleavage at A_3, giving rise to the $27SB_S$ pre-rRNA molecule and the remaining sequence is removed by nuclear exonuclease Rat1 together with its cofactor Rai1 (Henry et al., 1994; M.E. Schmitt & Clayton, 1993; Shuai & Warner, 1991). The cytoplasmic exonuclease Xrn1 can process the pre-rRNA from A_3 to B_S when Rat1 is not active, but it probably has no role in pre-rRNA processing under normal conditions (El Hage, Koper, Kufel, & Tollervey, 2008). In this context, Rrp17 was proposed to function as an exonuclease during 27S pre-rRNA processing (Oeffinger et al., 2009), but its involvement is not conclusively clarified yet, especially since Rrp17 has no typical nuclease domain. Moreover, homologs in human and rat were predominantly described to be RNA binding proteins with no conclusive studies supporting their nuclease activity (Scott et al., 2017; Suzuki et al., 2006). The minority of $27A_2$ pre-rRNA molecules (around 15%) is directly cleaved at the B_L site by a yet to be identified endonuclease. Both transcripts, the $27SB_S$ and $27SB_L$ pre-rRNA molecules, are further processed in an identical cascade of cleavage steps: Cleavage at C_2 by the endonuclease Las1 within ITS2 produces the corresponding $7SB_S$ and $7SB_L$ pre-rRNAs along with the 25.5S pre-rRNA, which is further processed by Rat1 into the mature 25S rRNA (Gasse, Flemming, & Hurt, 2015; Pillon, Sobhany, Borgnia, Williams, & Stanley, 2017; Schillewaert, Wacheul, Lhomme, & Lafontaine, 2012). The exonuclease Rex1 was also shown to play a role in 25S rRNA maturation, aside from its involvement in processing the independently transcribed 5S pre-rRNA (van Hoof, Lennertz, & Parker, 2000). Both 7S pre-rRNAs are processed by the RNA exosome in successive steps, giving rise to the $5.8S_S$ and $5.8S_L$ rRNA (Allmang et al., 1999; Briggs, Burkard, & Butler, 1998). During this reaction, the exosome trims the 7S pre-rRNAs to 5.8S pre-rRNAs containing 30nt long extensions. The extensions are then removed by the exosome-associated exonuclease Rrp6, which is assisted by the RNA helicase Mtr4. The resulting 6S pre-rRNAs are trimmed to the final 5.8S rRNAs by exonucleases Rex1 and Rex2 and subsequently Ngl2 (Faber, Van Dijk, Raue, & Vos, 2002).

The 5S rRNA, which is part of the LSU, is transcribed separately by Pol III from genes located in regions separating 35S rRNA genes. The transcribed 5S pre-rRNA only needs trimming at its 3' end, which carries about 12 additional nucleotides serving as termination signal for Pol III (Richard & Manley, 2009). 3' to 5' processing of the 5S pre-rRNA is dependent on the exonucleases of the RNase D family, Rex1, Rex2 and Rex3 (Y. Lee & Nazar, 1997; van Hoof et al., 2000). The 5S rRNA is stabilized by

L5 and L11 in the form of the 5S RNP and was shown to play a role in rRNA processing events occurring later in the 60S biogenesis pathway (Dechampesme, Koroleva, Leger-Silvestre, Gas, & Camier, 1999; Deshmukh, Stark, Yeh, Lee, & Woolford, 1995; Deshmukh, Tsay, Paulovich, & Woolford, 1993). Labeled 5S rRNA can be detected in very early pre-60S particles and was shown to be recruited with the help of Rpf2 and Rrs1 as well as the symportin Syo1 (Calvino et al., 2015; Kressler, Bange, et al., 2012; Trapman, Planta, & Raue, 1976; J. Zhang et al., 2007).

1.3 Assembly factors, snoRNPs and ribosomal proteins cooperatively produce translation competent ribosomes

Over the past decades, genetic and biochemical analyses of the eukaryotic ribosome assembly pathway identified a huge number of proteins and snoRNAs involved (reviewed in (Klinge & Woolford, 2018; Woolford & Baserga, 2013), for a list of AFs involved see Tables within). Ribosome biogenesis in eukaryotes is more complex and it takes place in different compartments of the cell, which makes a detailed spatial and temporal resolution of the process more difficult to obtain. With the TAP method and later cryo-EM analysis of isolated particles, the composition of distinct stages in the biogenesis pathway was revealed as well as a temporal and spatial map of assembly and disassembly steps that occur as the pre-ribosome matures to a functional 80S ribosome ready to engage in protein synthesis (Figure 1.5).

In bacteria, *in vitro* assembly studies showed a hierarchical formation of the ribosomal subunits from rRNA and ribosomal proteins, where r-proteins could be grouped into primary, secondary and tertiary binders (Held, Mizushima, & Nomura, 1973; Nierhaus & Dohme, 1974). The accessibility of bacterial ribosome formation for *in vitro* studies allowed for structural analyses as well as studies regarding the dynamics of the process (reviewed in (Davis & Williamson, 2017)). In eukaryotes it was shown that, similarly to ribosome assembly in prokaryotes, incorporation of r-proteins follows a hierarchical assembly mode: early, middle and late r-proteins are stably incorporated into domains in a consecutive manner (Ferreira-Cerca et al., 2007; Gamalinda et al., 2014; Kater et al., 2017; O'Donohue, Choesmel, Faubladier, Fichant, & Gleizes, 2010). The 60S maturation pathway begins with the stable incorporation of early r-proteins as they bind to the solvent exposed subunit side. Next, the region around the polypeptide exit tunnel is stabilized, followed by the subunit interface with the PTC and lastly, r-proteins around the CP are stably incorporated into nascent pre-60S particles. Similar to the *in vitro* results with bacterial small ribosomal subunits,

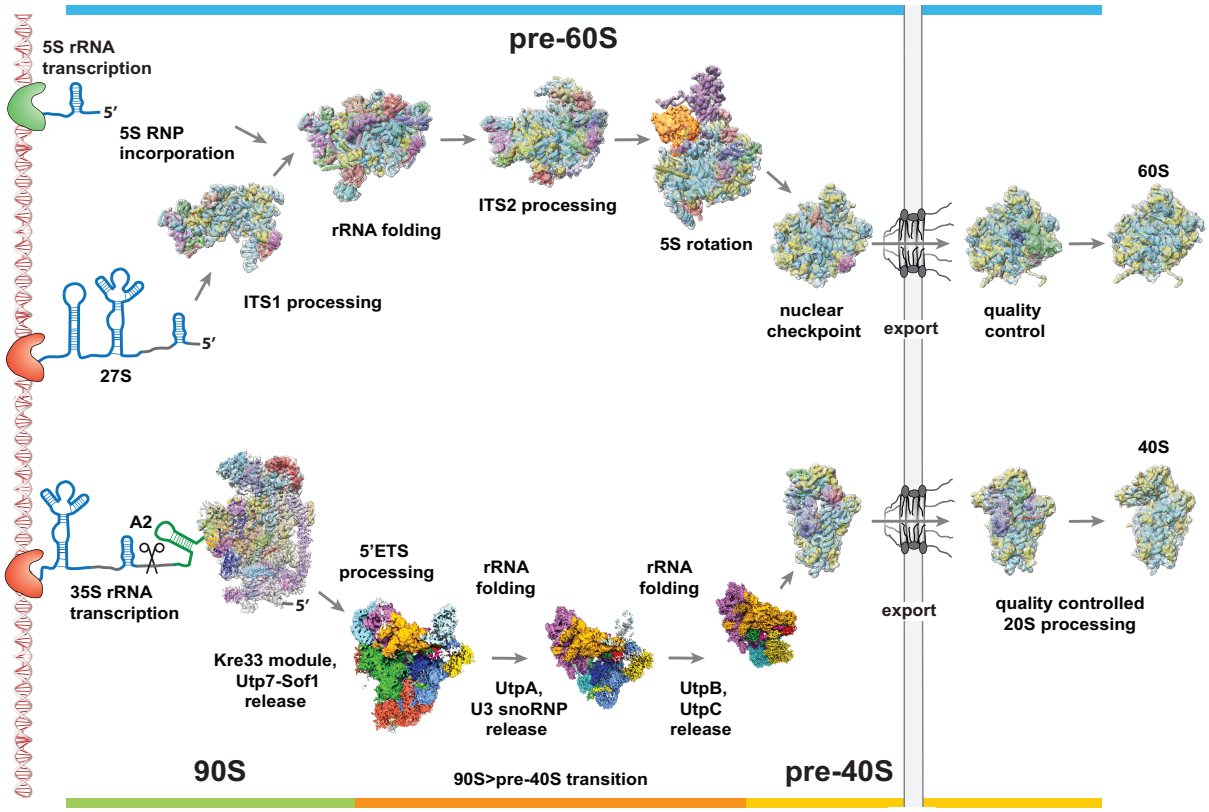


Figure 1.5 Structural depiction of ribosome biogenesis in yeast. Distinct pre-ribosomal states as captured via cryo-EM models of particles isolated by TAP-tagged AFs. rDNA is shown as double helix, Pol I is depicted in red, Pol III in green. Parts of the 35S pre-rRNA transcript is depicted in green indicating the part joining the 90S and pre-40S biogenesis pathway (indicated with a light green and light orange line, respectively), and in blue for the part joining the pre-60S biogenesis pathway (indicated with a light blue line). Major biogenesis steps are indicated. Figure adapted from (Bassler & Hurt, 2018) Figure 6. 90S to pre-40S transition was included and adapted from (J. Cheng et al., 2020) Figure 2.

in yeast r-proteins located in the body are required for early pre-rRNA processing steps, while r-proteins binding to the head region are required for cleavage steps occurring after export of pre-40S particles form the nucleus (Ferreira-Cerca, Poll, Gleizes, Tschochner, & Milkereit, 2005). These similarities in ribosome biogenesis between eukaryotes and prokaryotes indicate that the progressive compaction of pre-ribosomal particles is caused by properties of the pre-rRNA molecules and r-proteins. In this scenario, AFs would not produce the general hierarchical assembly mode but rather function in a complementary fashion by facilitating productive conformational changes or delaying certain maturation steps via established checkpoints. For example, late binding r-proteins of the small subunit (RpS2, RpS3 and RpS23) corresponding to tertiary binders in *E. coli* were absent in mutant cells where U3 snoRNP release and hence formation of the central pseudoknot was

blocked, which is a key architectural feature of the mature small subunit (Sardana et al., 2015; Shajani, Sykes, & Williamson, 2011). In this context, U3 snoRNP release functions as a key step enabling or preventing final maturation processes. Since r-proteins are RNA binding proteins, their free pool in the cell needs to be kept as small as possible to prevent aggregate formation. Studies showed that cells use two mechanisms to prevent a free pool of ribosomal proteins. In at least 10 cases (RpS2, RpS3, RpS14, RpS26, RpL3, RpL4, RpL23, RpL10, RpL5 and RpL11), r-proteins have been shown to associate with specific chaperones as soon as they are translated (for review see (Pillet, Mitterer, Kressler, & Pertschy, 2017)). Moreover, r-protein levels are managed by a conserved degradation mechanism sensing surplus r-proteins and removing them by the ubiquitin degradation system (Sung et al., 2016).

Most AFs are highly conserved and encoded by essential genes. They have diverse roles in ribosome biogenesis: they assist folding and processing the pre-rRNA and assembly of r-proteins. They facilitate structural rearrangements by providing a structural platform, help release or attract other AFs, or catalyze reactions that are necessary for the progression of the biogenesis pathway. They can serve as proteins monitoring the correct succession of assembly and processing steps and thus act as quality control checkpoints. As a general classification, AFs can be grouped in proteins (complexes) with or without enzymatic activity. AFs acting as endo- and exonucleases, which process pre-rRNAs (see section 1.2.2), snoRNPs, which modify pre-rRNAs at distinct sites (see section 1.2.3.1) and RNA helicases, which unwind rRNA regions or help release other AFs (see section 1.2.3.2) will be covered in greater detail.

Different classes of NTPases drive ribosome assembly by consuming energy and therefore bringing the maturation step forward with the introduction of irreversible changes. AAA-type ATPases like Rea1, Drg1 or Rix7 catalyze structural rearrangements and the release of AFs in the pre-60S maturation pathway (reviewed in (Kressler, Hurt, Bergler, & Bassler, 2012). ATPases like Rio1, Rio2 and Fap7 have roles in 40S biogenesis. Fap7 was shown to function as an RNA mimic of H23 18S rRNA for RpS14. ATP hydrolysis helps incorporate the r-protein by triggering release of RpS14 onto the 18S rRNA (Loc'h et al., 2014; Pena, Schutz, Fischer, Chang, & Panse, 2016). Rio kinase/ATPases found in yeast (Rio1 and Rio2) belong to an ancient conserved protein kinase/ATPase family. They are implicated in cytoplasmic pre-40S maturation steps (Belhabich-Baumas et al., 2017; Ferreira-Cerca, Kiburu, Thomson, LaRonde, & Hurt, 2014; Turowski et al., 2014). Moreover, Rio1 was described to

govern a signaling network affecting growth in a nutrient dependent manner (for review see (Berto, Ferreira-Cerca, & De Wulf, 2019)).

The functional role of GTPases involved in ribosome biogenesis largely remains unknown despite many genetic, biochemical and structural data (reviewed in (Karbstein, 2007)). Similar to other energy consuming NTPases, several scenarios are conceivable. Energy derived from GTP hydrolysis could be invested in structural rearrangements, binding or release of other proteins. GTPases could act as placeholders. They could be a regulation hub at the intersection of ribosome biogenesis and nutritional state mirrored by the GTP/GDP ratio. Bms1, which functions in complex with Rcl1, is the only GTPase known to be involved in 40S biogenesis. The GTPase Fun12 is involved in the final quality control step by proofreading 40S subunits in a translation-like cycle (B. S. Strunk, Novak, Young, & Karbstein, 2012). The inventory of 60S biogenesis factors includes five essential GTPases. Nog1, Nug1 and Nug2 are involved in nucleolar and nuclear pre-ribosomal stages, while Ria1 and Lsg1 are found in the cytoplasm.

Other enzymatic families involved in ribosome biogenesis are methyltransferases (pre-40S: Rrp8, Emg1, Bud23, Dim1; pre-60S: Spb1, Nop2, Rcm1, Bmt2), acetyltransferase (pre-40S: Kre33) and kinases (pre-40S: Cka1/2, Ckb1/2, Hrr25). In the following sections, snoRNPs, RNA helicases and structural proteins will be described in more detail.

1.3.1 Role of snoRNPs during pre-rRNA maturation

As the pre-rRNA molecule is transcribed, rRNA bases are chemically modified by snoRNPs. They contain proteins and snoRNA and one snoRNP can modify RNA bases at different sites (for review see (Decatur, Liang, Piekna-Przybylska, & Fournier, 2007; Ojha et al., 2020; Watkins & Bohnsack, 2012)). snoRNPs catalyze the reactions leading to 2'-O-ribosme methylation (box C/D snoRNPs), or pseudouridylation (H/ACA snoRNPs) (Figure 1.6A and 1.6B, respectively). 2'-*O*-methylation introduces a hydrophobic group into the ribose and thus can help the hydrophilic rRNA interact with more hydrophobic protein elements of the ribosome. Isomerization of uridine to pseudouridine introduces an additional hydrogen bond donor, increasing stability through hydrogen bond formation. These two classes of snoRNPs are named after the conserved secondary structure motif of the respective snoRNAs (Figure 1.6A and B, left panel) (Balakin, Smith, & Fournier, 1996). The protein enzyme in the

snoRNP catalyzes the chemical modification and the snoRNA guides the catalytic activity to the right position within the target RNA molecule by base-pairing. C/D box snoRNPs contain two copies of the methyltransferase Nop1, the homodimer Snu13 and the heterodimer Nop56-Nop58 (Figure 1.6A, right panel panel). H/ACA snoRNPs contain the pseudouridine synthase Cbf5, Nhp2, Nop10 and Gar1 (Figure 1.6B, right panel).

Among the snoRNPs involved in ribosome biogenesis, some stand out because they have other roles than chemical modifications. These snoRNAs are essential, in contrast to snoRNAs that guide modifications only and are nonessential genes (Samarsky & Fournier, 1999). Most rRNA modifications are not essential and their absence does not impair growth, but they often occur in functionally important regions and likely influence the ribosome in structure and function (Decatur & Fournier, 2002). Inhibiting the enzymatic activities of snoRNPs by point mutations in Cbf5 and Nop1 causes a severe phenotype. This points to an additive role of the chemical modifications, even though single deletions of snRNAs and the modifications they guide do not cause a dramatic phenotype in most cases (Esguerra, Warringer, & Blomberg, 2008; Tollervey, Lehtonen, Jansen, Kern, & Hurt, 1993; Zebarjadian, King, Fournier, Clarke, & Carbon, 1999). snR10 is an exception here since deletion causes a growth phenotype. Because snR10 is involved in processing events also, it is not straightforward to assign this growth phenotype exclusively to loss of modification only (Tollervey & Guthrie, 1985). In human cells, mutations in the H/ACA snoRNP were shown to cause the ribosomopathy X-linked Dyskeratosis Congenita. Specifically, mutations in the human Cbf5 homolog, dyskerin, were shown to alter translation of specific tumor suppressor genes, p27 and p53, as well as VEGF, a factor supporting tumor growth (Bellodi, Kopmar, & Ruggero, 2010; Bellodi, Krasnykh, et al., 2010; Montanaro et al., 2010; Rocchi et al., 2013). Noteworthy, the changes in translation were shown to be rooted in altered translation activity of ribosomes with defective pseudo-uridylation (Penzo et al., 2015).

C/D box RNA U3 was the first snoRNA to be identified in 1968, already described to be enriched in the nucleolus and associated with ribosomes (Hodnett & Busch, 1968; Prestayko, Tonato, & Busch, 1970; Weinberg & Penman, 1968). It is a highly conserved snoRNA among all eukaryotes (Marz & Stadler, 2009). It is absolutely essential for the formation of the 90S particle, which at the same time was described as particle containing U3 and 35S pre-rRNA and also gave many AFs of the small

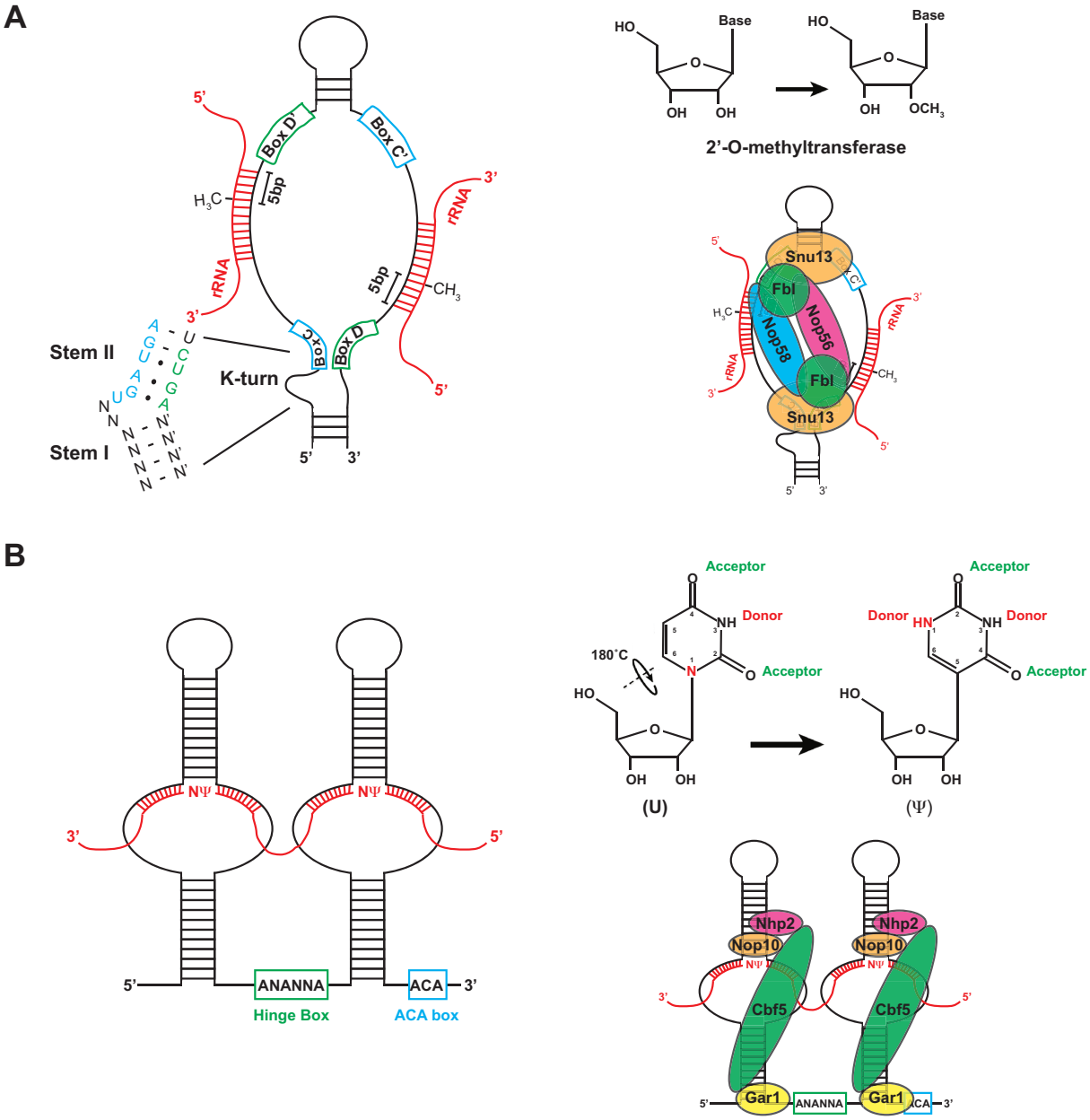


Figure 1.6 snoRNPs catalyze chemical modifications on pre-rRNA molecules. A) Left panel: 2D structure of C/D box snoRNAs indicating Box C/C' (blue), Box D/D' (green), rRNA hybrids (red) and site of methylation as 5bp from Box D/D'. Right panel: 2'-*O*-methylation reactions (upper panel) are catalyzed by C/D box snoRNPs (lower panel) consisting of snoRNA and proteins Nop56, Nop58, dimer Snu13 and methyltransferase Nop1. B) Left panel: Hairpin-hinge-hairpin-tail structure of H/ACA box snoRNAs with hinge box (H) in green, ACA box (ACA) in blue, rRNA hybrid in red as well as the pseudouridylation pocket (NΨ) at the base of the hairpins. Uridine (U) to pseudouridine (Ψ) isomerization (upper panel) are catalyzed by H/ACA snoRNPs (lower panel) consisting of snoRNA, Gar1, Nhp2, Nop10 and pseudouridin synthase Cbf5. Figure was adapted from (Ojha et al., 2020) Figure 1 and Figure 2 and (De Zoysa & Yu, 2017) Figure 1.

subunit their name (UTP – U three protein). Early cross-linking studies showed that U3 snoRNA base-pairs with the 5'ETS and 18S regions of the pre-rRNA and is required for processing of the 5'ETS as well as for chaperoning formation of the central

pseudoknot (Beltrame & Tollervey, 1992; J. M. Hughes & Ares, 1991; J. M. X. Hughes, 1996; K. Sharma & Tollervey, 1999). Duplex formation between U3 snoRNA and pre-rRNA is facilitated by Imp3, an RNA chaperone protein, which unfolds structures within the U3 sequence to allow for base pairing between U3 and the pre-rRNA (Gerczei & Correll, 2004; B. N. Shah, Liu, & Correll, 2013). This prevents central pseudoknot formation, an important and conserved RNA structure of the mature small subunit. It maintains the 40S architecture by coordinating the four RNA subdomains and setting up the decoding center. Consequently, U3 snoRNP release is an important maturation step in the 40S biogenesis pathway and occurs during the 90S>pre-40S transition (J. Cheng et al., 2020; Sardana et al., 2015). Another C/D box snoRNA proposed to have a role in aiding the formation of correct rRNA folding is the essential snoRNA U14 (also termed snR128), although in contrast to U3 it can also catalyze methylation (H. V. Li, Zagorski, & Fournier, 1990; W. Q. Liang & Fournier, 1995).

H/ACA box RNAs snR30 and snR10 have an important function in directing pre-rRNA processing (Bally, Hughes, & Cesareni, 1988; Martin et al., 2014; Morrissey & Tollervey, 1993; Tollervey, 1987). Despite their critical role in ribosome assembly, their molecular mechanism is not known. snR30 is the only essential H/ACA snoRNA and requires RNA helicase Rok1 for its release, unlike some other H/ACA box snoRNPs that do not require additional factors for dissociation from their substrate (Bohnsack, Kos, & Tollervey, 2008). snR10 is required for early processing steps but also guides pseudouridylation (King, Liu, McCully, & Fournier, 2003; Schattner et al., 2004).

RNase MRP (mitochondrial RNA processing) is another essential snoRNP catalyzing pre-rRNA cleavage at A_3 (Lygerou et al., 1996; M. E. Schmitt & Clayton, 1992; M.E. Schmitt & Clayton, 1993). It was originally discovered in mouse, but later homologs were found in human and yeast. Its RNA component, Nme1, does not belong to the C/D box or H/ACA box type of snoRNAs but is critical for processing at A_3. Recently revealed structures further elaborate on how MRP recognizes and processes short single stranded RNA target sequences (Lan et al., 2020). Components of the RNAse MRP complex include 10 protein members and eight of these are shared with another RNP, RNase P, adding another layer of complexity to the research field (Chamberlain, Lee, Lane, & Engelke, 1998).

1.3.2 DExD/H-box helicases involved in ribosome biogenesis

The first RNA helicase shown to have a role in ribosome biogenesis, Drs1, was discovered via a cold-sensitive phenotype inducing mutation and ribosome biogenesis defects (Ripmaster, Vaughn, & Woolford, 1992). Further studies uncovered 19 RNA helicases of the DEAD-box and DEAH-box family which have a function within the ribosome production pathway (reviewed in (Martin, Straub, Doebele, & Bohnsack, 2013; Rodriguez-Galan, Garcia-Gomez, & de la Cruz, 2013). The DExD/H motif consists of a conserved helicase core which comprises 13 individual motifs that participate in the helicase function ((Q, I, Ia, Ib, Ic, II, III, IV, IVa, V, Va, Vb, and VI). Generally, the helicase core folds into two Recombinase A-like (RecA-like) domains. Q-III form the Walker A and Walker B motif needed for ATP binding and hydrolysis. Motifs IV-VI build the second RecA-like domain, which is needed for ATP and RNA binding. The helicase core is flanked by variable C- and N-terminal domains, which are important for substrate recognition, nuclear import and binding of cofactors. Mutational analysis of conserved motifs and depletion of RNA helicases, polysome profiling, rRNA analysis by northern blotting of pulse-chase experiments and whole cell RNA extraction helped to group the identified helicases according to their involvement in ribosomal subunit assembly. Three have roles in biogenesis of both subunits (Prp43, Has1, Mtr4), seven have roles in the biogenesis of the small subunit (Rrp3, Fal1, Rok1, Dhr1, Dhr2, Dbp4, Dbp8) and nine are involved in large subunit assembly (Spb4, Mak5, Drs1, Dbp2, Dbp3, Dbp6, Dbp7, Dbp9, Dbp10). They belong to the SF2 superfamily, except for Mtr4, and are essential genes, except for Dbp2, Dbp3 and Dbp7, which induce a phenotype of decreased growth upon deletion. Catalytic mutants are often lethal and/or cause dominant negative phenotypes.

Depletion of RNA helicases involved in the biogenesis of both subunits, Has1 and Prp43, causes changed levels of mature subunits and hence mature rRNA species (Combs, Nagel, Ares, & Stevens, 2006; Emery, De la Cruz, Rocak, Deloche, & Linder, 2004; Lebaron et al., 2005). Disturbing the function of RNA helicases in 90S and 40S biogenesis usually causes defects in early processing steps (A_0, A_1 and A_2) and a decrease in 20S pre-rRNA as well as mature 18S rRNA (Bernstein, Granneman, Lee, Manickam, & Baserga, 2006). At the same time, the 35S pre-rRNA accumulates and alternative intermediates, 23S pre-rRNA and 21S pre-rRNA, can be detected. rRNA precursors of the large subunit are not affected significantly except for the $27SA_2$ pre-rRNA which reflects disturbed ITS1 processing. Impairment of RNA helicases

involved in large subunit assembly cause phenotypes depending on the ribosome maturation stage they are involved in. Early acting helicases cause accumulation of small subunit precursors and the alternative processing intermediate 23S pre-rRNA, with a small reduction in mature 18S rRNA levels (Bernstein et al., 2006; Bond, Mangus, He, & Jacobson, 2001; Weaver, Sun, & Chang, 1997). Other RNA helicases involved in later steps of large subunit biogenesis cause a typical accumulation of the 27SB pre-rRNA, suggesting an impairment in C_2 cleavage (Burger, Daugeron, & Linder, 2000; De la Cruz, Kressler, Rojo, Tollervey, & Linder, 1998).

Some RNA helicases have been shown to be activated by a cofactor protein. Dbp8, a DEAD-box helicase involved in 90S maturation, is stimulated by Esf2, which in turn was shown to interact with the U3 snoRNP (Granneman et al., 2006; Hoang et al., 2005). Prp43, a DEAH-box helicase involved in biogenesis of both subunits, was described to be tightly associated with Pfa1 (Lebaron et al., 2009; Leeds, Small, Hiley, Hughes, & Staley, 2006). Rrp5 was described as cofactor for the DEAD-box helicase Rok1 and both Esf2 as well as Rrp5 likely also recruit their RNA helicase partner (Vos, Bax, Faber, Vos, & Raue, 2004; Young, Khoshnevis, & Karbstein, 2013). Utp14 was shown to regulate the function of Dhr1 by recruiting it to the 90S particle and stimulating its activity (Zhu, Liu, Anjos, Correll, & Johnson, 2016). Similarly, Sgd1 stimulates the catalytic activity of the DEAD-box helicase Fal1 and likely also recruits it to its substrate pre-rRNA (Gallesio, Hackert, Bohnsack, & Bohnsack, 2020; Kressler, De la Cruz, Rojo, & Linder, 1997).

For most RNA helicases involved in ribosome biogenesis, their exact molecular function and RNA substrate is not known. Several RNA helicases were described to separate RNA duplex strands fueled by the energy that is generated upon ATP binding, while ATP hydrolysis promotes helicase release from the RNA and thus multiple substrate turnovers (Hilbert, Karow, & Klostermeier, 2009; Jankowsky, 2011; Liu, Putnam, & Jankowsky, 2008). In some cases, specific RNA helicases were shown to be important for snoRNP release. Since snoRNPs form base-pairing interactions with pre-rRNAs, they need to be removed for maturation to be able to proceed. As mentioned earlier, snoRNP guided chemical modifications are often clustered in regions that are important for the ribosome's functionality, which makes release of individual snoRNPs necessary for others to be recruited and do their job. Has1 is involved in the release of several snoRNPs, as is Prp43 (Bohnsack et al., 2009; X. H. Liang & Fournier, 2006). U14 snoRNP release requires Dbp4 (Kos & Tollervey, 2005)

and snR30 release requires the helicase Rok1 (Bohnsack et al., 2008; Khoshnevis et al., 2016; Martin et al., 2014). U3 snoRNP is released by the helicase Dhr1, governing a key maturation step on the way to mature 40S subunits (Sardana et al., 2015).

1.3.3 Structural roles of assembly factors and modules during ribosome biogenesis

Most of the AFs identified lack homology to proteins with enzymatic functions. However, they contain various structural motifs (for example HEAT/ARM, TPR, HAT, WD40) or RNA binding domains (for example KH, GAR, Brix, RRM, S1, Zinc fingers, dsRBD) (see Table 3 and Table 4 in (Woolford & Baserga, 2013). Some of the proteins were described as having a placeholder function due to their similarities to r-proteins (Mrt4 and RpP0, Rlp24 and RpL24) or to other non-ribosomal protein factors either involved in ribosome biogenesis (e.g. Dbp10 and Nmd3, Nog1 and Rei1, Bms1 and Tsr1, Tsr1 and Rio1, Krr1 and Pno1, formerly named Dim2,) or in translation (e.g. Ria1 and EF-2) (reviewed in (Espinar-Marchena, Babiano, & Cruz, 2017)). Some AFs contain domains similar to enzymatic motifs but lack the catalytic activity, suggesting that they could fulfill a placeholder role for their catalytically active counterpart. One example from the 90S biogenesis pathway is Utp23, which has a PIN like domain highly similar to Utp24, but no catalytic activity (Bleichert et al., 2006). Another example is Utp25, a DEAD-box like protein described to work in a protein network with Nop19 and the DEAH-box helicase Dhr2 (Charette & Baserga, 2010; Choque, Marcellin, Burlet-Schiltz, Gadal, & Dez, 2011).

Over the course of the past two decades, it was shown that many of the proteins without enzymatic activity work in complexes or modules. For the 90S and pre-40S maturation pathway, several such modules were identified and analyzed and are described in more detail in the section 1.3.1 (Figure 1.7A). The UTP-A module is one of the first to associate with pre-rRNA and consists of Utp4, Utp5, Utp8, Utp9, Utp10, Utp15 and Utp17 (J. E. Gallagher et al., 2004; J. E. G. Gallagher, 2019; Krogan et al., 2004). The UTP-B module comprises the proteins Utp6, Utp13, Utp18, Utp21, Pwp2 and Dip2 (Dosil & Bustelo, 2004; Krogan et al., 2004). The UTP-C module contains Utp22, Rrp7 as well as casein kinases II (CK2: Cka1/2 and Ckb1/2 subunits) (Krogan et al., 2004). The Mpp10 module is built up from Mpp10, Imp3 and Imp4 (Wehner, Gallagher, & Baserga, 2002). Bms1-Rcl1 also form a module as a heterodimer (Karbstein, Jonas, & Doudna, 2005; Wegierski, Billy, Nasr, & Filipowicz, 2001). The Noc4 module contains Enp1, Nop14, Rrp12, Noc4 and the methyltransferase Emg1

(J. Cheng et al., 2019; Kuhn et al., 2009). The Kre33 module contains the acetyltransferase/ATPase Kre33 and Enp2, Bfr2 and Lcp5 (J. Cheng et al., 2019). In the pre-60S maturation pathway the Rrp5-Noc1-Noc2 module (Hierlmeier et al., 2013) and Ytm1-Nop7-Erb1 module (Miles et al., 2005; Tang, Sahasranaman, Jakovljevic, Schleifman, & Woolford, 2008) were described.

1.4 The 90S pre-ribosome is the earliest ribosomal precursor

The 90S pre-ribosomal particle was initially defined by sucrose centrifugation as a precursor associated with human 45S or yeast 35S pre-rRNA (Tamaoki, 1966; Trapman et al., 1975; J. R. Warner & Soeiro, 1967). It is a huge, approximately 5 MDa precursor, which arises at the transcription site of the pre-rRNA in the nucleolus. As the 35S pre-rRNA is synthesized by Pol I, this first pre-ribosomal scaffold mediates the initial compaction of the emerging pre-rRNA molecule. Besides containing the 35S pre-rRNA and thus the rRNA content for the biogenesis pathways of both ribosomal subunits, the 90S particle also contains the U3 snoRNP, r-proteins of the SSU and AFs necessary for 40S biogenesis. Pre-60S factors are mostly absent as described first by our laboratory (Grandi et al., 2002). Containing the precursor for all rRNA species, this pre-ribosomal particle has a special position in the ribosome biogenesis pathway: separation of 40S and 60S biogenesis pathways occurs upon cleavage at the A_2 site, when the 90S particle, which matures into the pre-40S, is split from the maturation pathway of pre-60S particles. These particles mature independently with their own set of AFs, with only a few rare ones being reported as part of both pathways (Rrp5, Has1, Pol5, Prp43) (Braun et al., 2020; Emery et al., 2004; Lebaron et al., 2013). Around the same time as the 90S pre-ribosome, the SSU processome was described as an 80S pre-ribosomal assembly intermediate containing the U3 snoRNP and 28 proteins, but largely lacking pre-60S AFs. The absence of pre-60S factors gave the particle its name as small subunit (SSU) processome (Bernstein, Gallagher, Mitchell, Granneman, & Baserga, 2004; Dragon et al., 2002). Both terms, 90S particle and SSU processome, likely describe highly similar, if not the same, pre-ribosomal assembly stages as judged by their protein and rRNA composition. Hence, the earliest pre-ribosomal particles are referred to as 90S particles in this work.

1.4.1 Co-transcriptional assembly of protein modules and AFs with newly synthesized rRNA leads to the 90S pre-ribosome

As Pol I transcribes the 35S pre-rRNA, the earliest pre-ribosomal particle is assembled from approximately 70 individual AFs, including protein modules, snoRNPs and early binding r-proteins (Figure 1.7B). Their function has been described via depletion studies and ribosome biogenesis defects, identification of protein complexes and pre-ribosomal particles, aptamer-tagged RNA truncations and cryo-EM analysis of isolated pre-ribosomal particles (reviewed in (Bassler & Hurt, 2018; Klinge & Woolford, 2018)).

The 5'ETS is the first pre-rRNA segment to emerge as Pol I continues transcription and hence recruits the first AFs in a modular and hierarchical fashion. Depletion studies indicate that the UTP-A module is the first to contact the nascent pre-rRNA, forming a platform to recruit other modules, snoRNPs and AFs (J. E. Gallagher et al., 2004; Krogan et al., 2004; Perez-Fernandez, Martin-Marcos, & Dosil, 2011; Perez-Fernandez, Roman, De Las Rivas, Bustelo, & Dosil, 2007). It is sometimes referred to as tUTP module (transcriptional UTP) because depletion of its protein members inhibited pre-rRNA transcription. In comparison, depletion of proteins belonging to other modules led to pre-rRNA processing defects, which was accompanied by increased levels of 35S pre-rRNAs (J. E. Gallagher et al., 2004; Granneman & Baserga, 2005). UTP-A is the largest module containing seven proteins, which are highly interconnected by protein-protein interactions. UTP-B, composed of 6 proteins, is the second largest 90S protein module. Both modules are built from proteins with no enzymatic activities, instead carrying ß-propeller domains (WD40 repeat domains) and α-solenoid structures. Together with the U3 snoRNP, they are thought to be functioning as nucleation core and structural framework for the 90S particle. They bind to pre-rRNAs and serve as platform for further protein-protein and protein-RNA interactions, which build the 90S pre-ribosome (Champion, Lane, Jackrel, Regan, & Baserga, 2008; Hunziker et al., 2016; Pöll et al., 2014; C. Zhang et al., 2014).

The Mpp10 module contains Mpp10, Imp3 and Imp4, all proteins without enzymatic activity but a link to UTP-B via AF Utp3/Sas10 (Charette & Baserga, 2010). This module is described in the literature as essential component of the U3 snoRNP associated complex with an important role in stabilizing the 18S pre-rRNA::U3 hybrids and therefore chaperoning very early pre-rRNA remodeling events (Dunbar, Wormsley, Agentis, & Baserga, 1997; Gerczei & Correll, 2004; Gerczei, Shah, Manzo,

Walter, & Correll, 2009; S. J. Lee & Baserga, 1999; Wormsley, Samarsky, Fournier, & Baserga, 2001).

Bms1 and Rcl1 form a heterodimer, which associates with 90S pre-ribosomes and persists until early pre-40S stages (J. Cheng et al., 2020; Gelperin, Horton, Beckman, Hensold, & Lemmon, 2001). Rcl1 binds to Bms1 in the presence of GTP and GTP hydrolysis releases Rcl1 from the pre-ribosome (Karbstein & Doudna, 2006; Karbstein et al., 2005). It has been proposed to cleave pre-rRNAs at the A_2 cleavage site within ITS1 (Gelperin et al., 2001; Horn, Mason, & Karbstein, 2011; Karbstein et al., 2005; Wegierski et al., 2001). However, it is more widely accepted that the PIN domain containing protein Utp24 is the endonuclease mediating A_2 cleavage (Bleichert et al., 2006; Wells et al., 2016).

The UTP-C module contains Utp22, Rrp7 and CK2. Utp22 shows similarity to CCA enzyme, a tRNA nuleotidyltransferase, but harbors no enzymatic activity. It interacts with Rrp7 which in turn connects the module via its flexible RNA-binding C-terminus to the 90S particle (Lin, Lu, Feng, Sun, & Ye, 2013). CK2 has been proposed to have a potential regulatory role by phosphorylation of ribosomal proteins and/or AFs (Phipps, Charette, & Baserga, 2011; Wojda, Cytrynska, Frajnt, & Jakubowicz, 2002). Moreover, UTP-C has been shown to be part of the CURI complex, which contains the transcription factor Ifh1 that, together with promoter-bound Fhl1, controls expression of r-protein genes (Albert et al., 2016; Rudra, Mallick, Zhao, & Warner, 2007; Rudra, Zhao, & Warner, 2005). This connection offers an intriguing path to more global regulatory processes and how ribosome biogenesis, given its extraordinary energy expense, is integrated into the cellular energy budget (reviewed in (de la Cruz et al., 2018)). One such connection is the growth-promoting TORC1 (target of rapamycin 1) kinase which upon inactivation triggers Ifh1 dissociation from r-protein gene promoters (Schawalder et al., 2004). Another mechanism ensuring that ribosome biogenesis fits cellular demands occurs through balancing r-protein production with cellular demand of ribosomes via interplay of the transcription factors Ifh1 and Hsf1 (Albert et al., 2019).

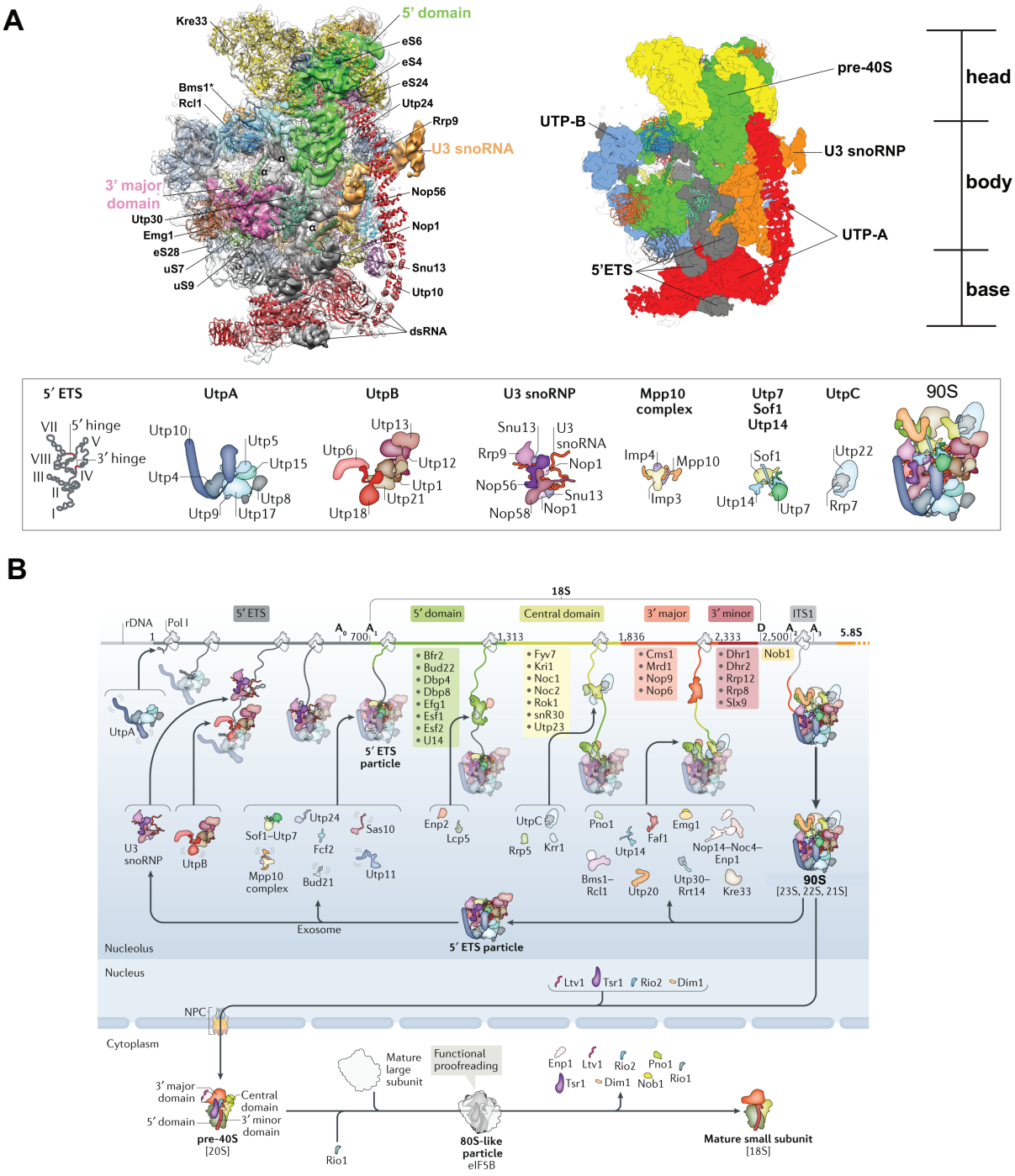


Figure 1.7 Modular architecture of the 90S pre-ribosome. A) Upper panel: Cryo-EM model of the front view of a 90S particle from *Chaetomium thermophilum* (left panel) as well as schematic representation of the main modules and rRNAs. Figure taken from (Kornprobst et al., 2016) Figure 7. Lower panel: Depiction of main modules of the 90S pre-ribosome as well as of the 90S particle in cartoon form. Figure taken and adapted from (Klinge & Woolford, 2018) Figure 2. B) Schematic representation of steps taking place during 90S assembly, maturation and pre-40S final maturation steps in the cytoplasm. NPC: nuclear pore complex, Pol I: RNA polymerase I, snoRNP: small nucleolar ribonucleoprotein. Figure taken and adapted from (Klinge & Woolford, 2018) Figure 2.

The Kre33 module consists of the SAS10-domain containing protein Lcp5, ß-propeller protein Enp2, Bfr2 and the RNA acetyltransferase Kre33 homodimer. Previous studies implicated the module members in a shared protein interaction network. Human Bfr2 (AATF) and Enp2 (NOL10) were described to exist in a complex with Lcp5 (NGD) and *ct*Bfr2 was shown as a strong Y2H pair with *ct*Kre33, which in the cryo-EM models mentioned earlier was positioned as homodimer in the 5' domain of the pre-rRNA (Bammert, Jonas, Ungricht, & Kutay, 2016; Bassler et al., 2017). Work from our lab showed via an extended network of Y2H interactions, *in vitro* reconstitutions as well *in vivo* biochemical analysis of protein interactions that these factors are part of a module, which binds to the 5' domain (J. Cheng et al., 2019).

Studies employing particles isolated via 3'-truncated aptamer tagged rRNA molecules further added information on when AFs could be recruited to or stably assembled with nascent pre-rRNAs (Chaker-Margot, Hunziker, Barandun, Dill, & Klinge, 2015; Hunziker et al., 2019; L. Zhang, Wu, Cai, Chen, & Ye, 2016). Based on these studies it was postulated that AFs are recruited to pre-rRNA subdomains in the order of their 5'>3' ongoing transcription (Figure 1.7B) and that this timely recruitment strictly governs further assembly events. However, the interpretation of these studies remains difficult since they do not give justice to the physiological complexity of long range rRNA interactions and thereby formed recruitment and binding sites as well as stabilized interactions for AFs or modules. Similarly, grouping AFs according to the pre-rRNA defects their mutation, depletion or knockout causes does not help to determine when an individual AF is first recruited to pre-ribosomal particles. Hence, the temporal resolution for the 90S particle is quite low. An exception are the UTP-A, UTP-B and U3 snoRNP, which are generally accepted to be recruited first co-transcriptionally.

Even though the aforementioned studies and methods identified many modules and AFs of the 90S assembly pathway, they were not sufficient in understanding the structural architecture and dynamics of the pre-ribosome. For most AFs as well as r-proteins, the precise binding site and molecular and biochemical function within the pre-ribosomal particle was unknown and difficult to access experimentally. The low resolution of the assembly process stems from the many transient interactions of AFs with pre-ribosomes, but also from structural changes that cannot be addressed with the standard genetic and biochemical approaches in yeast.

Here, first cryo-EM models of the 90S particle were immensely helpful. They showed pre-ribosomal assembly stages before A_1 cleavage has occurred and confirmed the modular structure of the 90S as well as the central role of the 5'ETS and U3 snoRNP in initiating and organizing the entire particle (Figure 1.7A) (Barandun et al., 2017; Kornprobst et al., 2016). For general orientation within this huge macromolecular protein-RNA assembly, the 90S pre-ribosome was divided in several regions. The base, or foot, is formed by evolutionary related molecular chaperones UTP-A and UTP-B covering the 5'ETS. The 5', central and 3' domains of 18S pre-rRNA are located on top of the particle's base. The 3' major domain of the 18S pre-rRNA and associated AFs form the backpack region of the 90S pre-ribosome. The 3' minor domain consists mainly of H45 and H44, which is part of the subunit interface in mature 40S subunits but is seen located far away from its mature position in the 90S pre-ribosome. The 3' domain and the central domain form the body of the 90S particle. The 5' domain and associated AFs define the head region in the 90S pre-ribosome.

The initial cryo-EM models gave us structural insights into how such an extraordinarily complex assembly as the 90S particle is the product of its underlying protein-protein and protein-RNA interaction network. Many AFs were seen to have long extensions providing structural support and interconnectivity for the particle, while other AFs formed more local interactions. Imp4, Faf1, Nop14 and Bms1 for example are extended proteins stabilizing RNA duplexes between the 5' domain, central domain and U3 snoRNA. Fcf2, Sas10 and Utp11 also have long extensions which can connect distant areas of the 90S particle. Some proteins cover the outer areas and clearly serve structural roles with their α-helical repeats (Utp10, Utp20, Rrp5, Noc4, Nop14). Utp20 and Utp10 for example are proteins containing elongated α-solenoid elements. They interact with each other in the head of the 90S which is wrapped by Utp20, and thereby form a scaffold reaching from the bottom to the top of the 90S particle. As described in section 1.2.3.1, the U3 snoRNP contacts both 5'ETS and 18S pre-rRNA. cryo-EM structures of the 90S pre-ribosome showed that the central pseudoknot is prevented from forming prematurely, while the domains of the 18S pre-rRNA are separated and chaperoned in different regions of the 90S pre-ribosome.

Even though the initial 90S cryo-EM models provided much needed structural information, it was not possible to visualize all r-proteins or AFs, which were identified by mass spectrometry in the samples used for cryo-EM analysis (Figure 1.7B, marked

with an asterisk). Moreover, A_1 as well as A_2 cleavages have not occurred yet in the particles described and neither has 5'ETS processing by the RNA exosome.

1.4.2 Shedding of 90S AFs liberates early 40S pre-ribosomes

Since the 90S particle contains factors needed for the production of functional 40S subunits, pre-40S biogenesis is initiated during 90S maturation. 90S pre-ribosomes serve as platform organizing pre-rRNA 18S domains in a way which leads to pre-rRNA cleavages, ultimately separating pre-40S biogenesis from the pre-60S maturation pathway. The transition of 90S to pre-40S pre-ribosomes has to involve the release of many AFs, but exactly how pre-40S particles emerge from 90S pre-ribosomes was unclear until recently (J. Cheng et al., 2020). In contrast to the previously assumed model of en bloc release of 90S modules, pre-40S particles were shown to emerge by continuous shedding of modules and AFs. For instance, based on previously reported data it was assumed that the 5'ETS RNP leaves the 90S particle as a whole during the 90S to pre-40S transformation (Chaker-Margot, Barandun, Hunziker, & Klinge, 2017; Chaker-Margot et al., 2015; Klinge & Woolford, 2018; Kornprobst et al., 2016; L. Zhang et al., 2016). However, the pre-40S emerges from the 90S particle through sequential simplification via release of the UTP-A module and U3 snoRNP protein components, followed by the dissociation of UTP-B and UTP-C (J. Cheng et al., 2020).

This transformative release of typical 90S factors is preceded by RNA exosome recruitment as well as A_1 cleavage and accompanied by higher flexibility of the 5'ETS region, which is almost completely dislodged after A_1 processing has occurred (Lau et al., 2021). Recruitment of the RNA exosome to the maturing 90S pre-ribosome is facilitated by the co-factor RNA helicase Mtr4 interacting with a platform region consisting of Utp6, Utp14 and the AIM-motif containing UTP-B protein Utp18 (Lau et al., 2021; Thoms et al., 2015). However, not all factors dissociate from 90S pre-ribosomes, as a few are also part of pre-40S intermediates. These factors include Pno1, Dim1, Nop14, Noc4, Enp1, Rrp12 and Slx9, which are implicated to also play a role in the export of pre-40S particles (U. Fischer et al., 2015; Milkereit et al., 2003; Moriggi, Nieto, & Dosil, 2014). Once exported into the cytoplasm, pre-40S subunits undergo a few last maturation steps before reaching the translation competent form. These last steps include assembly of late r-proteins, beak formation and 20S pre-rRNA cleavage at site D, while simultaneously premature engagement in translation needs to be prevented.

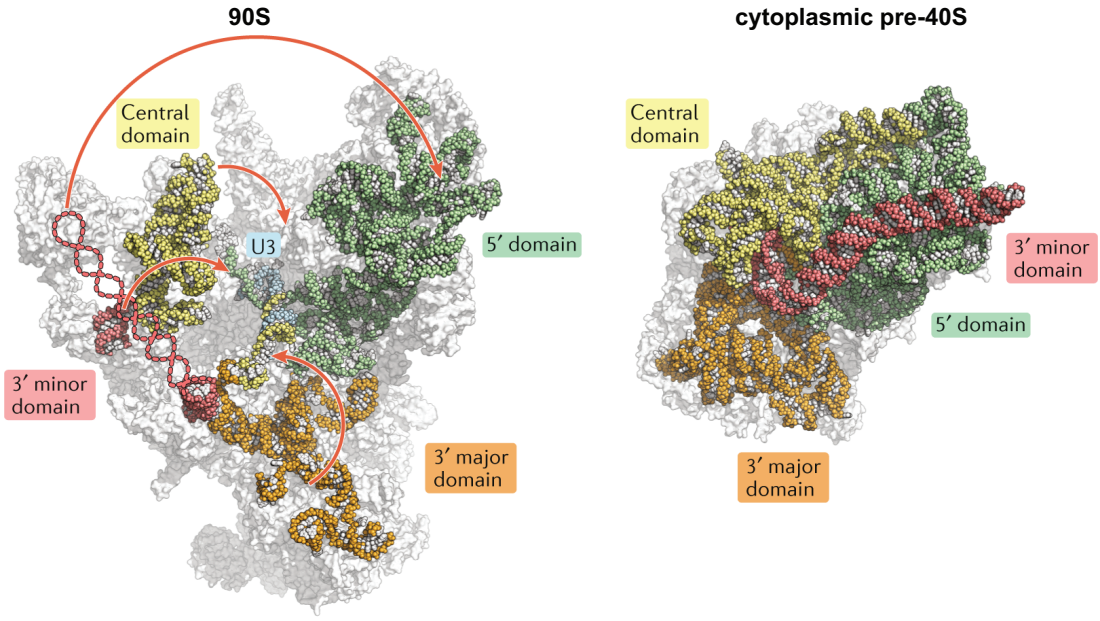


Figure 1.8 18S pre-rRNA subdomains are differentially arranged in 90S and pre-40S particles. Left panel: depiction of pre-rRNA subdomains and their movements relative to cytoplasmic pre-40S particles. Right panel: 18S pre-rRNA subdomains in their near mature conformation in cytoplasmatic pre-40S particles. Individual subdomains are color coded as indicated. Figure taken and adapted from Figure 6a (Klinge & Woolford, 2018).

Comparing the pre-rRNA domain organization in 90S pre-ribosomes and cytoplasmic pre-40S particles, major structural rearrangements can be observed for the 3' domain as well as, to a lesser extent, the central domain (Figure 1.8), again arguing for ribosome biogenesis as a progressive compaction of pre-rRNA domains.

Rrp12, Enp1 and Pno1 are still associated with the 3' domain in the pre-40S particle. Other factors assembled on the 90S pre-ribosome with the 3' domain of the 18S pre-rRNA have to be released during a transition, which also includes conformational changes of the pre-rRNA (Barandun et al., 2017; Heuer et al., 2017; Scaiola et al., 2018). Factors associating exclusively with early pre-40S particles, which contains the 20S pre-rRNA species, include Nob1, Tsr1, Hrr25, Rio1/2 and Ltv1 (Schafer, Strauss, Petfalski, Tollervey, & Hurt, 2003). They assemble with the pre-ribosome somewhere between the nuclear to cytoplasmic pre-40S intermediates, but their exact entry point is not known yet. Parts of Nop14 on the surface of Enp1 in the 3' domain is replaced by Ltv1, while Tsr1 replaces its structurally related GTPase Bms1 in the 5' domain (Heuer et al., 2017; Scaiola et al., 2018). Export of pre-40S particles is dependent on several factors and some of the involved factors indeed carry a nuclear export signal (NES) sequences, such as Rio2, Ltv1 and Pno1.

AFs involved in maturation steps of pre-40S particles also take part in preventing stable assembly of r-proteins. Pno1 prevents premature association of RpS26. Enp1 and Ltv1 prevent the formation of the beak structure of the mature 40S subunit, which forms upon assembly of r-proteins RpS3, RpS10, RpS12, RpS20 and RpS31. Phosphorylation of RpS3, Enp1 and Ltv1 leads to a dissociation of the three proteins. Subsequent dephosphorylation makes re-assembly of RpS3 possible, ultimately promoting beak formation (Johnson, Ghalei, Doxtader, Karbstein, & Stroupe, 2017; Schäfer et al., 2006; B. Strunk et al., 2011). Moreover, pre-40S AFs generally seem to occupy functional sites in the pre-40S particle, which in the mature form are bound by the translation machinery, thus preventing an immature cytoplasmic 40S subunit to enter the cycle of translation. Dim1, Rio2 and Tsr1 bind to the intersubunit side below the platform region close to the decoding center. Thereby, they prevent translation initiation factors eIF1 and eIF1A and mature 60S subunits to engage with immature 40S subunits (Johnson et al., 2017; Lebaron et al., 2012; McCaughan et al., 2016; B. Strunk et al., 2011; B. S. Strunk et al., 2012). Pno1 and Nob1 have overlapping RNA binding sites over cleavage site D indicating that Pno1 masks the pre-rRNA substrate for Nob1 until the right maturation stage is reached (Turowski et al., 2014). Within this context, a “translation-like cycle” was described as the last proofreading step, scanning cytoplasmic 40S pre-ribosomes for their competence to enter the translation pool (Pestova et al., 2000; B. S. Strunk et al., 2012). The GTPase translation initiation factor eIF5b (Fun12) is needed for a formation of a pre-40S-60S complex without mRNA or tRNA molecules and enables final cytoplasmic pre-rRNA processing, while Rio1 kinase is needed for Pno1 and Nob1 release (Lebaron et al., 2012; Parker, Collins, Korona, Ghalei, & Karbstein, 2019).

1.5 Aims of this study

In my PhD study, the initial goal was to investigate the role of the KH domain containing assembly factor Krr1 during 90S biogenesis, for which an interconnected function with another assembly factor Pno1 was suggested (Sturm, Cheng, Bassler, Beckmann, & Hurt, 2017). At that time, Krr1's role in ribosome biogenesis was largely defined by the presence of two KH domains, which are considered to mediate protein-RNA or protein-protein interactions (Karkusiewicz, Rempola, Gromadka, Grynberg, & Rytka, 2004; Sasaki, Toh-E, & Kikuchi, 2000; Zheng, Lan, Liu, & Ye, 2014). No information was available on the role of its conserved C-terminal extension.

As a highly resolved cryo-EM structures of the 90S pre-ribosome could be obtained in the Hurt lab during the course of my study, it revealed for the first time that Krr1 contacts the head and central region with its C-terminal extension. Moreover, interactions of the KH domain, which is positioned between the body and base region of the 90S particle, could be well resolved for the first time. Based on this new structural information, I wanted to comprehensively understand Krr1's essential role in early pre-ribosomal assembly processes. Therefore, I began with a mutational analysis of Krr1 to find out how its interactions within the different regions of the 90S particle are affected and if specific steps in 90S biogenesis could be disturbed. Because not all mutations in Krr1 gave a growth-related phenotype, the mutational approach also included genetic analysis with mutant versions of assembly factors that link Krr1 to the different 90S subdomains.

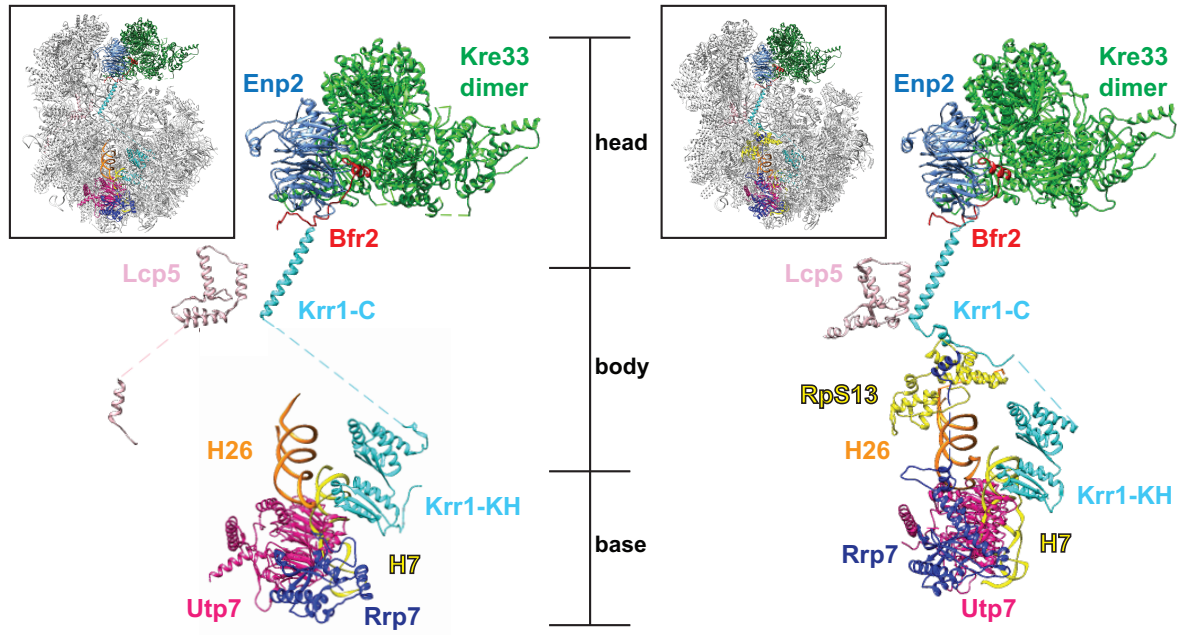
Since Krr1 has no enzymatic function but a strategic position within the 90S particle connecting different 90S subdomains, I sought to find out how Krr1 functions both in early and late 90S biogenesis steps, and finally how Krr1 can leave the 90S pre-ribosome. In this way, I wanted to decipher the timely progression of 90S pre-ribosome biogenesis and the events leading to the transition of 90S particles to pre-40S subunits.

2. Results

2.1 Krr1 contacts different regions within the 90S particle

Krr1 is a highly conserved AF among eukaryotes, which has been described in the literature as interaction partner of a few early 90S AFs (Kri1, Faf1, RpS14) and by its placeholding function for the 90S/pre-40S biogenesis factor Pno1 (see Introduction). Both functions were reported to be mediated by its KH domains, while the role of its conserved C-terminal extension has not been investigated yet. The C-terminal region harbors different structural elements and a putative NLS (Figure 2.1B and Supplemental Figure 5.1) (Sasaki et al., 2000).

A



B

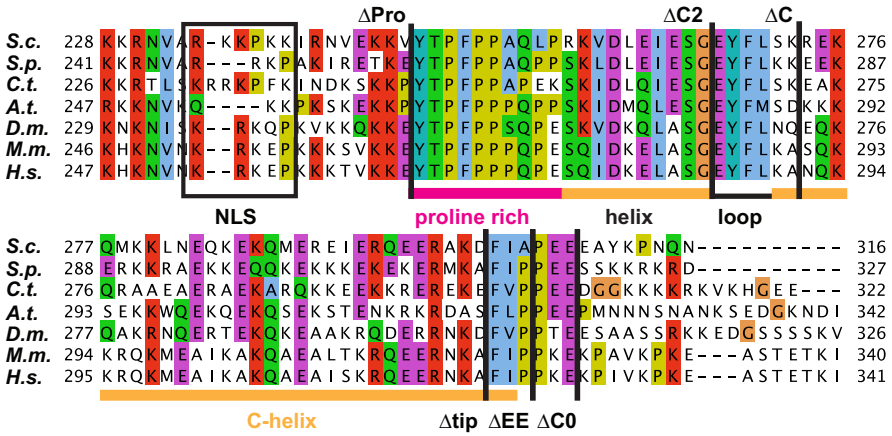


Figure 2.1 Krr1 spans the 90S from head to toe. (A) Cryo-EM model of Krr1 contacting different regions in state B2 with the whole 90S pre-ribosome depicted in a box in the upper left corner for orientation. Left panel: *Chaetomium thermophilum* (*ct*) *ct*90S PDB: 6rxv, right panel: *Saccharomyces cerevisiae* (*sc*) *sc*90S PDB: 6zqB. (B) Multiple sequence alignment of Krr1 with the C-terminus shown. Sequences were aligned with Clustal Omega and Jalview. C-terminal truncation mutants are indicated as well as the secondary structure elements seen in state B2 from the *ct*90S and *sc*90S Cryo-EM models. *S.c. Saccharomyces cerevisiae, S.p. Schizosaccharomyces pombe, C.t. Chaetomium thermophilum, A.t. Arabidopsis thaliana, D.m. Drosophila melanogaster, M.m. Mus musculus, H.s. Homo sapiens*

With the use of the split-purification technique in combination with cryo-EM analysis of isolated particles, our lab was able to reveal the structure of several 90S particles from the thermophile *Chaetomium thermophilum* and yeast (Figure 2.1A, left and right panel for *Chaetomium thermophilum* and yeast, respectively) (J. Cheng et al., 2019; J. Cheng et al., 2020). These structures, or assembly states, correspond to different snapshots and will be named with a prefix indicating the samples origin ("*sc*" for yeast, "*ct*" for *Chaetomium thermophilum*, e.g. *ct*90S for 90S pre-ribosome isolated from *Chaetomium thermophilum*, or *ct*B2 for state B2 of a 90S pre-ribosome isolated from *Chaetomium thermophilum*).

The biogenesis factor Krr1 is seen in 90S particles in state B2 from both species as a 90S factor spanning along the 90S particle, while contacting different proteins in the head, body and base region (Figure 2.1A). Parts of the C-terminal region of Krr1 were visualized for the first time as a long α-helical element in 90S particles in state B2 with a Noc4-ProtA/Kre33-FLAG split purification from *Chaetomium thermophilum* (Figure 2.1A, left panel). This helix was shown to point to the interface between the Kre33 module members Enp2 and Bfr2 in the head region of the 90S particle. 90S pre-ribosomes in state B2 from yeast additionally showed a short loop region, short helix and an unstructured proline-rich region in the central part of the 90S contacting RpS13 which interacts with the UTP-C module member Rrp7 (Figure 2.1A, right panel, and Figure 2.2, left panel for an isolated view of the C-terminal secondary structure elements of Krr1). Finally, in the base region of the 90S particle, the conserved KH domain of Krr1 is in close contact with H26, H22 and H23 of the central 18S rRNA domain and Utp7, which in turn contacts Rrp7. Moreover, *sc*90S particles in state B2 show both Krr1 and Utp7 contacting H7 of the 5'ETS rRNA.

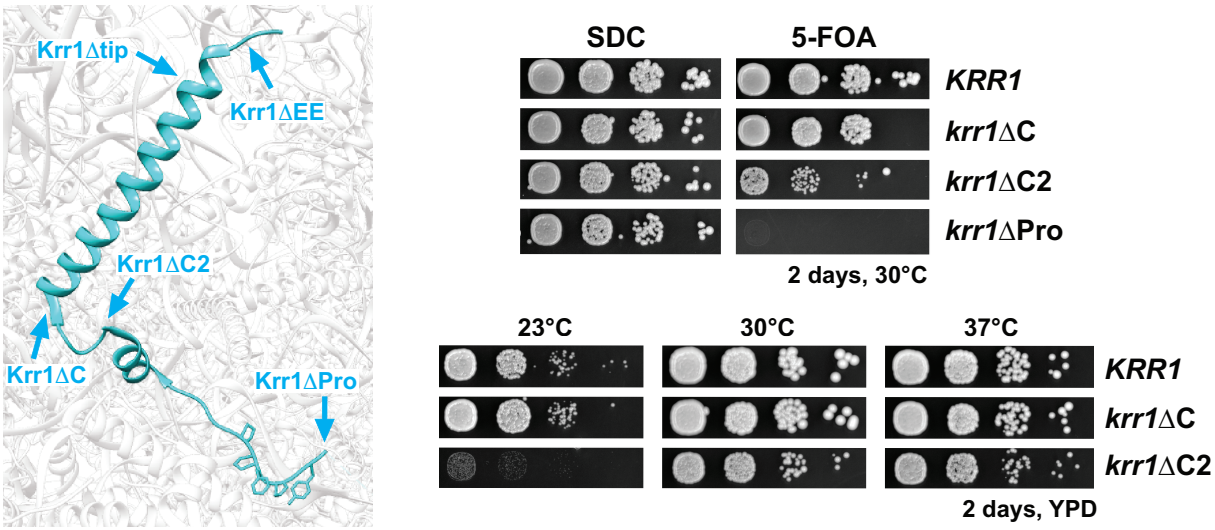


Figure 2.2 Structure based mutations of Krr1 show that its proline-rich region is essential. (A) Cryo-EM structure of the C-terminal region of Krr1 contacting the central platform and the C-helix pointing towards the Kre33 module in the head region (*sc*90S from B2, PDB: 6zqB). The respective C-terminal deletion mutants indicated in the MSA from Figure 1B are marked with an arrow. (B) Growth analysis of different C-terminal truncations of Krr1. Upper panel: A Δ*krr1* shuffle strain was transformed with pRS315 containing the indicated alleles. Cells were selected on SDC medium and plated in serial dilutions on SDC and SDC+5-FOA plates. Lower panel: Strains transformed with viable alleles of *KRR1* were selected on SDC+5-FOA and analyzed for their growth at the indicated temperatures by plating in 10-fold serial dilutions.

To decipher the structural and functional role of the C-terminus of Krr1, we created progressive deletion mutants. To our surprise, deletion of the C-helix (Krr1ΔC, aa1-272) supported growth and did not cause a growth phenotype at different temperatures (Figure 2.2, right panel, upper part for complementation and lower part for growth analysis). Accordingly, deletions of the helix tip or the negatively charged amino acids (*krr1*Δtip and *krr1*ΔEE, respectively) did not affect growth either (shown in Figure 2.6B). However, deletion of the C-helix and the small loop (Krr1ΔC2, aa1-266) slowed growth at all temperatures with a pronounced effect at 23˚C (Figure 2.2, right panel, lower part). Moreover, the C-terminal truncation including the proline-rich region (Krr1ΔPro, aa1-245) did not longer support growth in yeast (Figure 2.2, right panel, upper part). With the mutational analysis, we could extend the essential character of Krr1 beyond its KH domains, i.e. into its unstructured C-terminal region contacting the central domain. To further understand Krr1's involvement in the biogenesis of the 90S particle and its maturation, we analyzed Krr1's structural elements in the head, body and base region for a possible genetic link with the AFs in contact to Krr1 (Kre33 module members Enp2, Bfr2 and Kre33 in the head region; Utp7 in the base region).

Further, we characterized 90S biogenesis by isolating and analyzing 90S particles from mutant cells.

2.2 Krr1 has a genetic link to the Kre33 module via ß-propeller containing protein Enp2

2.2.1 Structure based mutational analysis of the Kre33 module members Enp2 and Bfr2

In the newly discovered structures of the 90S particle, Krr1's long C-helix was seen to contact the Kre33 module and connect it to the central region of the 90S particle. Despite its distinct location and connective character within the 90S pre-ribosome, deletion of the C-helix did not affect yeast cell growth (see previous section). To find out whether Krr1 is genetically linked to the Kre33 module, we sought to generate viable mutants of the essential Kre33 module members Enp2 and Bfr2 and analyze their combined effect on cell growth. A temperature-sensitive (ts) mutant of Kre33 was described previously and used in this study (Grandi et al., 2002). In the *ct*90S and *sc*90S structures revealed by our group, only the ß-propeller of Enp2 is visible while no density was assigned to the C-terminus of Enp2 (Figure 2.1A). The C-terminus is not very well conserved (Supplemental Figure 5.2), and likely flexible. We generated progressive C-terminal deletion mutants for Enp2, which were all viable (Figure 2.3A, upper panel). One mutant with the longest C-terminal deletion, Enp2ΔC (aa1-514), showed a growth defect at 23˚C (Figure 2.3A, lower panel), while other deletion mutants, Enp2ΔC1 (aa1-678) and Enp2ΔC2 (aa1-626), did not show any effect on growth of yeast cells incubated at the selected temperatures. To make sure that the slower growth rate is not based on a Kre33-module assembly problem, we purified full length and the truncated Enp2 version tagged with the FLAG-TEV-ProtA epitope. Analysis by SDS-PAGE, Coomassie and mass spectrometry showed that the Enp2ΔC protein assembled with Kre33, Bfr2 and Lcp5 (Figure 2.3 B left panel, lane 3 and 4 compared to lane 1 and 2), with no striking differences of the proteins isolated at 23˚C, where the growth defect is observed. Isolation of UTP-A-module member Utp10 (Figure 2.3B, middle panel), which is known to associate early with the emerging 35S rRNA (see Introduction), or the early to intermediate AF Utp7 (Figure 2.3B, right panel) showed a slightly increased incorporation into a 90S particle as judged by the increased intensity of the typical 90S band pattern visualized with Coomassie staining.

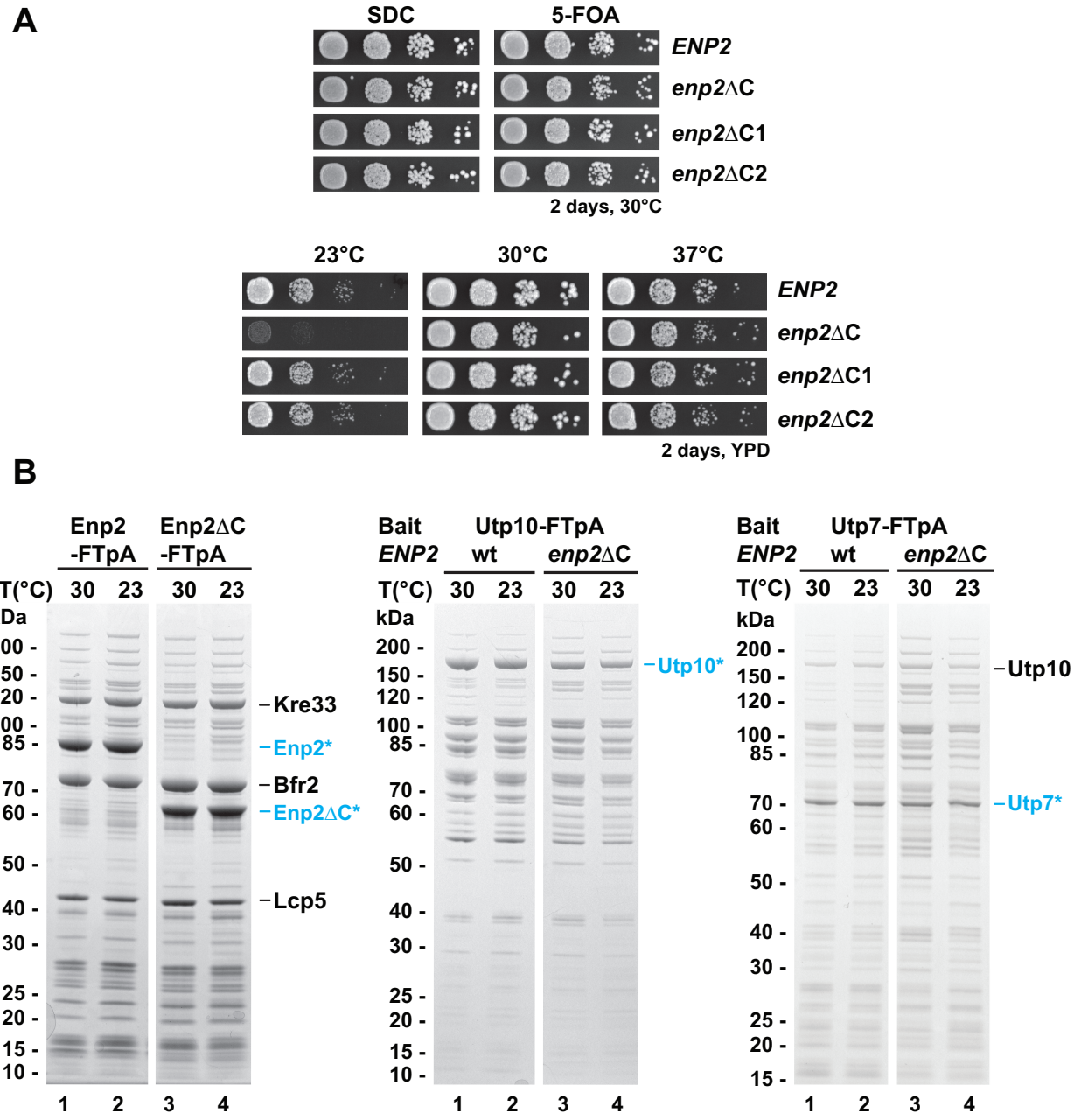


Figure 2.3 C-terminal truncation mutants of Enp2 are viable and *enp2*ΔC cells exhibit a cold sensitive phenotype. (A) Growth analysis of different C-terminal truncation mutants of Enp2. Upper panel: An Enp2 shuffle strain was transformed with pRS315 containing the indicated alleles. Cells were selected on SDC and plated on SDC and SDC+5-FOA in 10-fold serial dilutions. Lower panel: Strains transformed with viable alleles were selected on SDC+5-FOA and analyzed for their growth on YPD plates incubated at the temperatures indicated. (B) Biochemical analysis of proteins associated with different biogenesis factors in *enp2*ΔC cells. Left panel: A Δ*enp2*Δ*krr1* double shuffle strain was transformed with pRS314-Krr1 and pRS315-Enp2-FTpA or pRS315-Enp2ΔC-FTpA and the Enp2 or Enp2ΔC proteins were subsequently affinity purified. Cultures were grown either at 30℃ or shifted to 23℃ for 10h as indicated. Middle panel: The UTP-A module member Utp10 was genomically tagged with FLAG-TEV-ProtA at the C-terminus and purified from *KRR1 ENP2* or *KRR1 enp2*ΔC cells. Right panel: Early to intermediate AF Utp7 was genomically tagged at the C-terminus with FLAG-TEV-ProtA and purified from *KRR1 ENP2* or *KRR1 enp2*ΔC cells. Bait proteins are

shown in cyan and marked with an asterisk. Other labeled proteins were identified via mass spectrometry.

Taken together, the Enp2ΔC protein incorporates into the Kre33-module like its full-length counterpart and does not significantly alter the composition of AFs co-enriched with early 90S particles.

*Ct*90S and *sc*90S in state B2 both show a small C-terminal fragment of Bfr2 (Figure 2.4A, left panel): a small helix wedged between Enp2 and Kre33 is followed by an unstructured region. We progressively deleted parts of the C-terminus of Bfr2 according to the structural information provided by the cryo-EM model and parts of the not visible N-terminus of Bfr2, according to secondary structure predictions (Supplemental Figure 5.3). A short deletion of the region leading up to the small helix (Bfr2ΔC1, aa1-515) was viable and did not exhibit a growth defect at the temperatures tested (Figure 2.4A, right panel, and Figure 2.4B). The small wedge helix was not essential as a deletion supported growth (Bfr2ΔC2, aa1-487, Figure 2.4A, right panel). However, cells showed a decreased growth rate especially at 23˚C (Figure 2.4B). Further deletion beyond the unstructured region (Bfr2ΔC3, aa1-433) did not support growth (Figure 2.4A, right panel). The N-terminus of Bfr2 has many conserved negatively charged amino acids (Supplemental Figure 5.3). A short deletion of the weakly conserved first 65 amino acids (Bfr2ΔN1, aa 66-534) complemented a Δ*bfr2* deletion and did not affect growth at the temperatures tested (Figure 2.4A, right panel for complementation, and Figure 2.4B for growth at different temperatures). However, further deletion of the first 144 amino acids, including more conserved acidic regions, complemented a Δ*bfr2* deletion, but the growth was extremely slow at all temperatures tested (Figure 2.4A, right panel for complementation, and Figure 2.4B for growth at different temperatures). We tested whether the observed severe growth defect caused biochemical changes in pre-ribosomal particles isolated via different bait proteins, but did not observe any difference and hence did not investigate the cause of the growth impairment further (Supplemental Figure 5.4A).

To understand if deletion of the C-terminal helix of Bfr2 affects Kre33-module assembly, we isolated Enp2 tagged with the FLAG-TEV-ProtA epitope from wild-type (wt) and *bfr2*ΔC2 cells at 30˚C and 23˚C, where the growth defect of the mutant cells is pronounced. While Enp2 pulled down its other module partners Kre33, Bfr2 and Lcp5 and small amounts of 90S factors from wt cells (Figure 2.4C, left panel, lane 1 and 2),

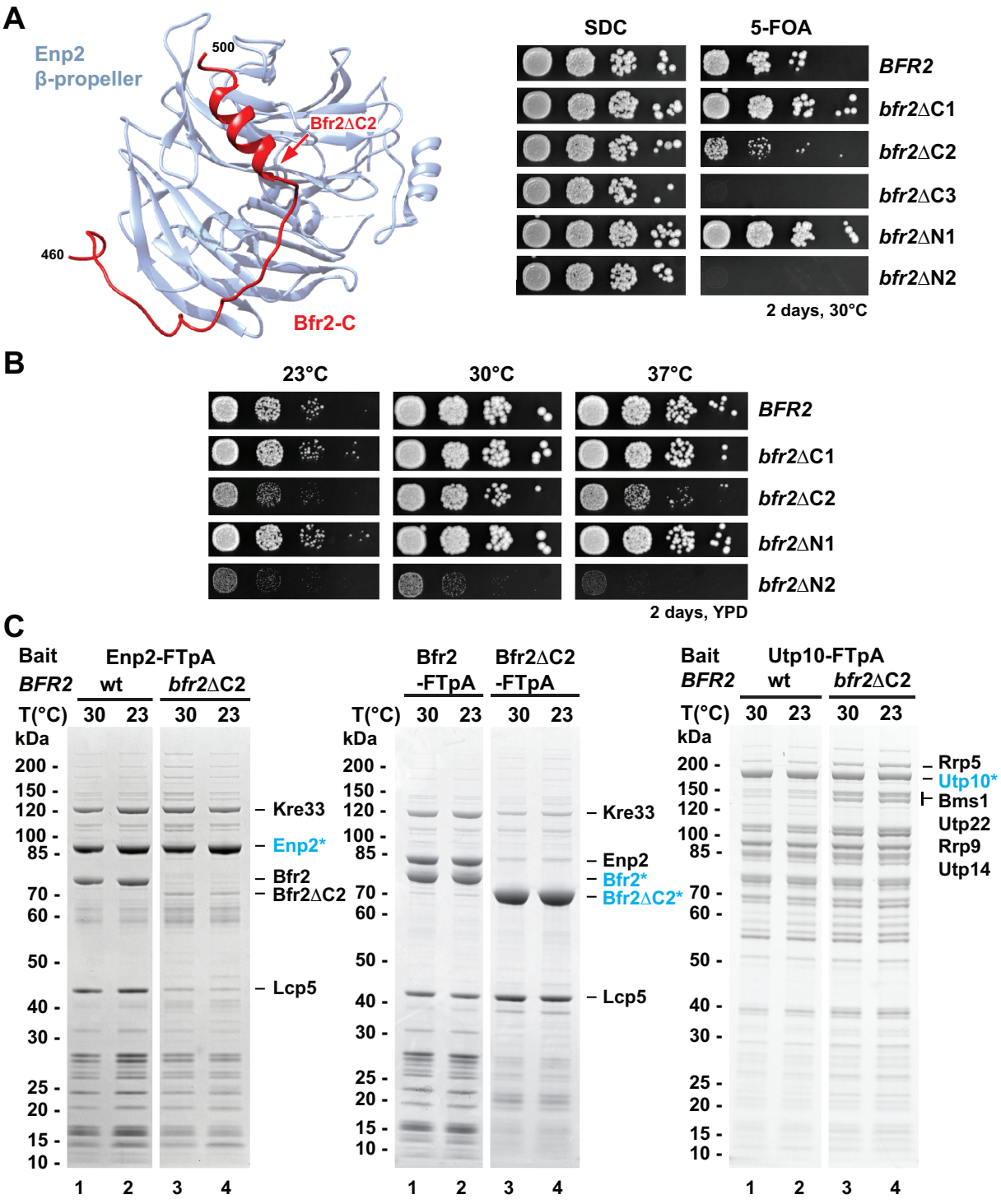


Figure 2.4 Structure based mutations of Bfr2 show importance of wedge helix for Kre33 module assembly. (A) Left panel: Cryo-EM model (*sc*90S, state B2 PDB: 6zqB) showing a C-terminal fragment of Bfr2 (red) with the ß-propeller of Enp2 (cornflower blue). Amino acid boarders and the Bfr2ΔC2 truncation are indicated. Right panel: Complementation analysis of N-terminal truncation mutants of Bfr2 and structure-based C-terminal truncations. A Δ*bfr2* shuffle strain was transformed with the alleles indicated, cells were selected on SDC and plated on SDC and SDC+5-FOA in 10-fold serial dilutions. (B) Strains transformed with viable alleles of *BFR2* were selected on SDC+5-FOA and analyzed for their growth on YPD plates incubated at the temperatures indicated. (C) Biochemical analysis of proteins associated with different biogenesis factors in *bfr2*ΔC2 cells. Left panel: In the Δ*bfr2* shuffle strain background, the Kre33 module member Enp2 was genomically tagged with FLAG-TEV-ProtA at the

C-terminus. The bait protein w was purified from *BFR2* or *bfr2*ΔC2 cells grown either at 30℃ or shifted to 23℃ for 10h as indicated. Middle panel: A Δ*bfr2* shuffle strain was transformed with plasmids expressing Bfr2-FTpA or Bfr2ΔC2-FTpA. Bait proteins were purified from cell cultures grown at 30℃ or shifted to 23℃ for 10h. Right panel: The UTP-A module member Utp10 was genomically tagged with FLAG-TEV-ProtA at the C-terminus and purified from *BFR2* or *bfr2*ΔC2 cells.

in *bfr2*ΔC2 cells, the association of Enp2 with Bfr2ΔC2 and Lcp5 was strongly diminished (Figure 2.4C, left panel, lane 3 and 4). We analyzed the Bfr2ΔC2 protein further by isolating the full length and truncated version of Bfr2 from cells grown at 30˚C and 23˚C (Figure 2.4C, middle panel). At both temperatures, wt Bfr2 associated in stoichiometric amounts with its module partners (Figure 2.4C, middle panel, lane 1 and 2). However, the Bfr2ΔC2 protein pulled down sub-stoichiometric amounts of Kre33 and Enp2, while its association with Lcp5 did not differ from wt Bfr2 (Figure 2.4C, middle panel, lane 3 and 4). This points to an important role of the small C-terminal helix in Kre33 module assembly.

Next, we wanted to investigate 90S biogenesis and for that we isolated the UTP-A module member Utp10. In wt cells, Utp10 pulled down its module members (Figure 2.4C, right panel, lane 1 and 2), while 90S factors were co-purified in sub-stoichiometric amounts. There was no difference observed for the proteins isolated from cultures grown at 30˚C or 23˚C. Utp10 isolated from *bfr2*ΔC2 cells showed a stronger incorporation into the 90S particle as judged by the increased band intensity of the Coomassie staining for the factors Rrp5, Bms1, Utp22, Rrp9 and Utp14 and others which were not identified with mass spectrometry. The amount of Utp20 associated with Utp10, a factor which shows stoichiometric association with isolated 90S particles that are more mature, did not change significantly. Enp1, a factor present both in late 90S and in pre-40S particles, co-purified more 90S particles in *bfr2*ΔC2 cells (Supplemental Figure 5.4B), underscoring the fact that efficient 90S progression was affected in cells that lack the C-terminal helix of Bfr2.

Taken together, with our mutational approach, we were able to generate viable *ENP2* alleles which do not affect Kre33 module assembly. Moreover, we identified a small α-helix in Bfr2, which plays a crucial role for Kre33 module assembly.

2.2.2 Genetic relationship analysis of Kre33 module mutants reveals connection to Krr1 via Enp2

After generating and characterizing the mutants described in the previous section, we aimed to search for synergistic effects on growth and potentially 90S biogenesis and maturation by combining the *krr1*ΔC mutant with other, viable mutants of the Kre33 module members. At the same time, we wanted to analyze the genetic relationship between Kre33 module mutants. To address this, we generated double shuffle strains as described in the Methods section and transformed them with a combination of wt and mutant alleles described in section 2.1 and 2.2.1.

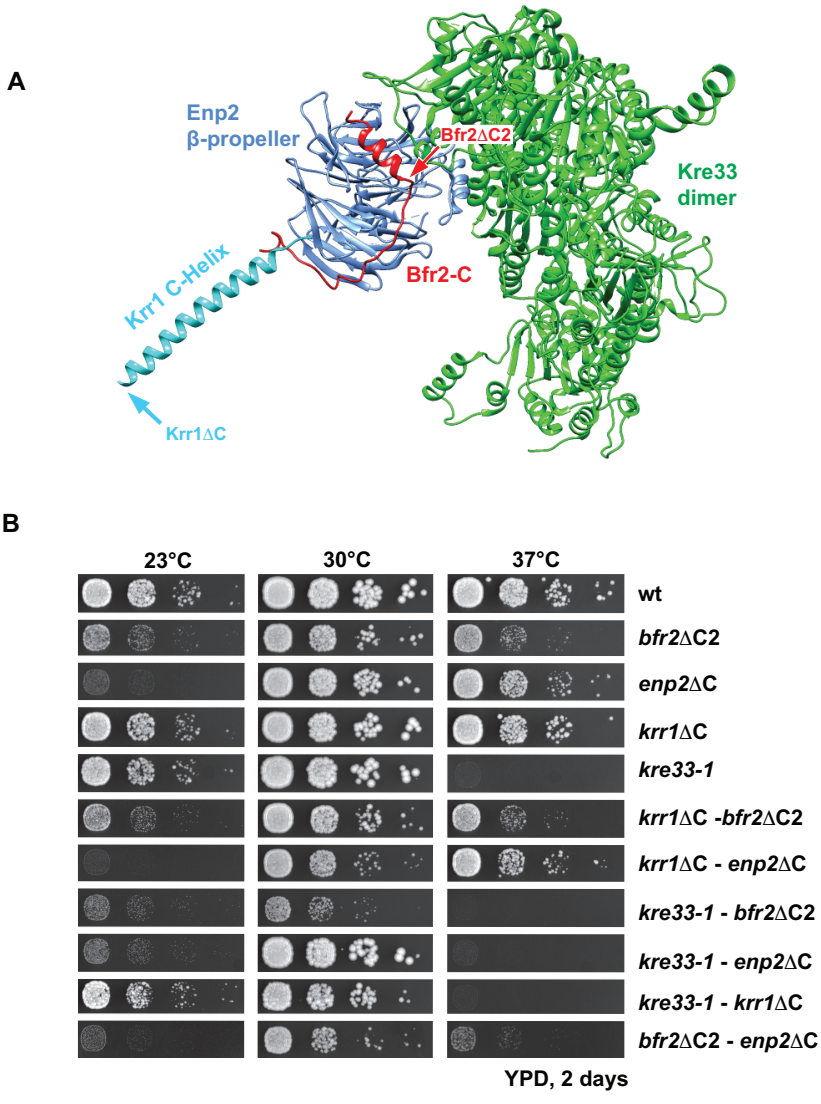


Figure 2.5 Genetic interactions show link of Krr1 to head region via the C-terminus of Enp2. (A) Cryo-EM structure (*sc*90S, state B2, PDB: 6zqB) depicts how Krr1 (cyan) contacts the composite surface of the C-terminal fragment of Bfr2 (red) with the ß-propeller of Enp2 (cornflower blue) which in turn both contact the Kre33 dimer (green). C-terminal truncations are highlighted whenever visible in the structure. (B) Double shuffle strains were transformed

with varying combinations of wt and mutant alleles created in the course of this study (alleles inserted into vectors pRS314 and pRS315 as well as strains are listed in the Methods section). Cells were selected on SDC+5-FOA, and plated on YPD in 10-fold serial dilutions and incubated for 2 days at the indicated temperatures.

The *bfr2*ΔN2 allele was omitted from this analysis, since the growth defect was very severe and yet we did not observe any biochemical difference in the 90S particles isolated. Within the Kre33 module, Bfr2 and Kre33 showed a genetic link in our analysis (Figure 2.5B). The combination of *kre33-1* and *bfr2*ΔC2 alleles showed a combined effect on growth when compared to either single mutant. The same was observed when *bfr2*ΔC2 was combined with the *enp2*ΔC allele, albeit to a lesser extent. No effect on growth was observed, when *enp2*ΔC was combined with *kre33-1*. Remarkably, when we combined the *krr1*ΔC and *enp2*ΔC mutants, we observed a synergistically enhanced growth phenotype: the double mutant strain grew slower at 30˚C and the growth defect was even more pronounced at 23˚C (Figure 2.6A, right panel). Such a combined effect on growth was neither observed between *krr1*ΔC and mutant alleles *bfr2*ΔC2 and *kre33-1*, nor between *enp2*ΔC and the other Kre33 module mutants suggesting an epistatic relationship between *enp2*ΔC and the *KRR1* allele.

2.2.3 Anchoring of Krr1's C-helix to the Kre33 module is crucial for cell growth when the C-terminus of Enp2 is missing

Having established a genetic relationship between the C-termini of Enp2 and Krr1, we wanted to understand the biochemical implications for 90S biogenesis. The C-terminus of Enp2 is not visible in our cryo-EM structures, but we looked closer at the interface of Krr1, Bfr2 and Enp2 (Figure 2.6A). In the cryo-EM model of *sc*90S in state B2, the C-terminus of Krr1 is resolved until E307, which is situated in close proximity to a positively charged arginine R171 within a loop of the Enp2 ß-propeller. Moreover, the aromatic phenylalanine F303 is in the vicinity of another aromatic amino acid, tyrosine Y466, which is part of the unstructured Bfr2-C region.

The helix tip of Krr1's C-helix is highly conserved, with a proline marking the helix end and a subsequent negatively charged glutamate. In yeast, two glutamates follow the helix breaker proline, and the negative charge is conserved in fungi and plants. We tested additional C-helix mutants on their ability to cause a pronounced growth defect in *enp2*ΔC cells. For this, we progressively shortened the helix tip (see Figure 2.1B for sequence alignment, conservation and indicated truncations, and

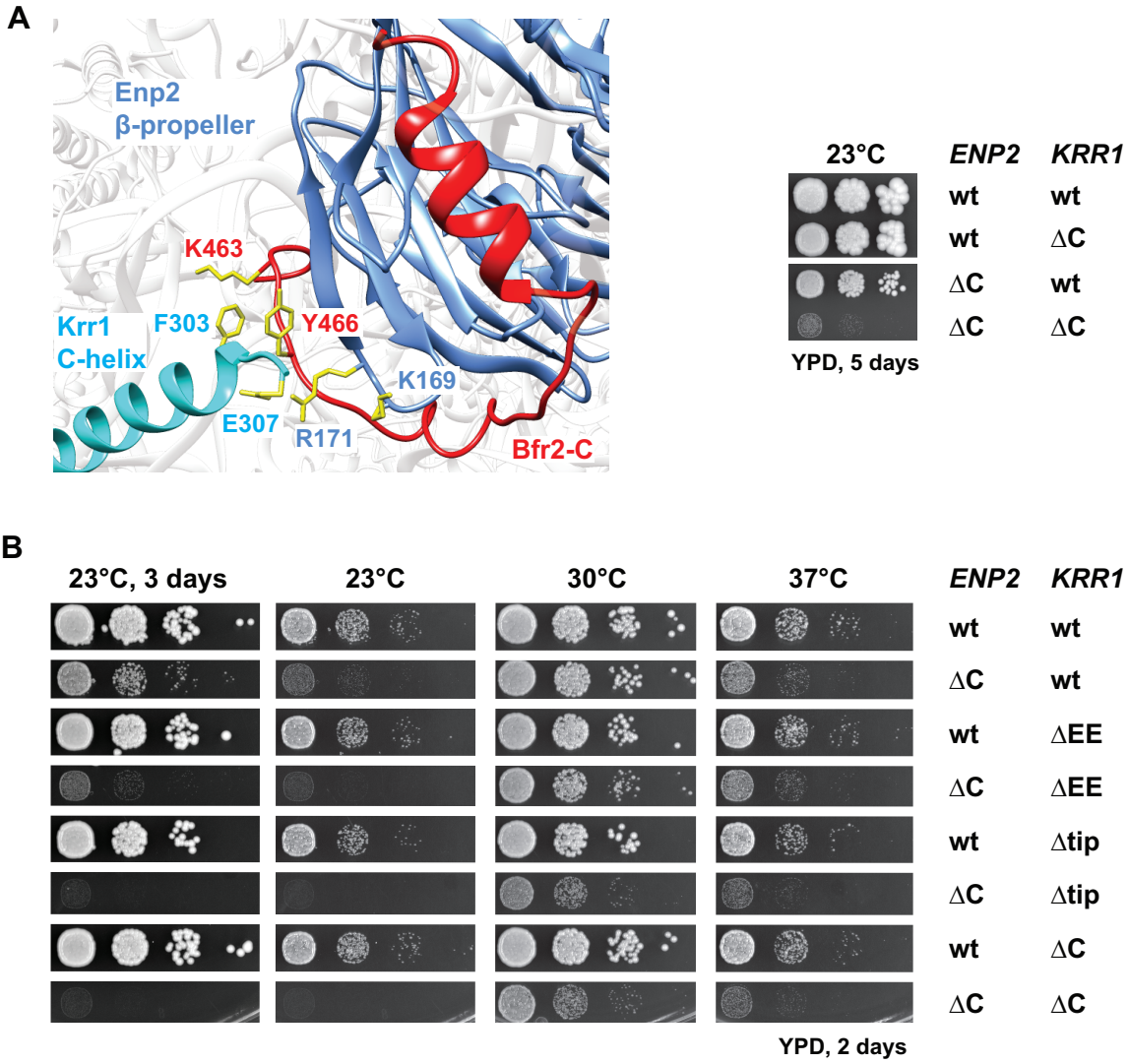


Figure 2.6 Enp2 C-terminus is linked to Krr1 via Krr1's helix tip which points to the interface between the C-terminus of Bfr2 and Enp2's ß-propeller. (A) Cryo-EM structure (*sc*90S, state B2, PDB: 6zqB) of Krr1 C-helix and its tip (cyan) contacting the C-terminal fragment of Bfr2 (red, Bfr2-C) and the ß-propeller of Enp2 (cornflower blue). Critical amino acids are shown with atom bonds and are colored accordingly. (B) Double shuffle strain Δ*enp2*Δ*krr1* was transformed with varying combinations of wt and mutant alleles of *KRR1* and *ENP2* (alleles inserted into vectors pRS314 and pRS315 as well as strains are listed in the Methods section). Cells were selected on SDC+5-FOA, and plated on YPD in 10-fold serial dilutions and incubated for 2 days at the indicated temperatures.

Figure 2.2 for structural depiction and growth analysis of mutants). *krr1*ΔC0 does not cause a growth defect on its own nor in combination with *enp2*ΔC (not shown). C-terminal deletions including the helix tip did not influence growth at any temperatures tested (Figure 2.6B), just as a deletion including the whole C-helix did not cause a growth defect. We observed that a C-terminal deletion including the two negatively charged amino acids (*krr1*ΔEE) caused a pronounced growth defect when combined

with *enp2*ΔC. However, the synergistic growth defect did not reach the severity of the *krr1*ΔC *enp2*ΔC allele combination. Interestingly, in *enp2*ΔC cells, deletion of the helix tip (*krr1*Δtip, including the highly conserved F303) caused a growth defect similar to the deletion of the whole C-helix indicating that proper anchoring of Krr1's C-helix is important in *enp2*ΔC cells.

We wanted to understand the observed phenotype better in terms of ribosome biogenesis defects and hence chose to purify 90S AFs in order to monitor 90S assembly and progression of maturation. We chose the UTP-A module member Utp10 as an early 90S biogenesis factor that showed a slightly increased incorporation into the 90S particle in *enp2*ΔC cells (Figure 2.3B, middle panel, lane 3 and 4) and no significant difference of isolated proteins when purified form *krr1*ΔC cells (Figure 2.7A, left panel, lane 1 and 2). Strikingly, when Utp10 was purified from *krr1*ΔC *enp2*ΔC double mutant cells at the restrictive temperature, it was mainly found associated with its cognate UTP-A module members (Figure 2.7A, left panel, lane 4) while other 90S biogenesis factors were dramatically decreased. Next, we asked whether the observed gradual increasing synergistic effects on growth in *enp2*ΔC cells with progressive C-terminal deletions of Krr1 can be mirrored in the composition of proteins isolated with Utp10. For that, we wanted to monitor Utp10 association with the 90S particle in *enp2*ΔC cells when the negatively charged glutamates (*krr1*ΔEE) or the whole helix tip was missing (*krr1*Δtip). While Utp10 isolated from *krr1*ΔEE *enp2*ΔC cells showed similar quantities of proteins isolated compared to wt cells (Figure 2.7A, right panel, lane 3 and 4), deletion of the helix tip caused a decreased association with 90S factors (Figure 2.7A, right panel, lane 5 and 6), similar to the effect caused by deletion of the whole C-helix (Figure 2.7A, right panel, lane 7 and 8). Note that in this preparation, more material was loaded (final FLAG eluate corresponding to 1500 OD_{600} of YPD cell culture) compared to the preparation in the left panel of Figure 2.7A (final FLAG eluate corresponding to 750 OD_{600} of YPD cell culture) which is why the loss of 90S biogenesis factors appears less dramatic. Further analysis was performed with the *krr1*ΔC *enp2*ΔC allele combination. Another 90S biogenesis factor which can be isolated from wt cells mostly in its free form is UTP-C module member Utp22 (Figure 2.7B, lane 1 and 2). When purified from *enp2*ΔC or *krr1*ΔC *enp2*ΔC cells at the restrictive temperature, Utp22 pulled down an increased amount of 90S particles and lost association with its CURI complex member Ifh1 (Figure 2.7B, left panel, lane 4 and

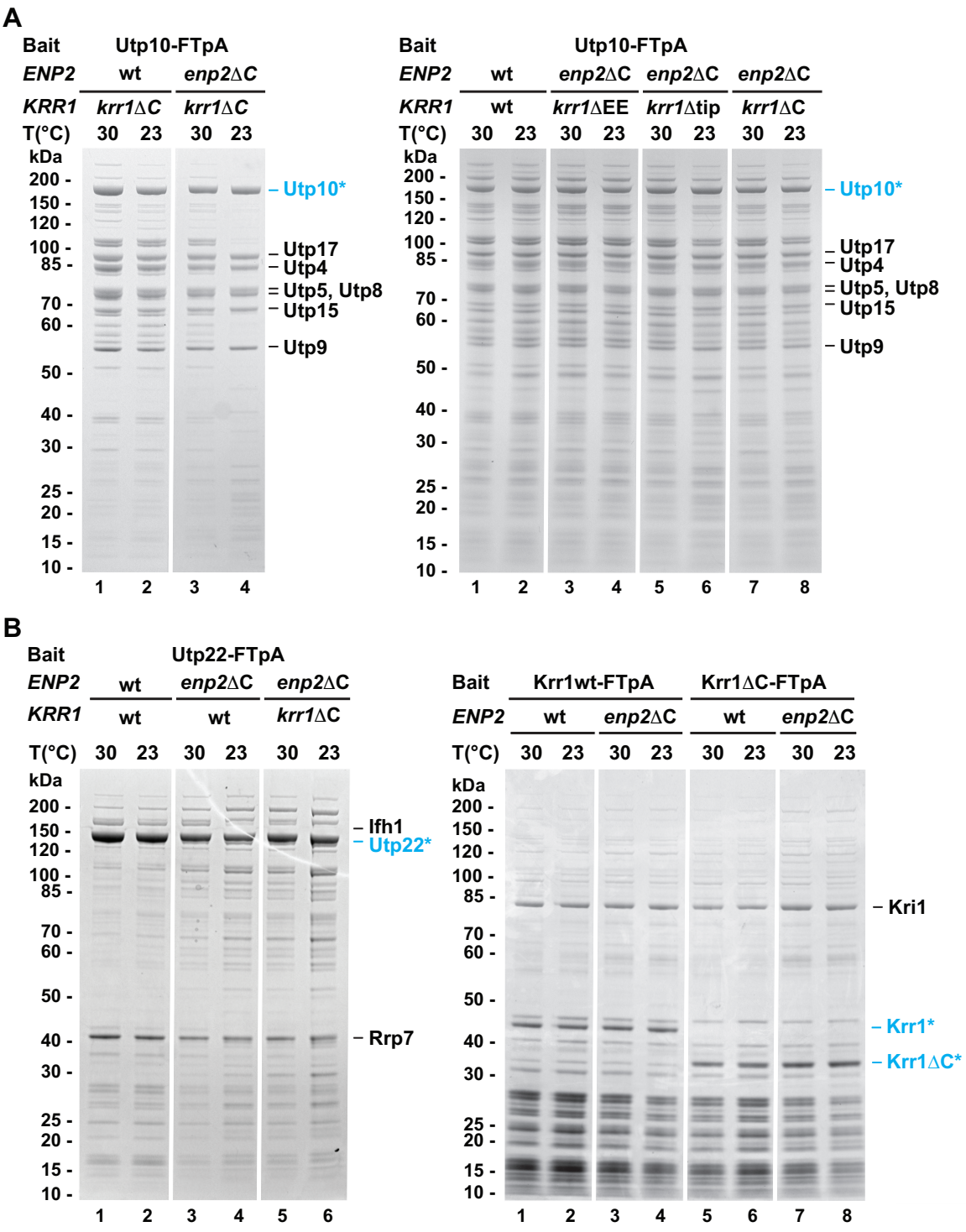


Figure 2.7 Deletion of the C-terminus of Krr1 and Enp2 has an effect on 90S formation and maturation. (A) Left panel: The UTP-A factor Utp10 was genomically tagged with FLAG-TEV-ProtA in a Δ*krr1* shuffle strain at the C-terminus and purified from *krr1*ΔC *ENP2* or *krr1*ΔC *enp2*ΔC cells grown at the indicated temperatures. Right panel: Utp10 was genomically tagged with FLAG-TEV-ProtA in a Δ*krr1*Δ*enp2* double shuffle strain at the C-terminus and purified from wt, *krr1*ΔEE *enp2*ΔC, *krr1*Δtip *enp2*ΔC or *krr1*ΔC *enp2*ΔC cells grown at the indicated temperatures. (B) Left panel: The UTP-C factor Utp22 was genomically tagged with FLAG-TEV-ProtA in a Δ*krr1* shuffle strain at the C-terminus and purified from *krr1*ΔC *ENP2* or *krr1*ΔC *enp2*ΔC cells grown at the indicated temperatures. Right panel: A Δ*krr1*Δ*enp2* double shuffle

strain was transformed with pRS315-Krr1-FTpA or pRS315-Krr1ΔC-FTpA and the Krr1 or Krr1ΔC proteins were affinity purified from *ENP2* or *enp2*ΔC cells. Bait proteins are highlighted in blue and protein bands identified by mass spectrometry are indicated.

6), suggesting that 90S progression is stalled at a certain stage in these particles (Albert et al., 2016). Compared to wt cells, an increased association of 90S biogenesis factors, albeit less dramatic, was also observed when Krr1ΔC was purified from *enp2*ΔC cells (Figure 2.7B, right panel, lane 7 and 8 compared to lane 5 and 6), or compared to Krr1 isolated from either background (Figure 2.7B, right panel, lane 1 to 4). Krr1ΔC was still able to associate with its binding partner Kri1, showing that the observed defect was unlikely to be based in Krr1's recruitment or assembly into the 90S. Taken together, the genetic analysis combined with biochemical investigation of 90S pre-ribosomes from mutant cells revealed that 90S biogenesis is disturbed when Krr1's and Enp2's C-termini are missing. Furthermore, anchoring Krr1's C-helix to the Kre33 module at the Bfr2-Enp2 interface is crucial in cells where the C-terminus of Enp2 is missing.

2.3 Krr1 C-terminus has an important role in contributing to the organization of the central domain in the 90S particle

In our mutational analysis (Figure 2.2, right panel), we saw that C-terminal deletions beyond the C-helix of Krr1 caused a growth defect (*krr1*ΔC2) or were lethal (*krr1*ΔPro). This essential region of Krr1 is visible in the cryo-EM structure in the body of the *sc*90S particle, where many helices of the 18S rRNA central domain meet (Figure 2.8A, upper panel). Especially the proline-rich part of Krr1 is close to two α-helices of RpS13 (Figure 2.8B, upper panel), which in turn is contacted by Rrp7 through a small, C-terminal α-helical structure (Figure 2.8B, lower panel).

To investigate the role of this flexible region in the Krr1 C-terminus in the maturation of the central domain, we tested whether overexpression of the lethal *krr1*ΔPro mutant caused a growth defect in cells with a chromosomal *KRR1* allele. Indeed, when placed under the inducible *GAL10* promoter, *krr1*ΔPro resulted in an enhanced growth defect when compared to cells carrying an empty plasmid or overexpressing the wt Krr1 protein (Figure 2.8B, lower panel). This assay allowed us to further analyze the *krr1*ΔPro mutant biochemically by isolating different pre-ribosomal particles via FTpA-tagged biogenesis factors from cultures, where overexpression of Krr1ΔPro was induced by adding 2% galactose to the growth

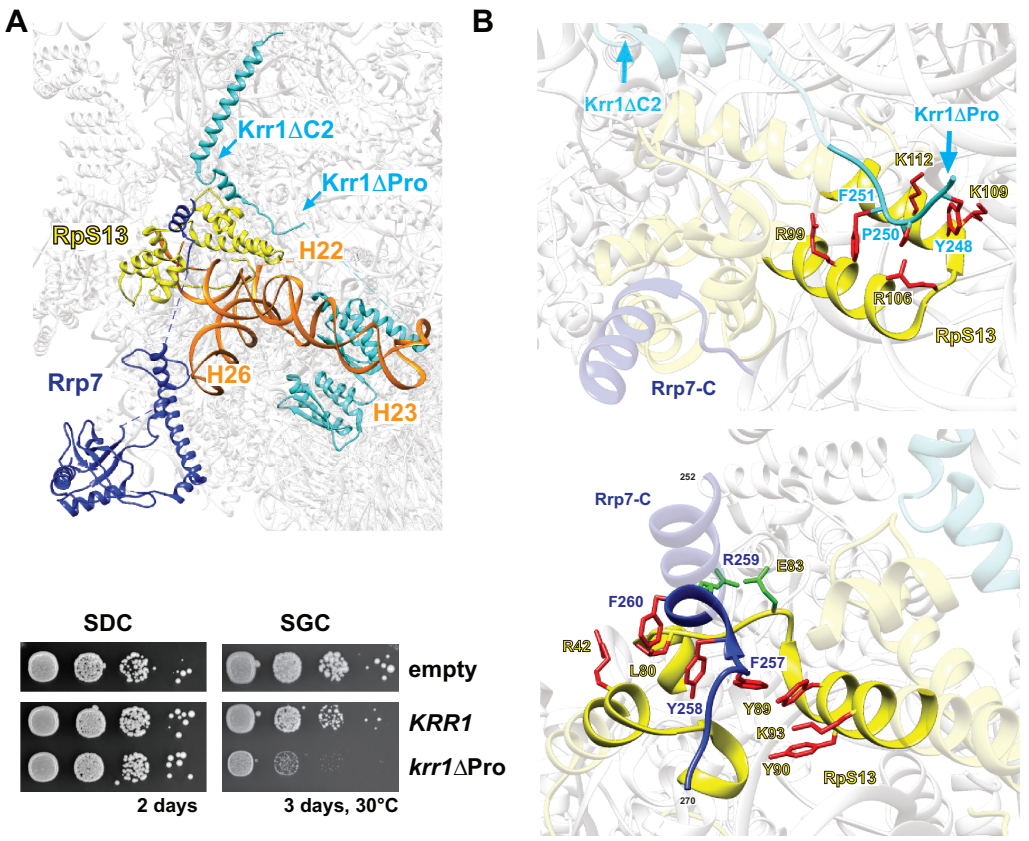


Figure 2.8 Region between Krr1's KH1 domain and its C-helix is important for stabilization of the central platform domain. (A) Upper panel: Cryo-EM structure (*sc*90S, state B2, PDB:6zqB) showing how Krr1 (cyan) contacts helical elements of RpS13 (yellow) which in turn interacts with a small alpha-helical element of Rrp7 (blue). rRNA helices H22, H23 and H26 of the central domain 18S rRNA are shown in orange. The lethal deletion mutant *krr1*ΔPro and the viable *krr1*ΔC2 mutant are marked with an arrow. Lower panel: Wt cells were transformed with an empty plasmid or 2µ plasmids containing the *KRR1* or *krr1*ΔPro allele under the control of the inducible GAL promoter. Cells were plated in 10-fold serial dilutions on either SDC or SGC plates containing 2% galactose for gene induction. Plates were incubated at 30℃ and photographs were taken after the indicated period of time. (B) Zoom into the interaction between Krr1, RpS13 and Rrp7 as seen in *sc*90S state B2 (PDB:6zqB). Krr1 is depicted in cyan, RpS13 in yellow and Rrp7 in blue. Amino acid residues are shown with atom bonds and their labels have the same color code. Atom bonds of amino acid residues involved in potential aromatic interactions or ion pair formation are colored in red and green, respectively. Upper panel: Krr1 contacts two α-helices of RpS13 via its proline-rich region. Lower panel: RpS13 anchors the C-terminus of Rrp7.

medium. Strikingly, when we isolated intermediate to late 90S AF Noc4, we found a significant decrease of Rrp5 and UTP-C module member Utp22 in cells where *krr1*ΔPro was overexpressed (Figure 2.9A, upper panel, lane 3 and 4, and lower panel for zoom into high molecular region). We were able to identify Krr1ΔPro in this preparation by mass spectrometry, indicating that incorporation of the shortened

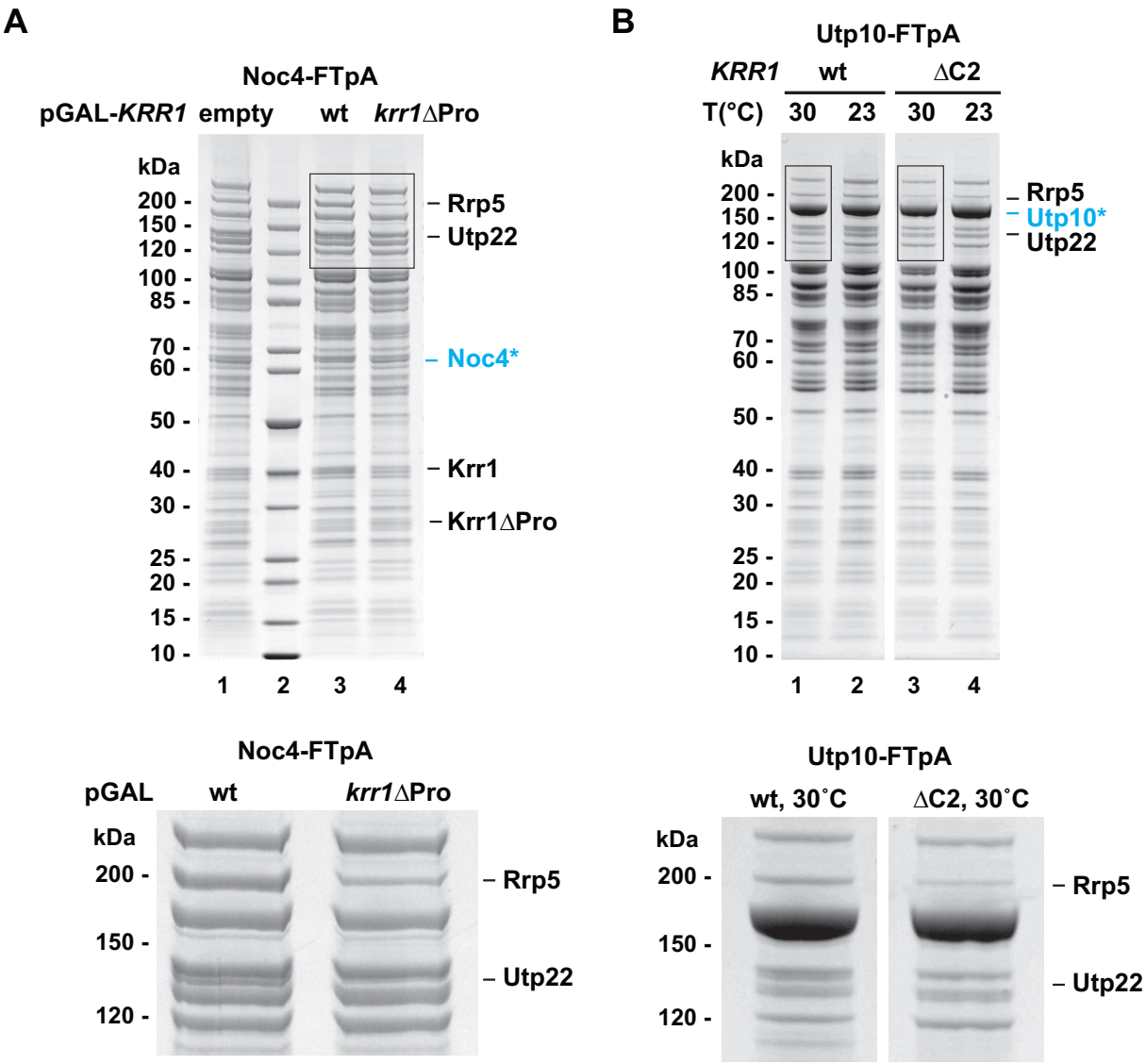


Figure 2.9 Mutations of Krr1 within the region contacting the central domain lead to depletion of Rrp5 and Utp22. (A) Upper panel: The middle to late 90S factor Noc4 was tagged genomically at the C-terminus with the FLAG-TEV-ProtA epitope and transformed with and empty plasmid or a plasmid expressing *KRR1* or *krr1*ΔPro under the control of the GAL promoter. The bait protein is highlighted in blue and protein bands identified with mass spectrometry are indicated. The black box indicates the gel region shown with a zoom in the lower panel. Lower panel: Zoom of gel region highlighted in the upper panel to better display the depletion of Rrp5 and Utp22. (B) Upper panel: The UTP-A factor Utp10 was genomically tagged with FLAG-TEV-ProtA at the C-terminus and purified from *KRR1* or *krr1*ΔC2 cells at the temperatures indicated. The bait protein is highlighted in blue and protein bands identified with mass spectrometry are indicated. The black box indicates the gel region shown with a zoom in the lower panel. Lower panel: Zoom of gel region from lane one and 3 highlighted in the upper panel to better visualize depletion of Rrp5 and Utp22.

protein in 90S particles is causing the growth defect observed upon overexpression of the *krr1*ΔPro allele. Moreover, Rrp5 and the UTP-C module are both associated with the central domain, indicating a role for Krr1's unstructured region in the assembly

events of this 18S rRNA subdomain. Similarly, *krr1*ΔC2 caused a visible depletion of Rrp5 and Utp22 when 90S AF Utp10 was affinity-purified (Figure 2.9B, upper panel, lane 3 and 4, and lower panel for zoom into high molecular region). To get more information on changes of the particle composition upon overexpression of the lethal *krr1*ΔPro allele or expression of the viable but phenotype inducing *krr1*ΔC2 allele, we analyzed the affinity-purified pre-ribosomal particles isolated via bait proteins Noc4 and Utp10 by semi-quantitative mass spectrometry (semiQ-MS). We were able to confirm that Utp22 and with it the UTP-C module were depleted upon *krr1*ΔPro overexpression or when *krr1*ΔC2 is expressed as the only Krr1 version in the cell (≥5fold reduction). Moreover, in all preparations, components of the nuclear exosome were less abundant, while other prominent 90S modules like UTP-A or UTP-B were not significantly changed (Supplemental Figure 5.5, left panel). Additionally, Rrp5 and its binding partners Rok1 and Noc2 were strongly depleted in all three samples (Supplemental Figure 5.5, right panel). The depletion of Rrp5 was visible by Coomassie staining of the SDS-PAGE gel, but since Rok1 is migrating at the same height as AF Utp7, this reduction was only uncovered following semiQ-MS analysis.

Taken together, the biochemical analysis of 90S particles isolated from cells, where most of Krr1's conserved C-terminus is missing, revealed its importance for the association of AFs with the central domain.

2.4 Krr1's KH domains have functions beyond acting as placeholder for Pno1

In a recent study by our lab, Krr1 was shown to function as placeholder for Pno1 as both factors share highly similar KH domains. It was further described in the literature, that the KH domains are needed for interaction with the AF Kri1, RpS14 and Faf1 (see Introduction). While Kri1 was not yet visualized in 90S pre-ribosomes by cryo-EM, the two KH domains of Krr1 were shown to be clamped between AFs and r-proteins of the small subunit, with KH domain 1 (KH1) interacting with RpS14 and RpS1 while Faf1 was shown interacting with KH domain 2 (KH2) on the opposite side. In our recent structures, we noticed a potential interaction of KH1 with a C-terminal region of Utp7 via two loops contacting each other and thereby establishing a ß-sheet-type interaction (Figure 2.10A, left panel). Utp7 is as a WD40 containing AF and is, together with Sof1 and Utp14, strategically placed between the UTP-A and UTP-B modules as part of the

90S base. In the vicinity of this contact, both Krr1 and especially one small α-helix of the Utp7 C-terminus, termed helix2 here, are intertwined with H7 of the 5'ETS rRNA. The interaction of Krr1 and Utp7 occurs in a conserved region of Krr1's KH1 (Supplemental Figure 5.1) and a less conserved region of Utp7 (not shown), with hydrophobic residues surrounding negatively charged aspartates (Figure 2.10A, right panel).

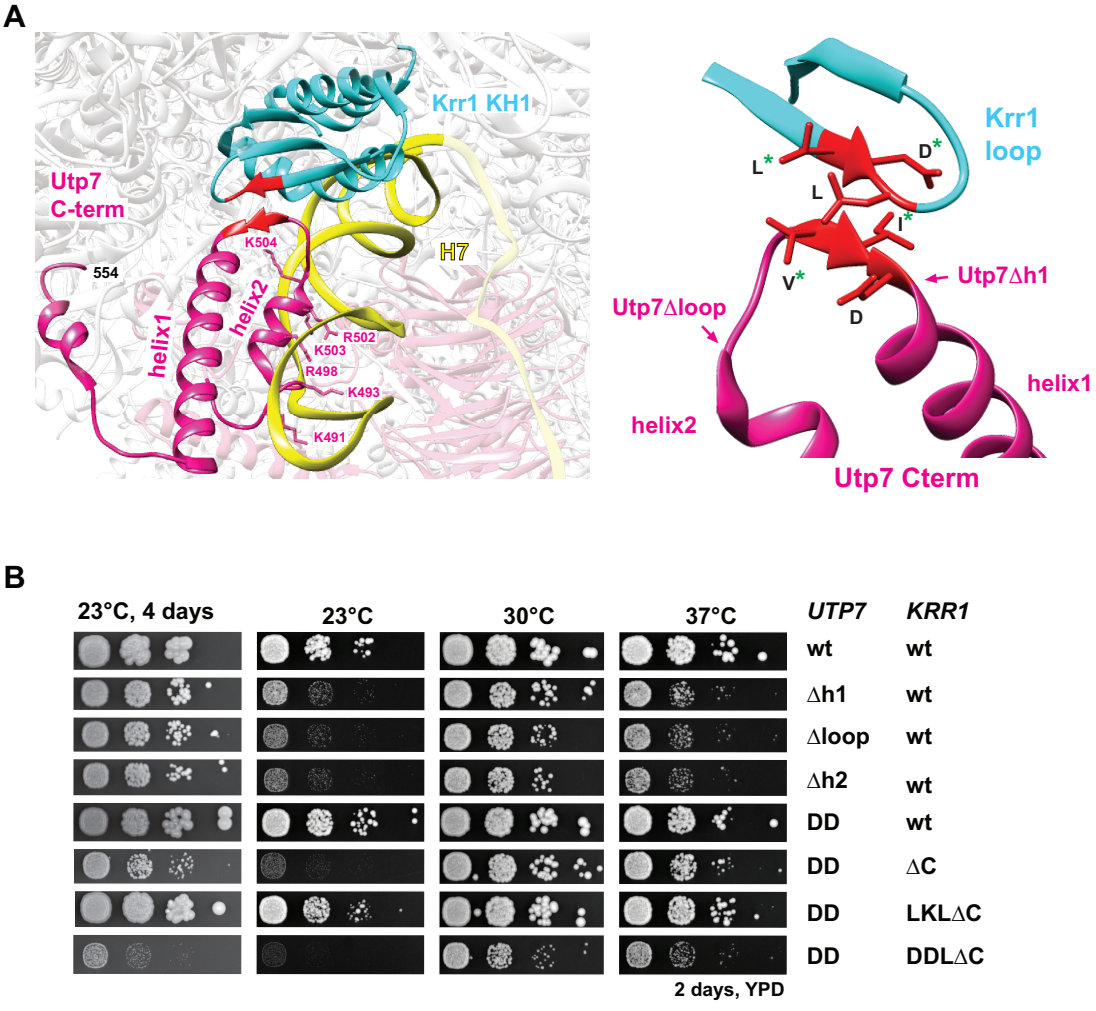


Figure 2.10 Krr1 KH domain 1 is genetically linked to Utp7 via a loop-loop interaction. (A) Left panel: Cryo-EM structure (*sc*90S, state B2, PDB:6zqB) displaying how Utp7 (deep pink) interacts via its C-terminus with h7 of the 5'ETS (yellow) and one of the KH domains of Krr1 (cyan). Loop regions involved in the Krr1-Utp7 interaction are highlighted in red. Right panel: Zoom of the loop-loop interaction with critical amino acids displayed with atom bonds. Labeled amino acids are highlighted with a green asterisk when mutated in genetic analysis in (B). C-terminal truncation mutants of Utp7 are marked with an arrow. (B) Genetic analysis of Utp7 and Krr1 mutants affecting loop-loop interaction. A double shuffle Δ*krr1*Δ*utp7* strain was transformed with different combinations of wt and mutant alleles as indicated. Cells were selected on SDC+5-FOA and plated in 10-fold serial dilutions on YPD plates. Plates were incubated at the indicated temperatures for the indicated period of time until photographs were taken.

This contact site places Krr1 in a strategic position connecting the head region via the Kre33 module to the base region via Utp7 which in turn is positioned between the UTP-A and UTP-B modules. Hence, we wanted to test whether the Krr1-Utp7 interaction contributes to 90S biogenesis and if or under which circumstances this interaction is of particular importance for 90S maturation. For this, we generated point mutations at the contact sites of Krr1 and Utp7 as well as C-terminal truncation mutants of Utp7 (Figure 2.10A, right panel).

Deletions of helix1 (*utp7*Δh1) slowed growth at all temperatures tested. This observed growth defect was exacerbated with further deletions including the loop region (*utp7*Δloop) or helix2 (*utp7*Δh2), both showing similarly reduced growth rates (Figure 2.10B). This indicates that the helix-loop-helix arrangement in the C-terminus of Utp7 is important for ribosome biogenesis. We ruled out decreased protein stability of the truncated versions because when we isolated Noc4-FpA from *utp7*Δh1 or *utp7*Δloop cells, a Coomassie stainable band appeared around the expected size indicating that truncated Utp7 is incorporated into the 90S particle (see next section, Figure 2.12A, right panel). While the *utp7*Δloop and *utp7*Δh2 truncations both abolish the contact site to Krr1, in *utp7*Δh2 cells additionally the interaction with the 5'ETS rRNA is missing. In order to specifically disrupt the loop-loop interaction between Krr1 and Utp7, we introduced point mutations in the amino acid sequence of each loop (marked with a green asterisk in Figure 2.10A, right panel). First, we mutated the Utp7 loop by introducing more negative charge instead of the hydrophobic amino acids (*utp7*DD). This change likely contributes to a repulsive electrostatic force between the mutated Utp7 loop and the aspartate in the Krr1 loop. However, no effect on growth was observed for this mutant indicating that destabilization of this contact site alone was not sufficient to dramatically alter the course of ribosome biogenesis.

However, when combined with the *krr1*ΔC mutant, where the long C-helix of Krr1 pointing to the Kre33 module is missing, we observed a strong growth defect especially at 23˚C (Figure 2.10B). Changing the aspartate in the loop of the Krr1ΔC protein into a positively charged lysine (*krr1* LKLΔC) reverses the quality of the electrostatic forces from repulsion to attraction. We were able to obtain a phenotypic reversion of the *utp7*DD mutant by the introduction of this second-site mutation. In agreement with this observation, the introduction of more negative charge in the loop of the Krr1ΔC protein (*krr1* DDLΔC) dramatically enhanced the growth defect, especially at 23˚C, where cells grew extremely slow.

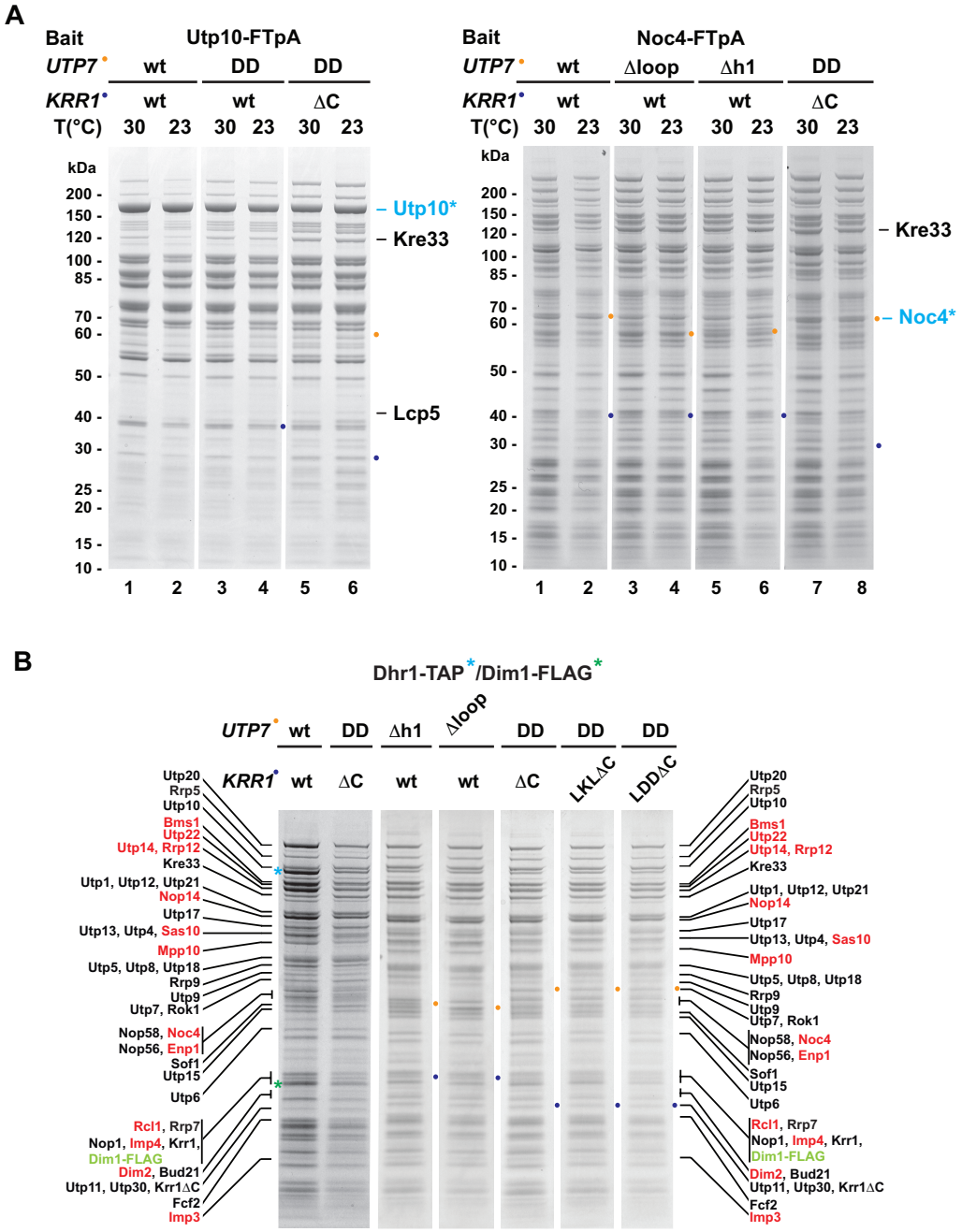


Figure 2.11 Mutations in the Krr1-Utp7 contact site cause defects in the progression of 90S maturation in *krr1*ΔC background. (A) Left panel: The UTP-A factor Utp10 was genomically tagged with FLAG-TEV-ProtA at the C-terminus in a Δ*krr1*Δ*utp7* shuffle strain and purified from cells expressing the indicated alleles at 30 ℃ or 23 ℃. Right panel: The AF Noc4 was genomically tagged with FLAG-TEV-ProtA at the C-terminus in a Δ*krr1*Δ*utp7* shuffle strain and purified from cells expressing the indicated alleles at 30 ℃ or 23 ℃. The bait protein is highlighted in blue and protein bands identified with mass spectrometry are labeled. Orange circles show where wt and mutant Utp7 migrate in the SDS-PAGE, violet circles indicate where wt and mutant Krr1 migrate. (B) Dhr1 and Dim1 were genomically tagged in a Δ*krr1*Δ*utp7* shuffle strain at the C-terminus with the TAP and FLAG-tag, respectively. Particles were purified from cells expressing the indicated alleles at 30 ℃.

Taken together, while the loop-loop interaction between Utp7 and Krr1 is dispensable for growth in wt cells, it becomes important when the interaction of Krr1 with the Kre33 module is disturbed, for example in cells where the C-helix of Krr1 is missing. Likewise, either C-terminal deletion of Utp7 (*utp7* ∆h1/∆loop/∆h2) is not compatible with life when combined with either mutation in the C-terminal helix of Krr1 (not shown). This genetic data points to an important relationship between the C-termini of the two proteins as well as to a functionally important connection between the head and base region of the 90S.

The intriguing connection between the base of the 90S particle and the Kre33 module in the head region mediated through Krr1 prompted us to analyze the composition of 90S pre-ribosomes affinity-purified via different AFs. We isolated FTpA-tagged Utp10 as an early 90S AF (Figure 2.11). The *utp7*DD mutant alone did not cause a significant difference in protein composition of associated factors in the Utp10-FTpA Flag eluate (Figure 2.11A left panel, lane 3 and 4 compared to lane 1 and 2). Interestingly, the combined disruption of the contact site between Krr1 and Utp7 and Krr1 and the Kre33 module in the double mutant *utp7*DD *krr1*∆C resulted in an increased association between the bait protein and typical 90S factors (Figure 2.11A, left panel, lane 5 and 6). Especially the increased amounts of Kre33 and Lcp5, which is otherwise not visible in the Coomassie staining, stood out, indicating that the Kre33 module is enriched in this preparation.

Next, we wanted to find out whether Noc4 as intermediate AF would give further evidence on potential 90S maturation problems in the double mutant cells. Here, we purified the bait protein from different mutant cells, including C-terminal truncations of Utp7 introduced in Figure 10B (Figure 2.11A, right panel). Again, we saw a strong accumulation of Kre33 on the 90S particles. We also analyzed the Noc4-FTpA preparation from different mutant backgrounds with semiQ-MS, confirming the enrichment of the Kre33 module (Supplemental Figure 5.6, right panel). Moreover, semiQ-MS analysis showed that Noc4 is incorporated more efficiently into the 90S particle as all classic 90S modules are enriched in *utp7*∆h1, *utp7*∆loop and *utp7*DD *krr1*∆C cells. For the transition of 90S to pre-40S, the Kre33 module needs to be released, while in later steps Dhr1 removes the U3 snoRNP (J. Cheng et al., 2020; Sardana et al., 2015), indicating that in our mutant background Kre33 is not efficiently removed and hence later 90S biogenesis steps and the 90S to pre-40S transition is affected. To test this, we purified particles via Dhr1-TAP/Dim1-FLAG

(Dhr1/Dim1 particle). This split-bait approach allows us to isolate late 90S and early pre-40S particles and several states in between (J. Cheng et al., 2020). Indeed, the disruption of the Kre33-Krr1-Utp7 connection lead to a decrease of pre-40S factors (Figure 2.11B, highlighted in red). Moreover, an accumulation of Kre33 was observed compared to wt cells, again supporting the notion that in these mutants, stages in the 90S maturation pathway accumulated, in which the Kre33 module cannot be released.

To understand the defect in the 90S to pre-40S transition in greater detail, we wanted to find out if pre-rRNA processing was affected in cells lacking the C-terminus of Utp7 or the Utp7-Krr1-Kre33 module link. For that, we isolated RNA from the Dhr1/Dim1 particle purified from wt and mutant cells and analyzed the rRNA species by Northern hybridization (Figure 2.12).

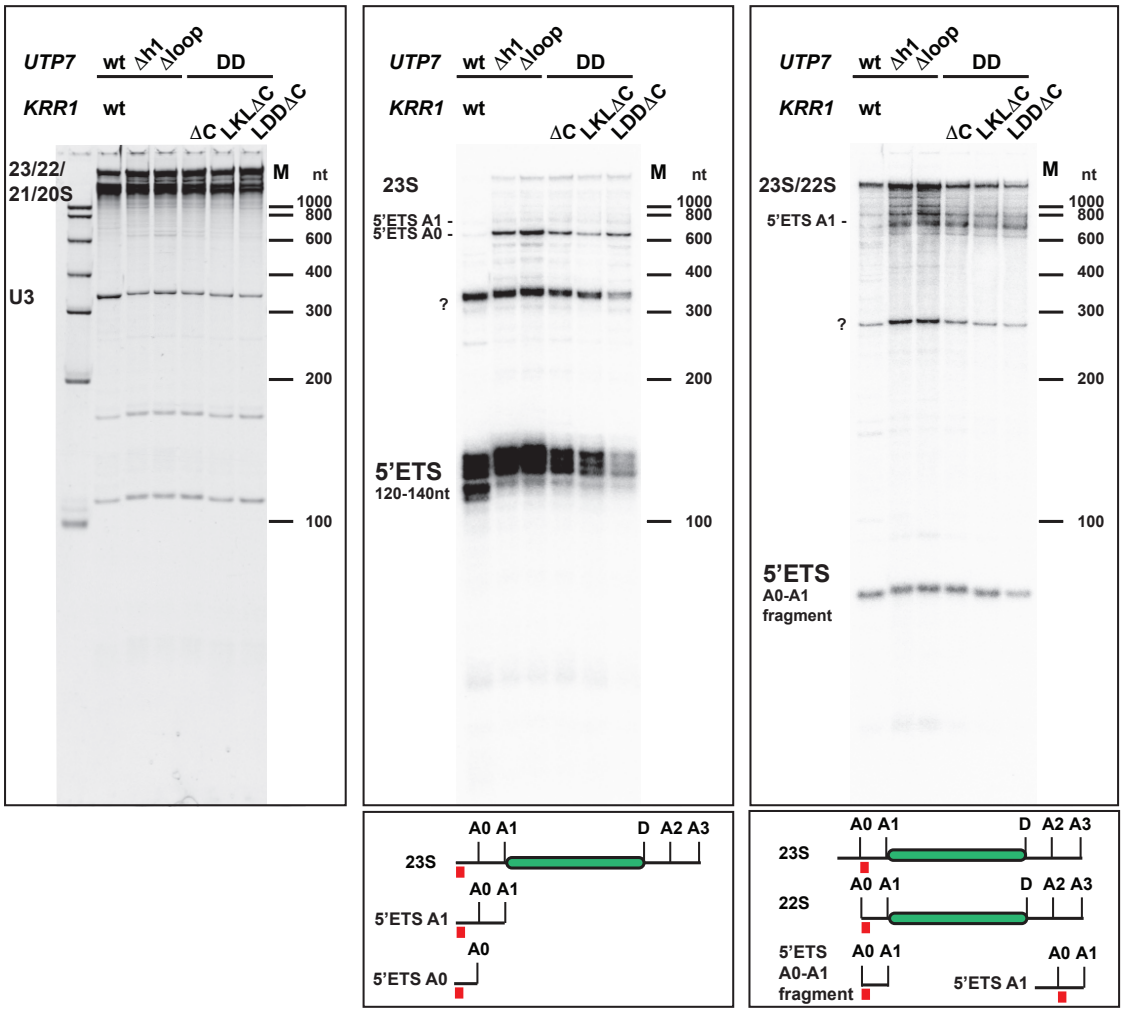


Figure 2.12 Mutations in the Krr1-Utp7 contact site lead to defects in A_1 processing of the 35S pre-rRNA in *krr1*ΔC background. Northern blot analysis of rRNA species purified via split-tag particles Dhr1-TAP/Dim1-FLAG. RNA was extracted from particles isolated via the bait proteins from cells grown at 30 ℃ and expressing the indicated alleles of KRR1 and UTP7. 0.7µg RNA was separated on an 8% acrylamide gel and blotted on nylon membrane subsequent incubation of the probes indicated in the box below the autoradiograph. Note that

for the last two lanes (utp7DD combined with krr1 LKLΔC or krr1 LDDΔC), less RNA was loaded because of an error in the measurement of RNA concentration which makes absolute quantitative statements about the rRNA species difficult. Left panel: Cybr green staining of 8% acrylamide gel. Middle panel: Autoradiograph of the membrane incubated with a probe hybridizing upstream of the A_0 cleavage site. Right panel: Autoradiograph of the membrane incubated with a probe hybridizing downstream of the A_0 cleavage site.

Compared to wt cells, SYBR green staining showed a decreased amount of U3 snoRNA in Dhr1/Dim1 particles from mutant cells (Figure 2.12, left panel). This finding was in line with the reduced amount of early pre-40S factors associated with the Dhr1/Dim1 particle (Figure 2.11B), because the reduced early pre-40S pool decreases the overall amount of U3 snoRNA in the preparation (J. Cheng et al., 2020). To identify pre-rRNA species linked to A_1 cleavage, we used two probes hybridizing either upstream or downstream of the A_0 processing site as described before (Figure 2.12, lower panel) (J. Cheng et al., 2020). The probe hybridizing to the 5'ETS region upstream of the A_0 cleavage site gave a very faint signal in the RNA sample isolated from wt Dhr1/Dim1 particles. In all mutant cells, the signal for the 5'ETS A_0 fragment was strongly increased, with particles isolated from *utp7*Δloop cells giving the strongest signal (Figure 2.12, middle panel). Moreover, a signal corresponding to 23S rRNA could be detected in the mutant cells, suggesting either an increased accumulation or a slower processing of this rRNA species. The 5'ETS 120-140nt fragment consists of 4 bands and is probably a degradation product produced during ribosome biogenesis and still attached to the 90S particle. Compared to the particle isolated from wt cells, the lowest band is strongly decreased, while the three upper bands were detected with increased or wt intensity. The significance of this finding is unclear since this pre-rRNA fragment is not well defined yet.

When we used a probe hybridizing in the 5'ETS downstream of the A_0 cleavage site, we detected the 23S/22S rRNA species in all particles isolated. Compared to particles isolated from wt cells, the preparations from cells expressing Utp7 truncations (Utp7Δh1 and Utp7Δloop) contained an increased amount of this rRNA species. Moreover, the 5'ETS A_0-A_1 fragment could be detected in all particles, with no significant difference in intensity. These findings suggest that cleavage at A_1 is delayed because an increased amount of 23S/22S should result in an increased amount of 5'ETS A_0-A_1 fragment (Figure 2.12, right panel).

Taken together, the biochemical analysis of the genetic connection between Krr1 and Utp7 indicate a link between release of the Kre33 module, rearrangements leading to A_1 cleavage and the transition of 90S particles to pre-40S particles.

3. Discussion

Assigning the exact roles to the many different AFs involved in ribosome biogenesis has been a tedious task in the past. It started with isolation of mutants causing pre-rRNA processing and ribosome biogenesis defects several decades ago and, recently, culminated in a vast number of structural data obtained by cryo-EM. With my PhD study, I could contribute to a better understanding of the role of the AF Krr1 during early ribosome biogenesis. Krr1 has no enzymatic activity, but structural elements contacting multiple domains of the 90S pre-ribosome revealed an importance for different steps of 90S biogenesis. Thus, Krr1 could act as AF which senses, conveys and possibly helps to integrate information about maturation states of distant domains in the 90S pre-ribosome, ultimately leading to A_1 processing (Figure 3.1).

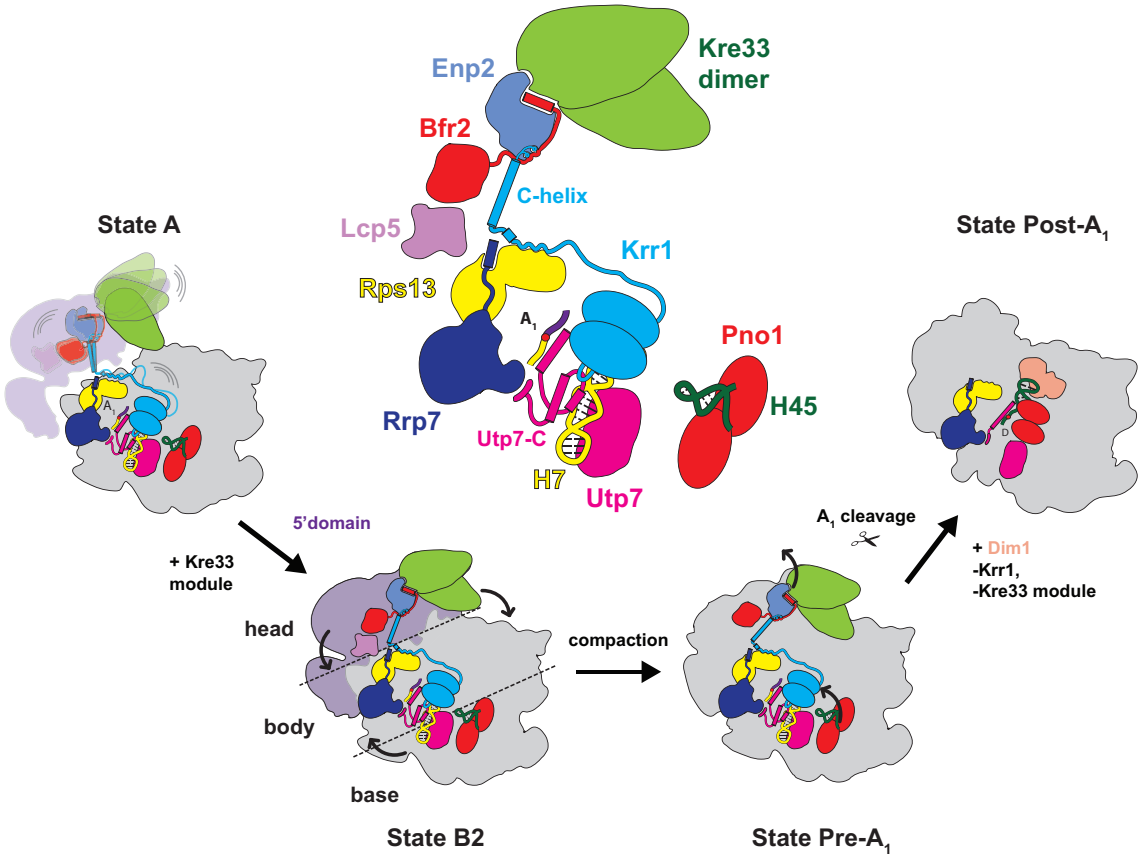


Figure 3.1 Model highlighting the role of Krr1 in 90S biogenesis. Stable incorporation of the 5' domain of the 18S pre-rRNA involves the assembly of the Kre33 module (Kre33, Enp2, Bfr2, Lcp5), which can be relayed to distant 90S regions via Krr1's C-terminus (State A to State B2). The 90S compaction processes involve the head, body and base region, which Krr1 can sense via its C-helix, unstructured C-terminus and KH domains, respectively (State B2). Next, A_1 cleavage site is processed as the Kre33 module is released, Krr1 is replaced by Pno1-H45 and the 5'ETS is deconstructed (State Pre-A_1 to State Post-A_1). Parts of Utp7-C are then

transformed into an elongated helix, which stabilizes Pno1-H45-Dim1 and shields the newly visible D cleavage site (State Post-A_1). Utp22 was omitted from the model because it covers most of the depicted proteins in the 90S body. The 5'ETS (H7 and downstream sequence of A1 cleavage site): yellow, central domain (upstream sequence of A1 cleavage site): orange, 3' domain (H45): forest green. α-helical protein segments: cylinders, KH domains: oval shapes, conformational changed within the 90S particle are depicted with arrows. C-helix: C-terminal helix of Krr1, Utp7-C: C-terminus of Utp7. See text for details.

3.1 Krr1 contacts the 5' domain in the head region with its C-helix via the Kre33 module

Improved particle isolation techniques from the thermophile *Chaetomium thermophilum* in combination with cryo-EM analysis resulted in a sequence of 90S pre-ribosomal cryo-EM models before A_1 cleavage has occurred (J. Cheng et al., 2019). Similarly to the previously described stable incorporation of pre-rRNA subdomains in the pre-60S pathway (Kater et al., 2017), the *ct*90S cryo-EM models support the view that 90S particles serves as a platform for the folding, stabilization and compaction of pre-rRNA subdomains. This gradual stable incorporation occurs independently of the order of transcription (5'>3'), but starts with the 5'ETS nucleation in the base of the 90S particle, followed by the 3' and central domain in the body region and finally concludes with the 5' domain in the head region. In a series of cryo-EM structures from yeast, the reported findings from *Chaetomium thermophilum* were essentially validated and extended with more structural information, such as a better resolved C-terminus of Krr1 (Figure 3.2) (J. Cheng et al., 2020).

The Kre33 module appears to have a key role in the interconnection and stabilization of the 5' domain together with Utp20, which is observed to be wrapped around the whole 5' domain (Figure 3.2 State B2 and Pre-A_1). In the first *ct*90S state of the series, the proximal copy of Kre33 is stably attached to the 90S particle, while the distal Kre33 molecule is more flexible and hence less well resolved. In contrast to later states, Enp2-Bfr2-Lcp5 cannot be observed in this early intermediate yet, indicating that structural stabilization of the Kre33 dimer and consequently the 5' domain needs the Enp2-Bfr2-Lcp5 trimeric complex. One possible mechanism behind 5' domain stabilization can be inferred from the genetic and biochemical analysis presented in this work. Mutational analysis revealed that the small wedge helix of Bfr2 is necessary for efficient Kre33 module assembly. This finding was in line with other results showing that the recruitment of the Bfr2-Enp2-Lcp5 heterotrimer to the 90S

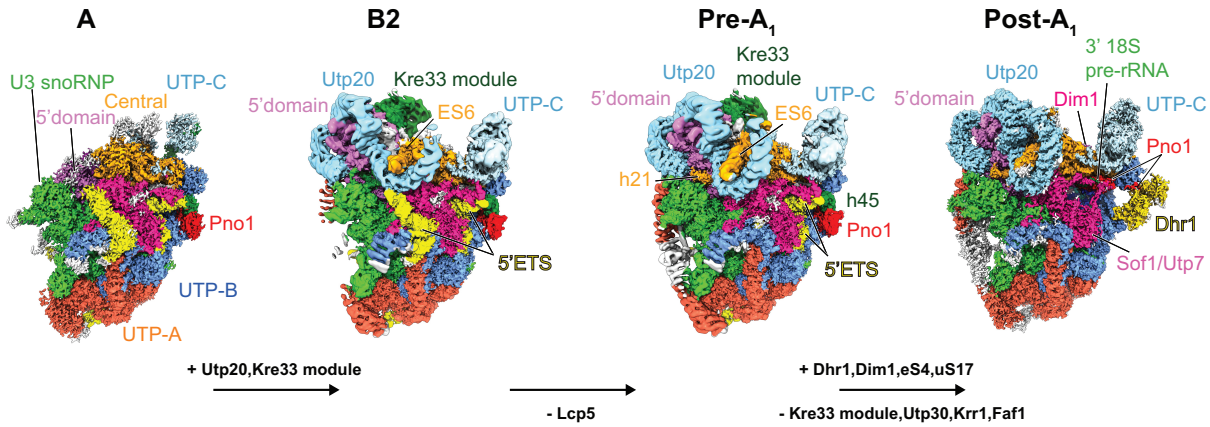


Figure 3.2 Sequential stable integration of the 5' domain and compaction of the 90S pre-ribosome visualized by a series of yeast cryo-EM models. Depiction of cryo-EM structures of states (A, B2, Pre-A_1, Post-A_1) leading to a 90S particle competent for A_1 cleavage. AFs/modules are labeled as well as pre-rRNA subdomains. Figure was taken and adapted from Figure 2 (J. Cheng et al., 2020)

particle is independent of Kre33 (J. Cheng et al., 2019). Consistent with our data, Bfr2, Enp2 and Lcp5 are reported as early binders of the 5' domain in the analysis of factors associated with truncated pre-rRNA molecules (L. Zhang et al., 2016). Moreover, Kre33's conserved substrate sites are located in the 3' domain, which is buried inside the 90S pre-ribosome and hence inaccessible (Chimnaronk et al., 2009; S. Sharma et al., 2015). Consequently, there must be a window of substrate accessibility for Kre33, including a more flexible 3' domain. One elegant mechanism could be that one Kre33 copy exerts its enzymatic function transferring an acetyl group to its target sites while the other Kre33 copy functions as anchoring agent bringing the dimer to its location in the 90S head region.

Taken together, these findings support a model where the Kre33 homodimer is docked onto the 90S particle, while the Bfr2-Enp2-Lcp5 trimer is attached to the flexible 5' domain of the 18S pre-rRNA (Figure 3.1 State A). Keeping the 5' domain flexible could be a means to allow the complicated maturation of this rRNA subdomain enough time to occur. A number of snoRNAs and AFs participate in this processes, including snoRNAs U14 and snR30, helicases Rok1 and Dbp4 or proteins without enzymatic function such as Esf1, Esf2, Efg1 and Bud22 (Choque, Schneider, Gadal, & Dez, 2018; Fayet-Lebaron, Atzorn, Henry, & Kiss, 2009; Kos & Tollervey, 2005; Martin et al., 2014; Shu & Ye, 2018; Soltanieh, Lapensee, & Dragon, 2014; Soltanieh et al., 2015). Thus, stable incorporation of the 5' domain supported and/or driven by the assembly of the Kre33 module could be a way to give a signal for the next maturation steps to occur.

In this scenario, Lcp5 serves as a connection between the body of the 90S and the 5' domain (Figure 3.1 State B2) but also U3 snoRNP via Rrp9. Moreover, the composite interface of Enp2 and Bfr2 offers an anchoring point for the C-helix of Krr1, which emerges from the central domain and reaches to the Kre33 module, thus bridging both subdomains of the 90S particle. Krr1's C-terminus is genetically linked to the C-terminal part of Enp2, which is not visible in the cryo-EM structures. We cannot say how both C-termini functionally act together within the 90S particle, if there is a protein-protein interaction involved or if they both act on the same structural or conformational changes occurring during ribosome maturation. Our biochemical data shows a clear defect in 90S biogenesis in mutant cells. In combination with our genetic analysis of the C-helix tip, we can conclude that proper anchoring of Krr1's C-helix to the Kre33 module is important in cells where Enp2's C-terminus is missing. However, the C-helix is not essential for cell growth or 90S biogenesis and other AFs likely contribute to this process in a redundant way. Although not essential under normal growth conditions, it has an important role in maturation of the 90S particle, perhaps by bridging and thus stabilizing subdomains of the 90S pre-ribosome. With its strategic positioning, the C-helix could act as sensor of 5' domain incorporation or even act as lever supporting conformational changes. This could facilitate further compaction of the 90S pre-ribosome, culminating in a state ready for A_1 cleavage to occur.

A reverse order of stable incorporation of pre-rRNA subdomains is in contrast to previous studies describing the temporal hierarchy of 90S subdomain assembly events as following the 5'>3' direction of Pol I transcription. In particular, mutational approaches of pre-rRNA fragments were used for particle isolation and biochemical analysis of AFs associated with the truncated pre-rRNAs (see Introduction). Subsequently, conclusions about the temporal order of AF recruitment to the 90S particle, and hence hierarchy of assembly events, were drawn. However, it was not taken into full account that the *in vivo* association of AFs with truncated pre-rRNA species does not necessarily resemble physiological relevant assemblies leading to productive pre-ribosomal intermediates. This approach ignores the intimate entanglement of AFs, r-proteins and pre-rRNA domains and their dependency on long range interactions. Moreover, the cell needs to make sure that 3' truncated pre-rRNA versions arising from premature terminated Pol I transcription do not further engage in the ribosome biogenesis pipeline. Hence, the pre-rRNA truncations most-likely yield dead-end products as they would fail the outlined route of hierarchical integration of

pre-rRNA subdomains into functional ribosomes. While recruitment of an AF or r-protein to a specific region of the pre-rRNA molecule can be detected via aptamer-tagged pre-rRNA fragments, their stable structural incorporation might depend on higher level and long-range interactions as well as the overall compaction state of the 90S pre-ribosome. With our study, we proposed a well-founded separation of the process of assembly into recruitment of an AF or r-protein and their stable incorporation into the 90S pre-ribosome illustrated by the stable incorporation of the Kre33 module and 5' domain in the head region of the 90S particle.

3.2 Krr1's unstructured C-terminal extension contributes to maturation of the central region of the 90S particle

In contrast to the 5' and 3' domain, the central domain of the 18S pre-rRNA is not well resolved in cryo-EM models. Hence, many AFs necessary for central domain formation have not been observed in recently solved cryo-EM structures of the 90S pre-ribosome. In mature 40S subunits, the central domain is part of the platform which additionally contains the 3' minor domain (H44 and H45) and r-proteins (RpS1, RpS7, RpS13, RpS14, RpS22, RpS26 and RpS27). Knitting the central domain together is one of the crucial events early in the biogenesis of the 90S particle. This is supported by depletion experiments of r-proteins found in the central domain (RpS14, RpS13, RpS1 and RpS27), which leads to a reduction of cellular 20S pre-rRNA levels (Ferreira-Cerca et al., 2005). Consequently, AFs involved in the correct formation of the central domain contribute to very early formation of pre-ribosomal particles. These include the UTP-C module, Rok1 and its cofactor Rrp5 and factors associated with snR30.

In the recently revealed *sc*90S particle series, we could observe for the first time that Krr1's unstructured, proline-rich region contacts the central domain via RpS13 (Figure 3.1 State B2 and Pre-A_1) (J. Cheng et al., 2020). Previous findings demonstrated that Krr1 is able to interact with Utp22 and Rrp7 *in vitro*, further adding to the evidence that Krr1 contributes to a stable association of AFs of the central domain (Sturm et al., 2017). Moreover, Krr1 was shown to interact with Kri1 via its KH1 domain, offering another link to the central domain via the Utp23-snR30 network (Sasaki et al., 2000; Zheng et al., 2014). This protein-protein and protein-snoRNA interaction network extends to Rrp5 and the DEAD-box helicase Rok1 via the essential H/ACA snoRNA snR30 (see Introduction). Besides H/ACA snoRNP components (Cbf5, Nop10, Nhp2, Gar1; see section 1.2.3.1) and Rok1, snR30 has been reported

to interact with Nop6 and the DEAD-box helicase Has1 (Lemay, Hossain, Osheim, Beyer, & Dragon, 2011; X. H. Liang & Fournier, 2006; Lübben, Fabrizio, Kastner, & Lührmann, 1995). Additionally, Utp23 was shown to directly interact with H/ACA snoRNP component Nhp2, Kri1, Utp24 as wells as Rrp7 and Rok1, both factors associated with the central domain and ES6 as well as snR10, snR30 and U14 (Lin et al., 2013; Martin et al., 2014; Wells et al., 2017).

This interconnectivity of the AFs in the central domain makes it a complicated task to reveal Krr1's exact role in this subdomain's organization. Deletion of Krr1's C-terminus including the proline-rich region is lethal, revealing that not only the KH domains of Krr1 fulfill an essential function in ribosome biogenesis as described in the literature. At this point we cannot conclusively say why deletions up until the small helix cause slower growth while deletions including the proline-rich region are lethal. Unfortunately, the region around Krr1's C-terminus including the long C-helix, the small helix and the unstructured proline-rich region is not resolved in current cryo-EM models and, except for RpS13, void of possible protein-protein interactions. However, C-terminal truncations beyond the C-helix of Krr1 significantly affect the composition of AFs in the central domain. In this context, Krr1's proline-rich region could stabilize a conformation needed for efficient coupling of RpS13 to Rrp7 and Utp22. Moreover, deletions beyond the C-helix could render the unstructured region fully flexible. As a consequence, an unhinged, unstructured C-terminus of Krr1 could disturb interactions we do not see yet, which under normal circumstances could lead to stable incorporation of the UTP-C module. Alternatively, the alterations in the central domain caused by a mutated C-terminus of Krr1 could first affect Rrp5 and Rok1, which would subsequently prevent efficient assembly of the UTP-C module as described before (Perez-Fernandez et al., 2007). Moreover, Krr1's small helix could fix the long C-helix at the central domain. This could be an elegant way to transmit information about the assembly status of the head region to the central domain via Krr1's C-terminus. However, since deletion of the small helix is not lethal, other protein-protein or protein-RNA interactions likely substitute and support proper conformations, ensuring that central domain maturation continues. Alternatively, premature release of the factors mentioned above could be stimulated when the interactions around Krr1's unstructured C-terminal part are altered.

Interestingly, the *ct*90S particle series hints at an important role for the UTP-C complex. As the module's association with the *ct*90S pre-ribosome tightens, it contacts

rRNA helices and r-proteins in the central domain (H22, H26, RpS1, RpS27) and H44 in the 3' minor domain. The association of the UTP-C module with the 90S particle is mediated by the C-terminal tail of Rrp7, as reported in earlier cryo-EM models or suggested by crosslinking experiments (Lin et al., 2013; Sun et al., 2017). In the *sc*90S particle cryo-EM series, Rrp7 is seen to contact RpS13 with a small C-terminal helix (Figure 3.1) (J. Cheng et al., 2020). The importance of this α-helical anchor, but also of RpS13 as organizing molecule of the central domain, is underscored by the fact that depletion of RpS13 was reported to dramatically reduce the UTP-C module on 90S pre-ribosomes (Jakob et al., 2012). In this context, Krr1's C-terminus could provide information about the maturation of the head domain as its C-helix could monitor weather the Enp2-Bfr-Lcp5 trimer is assembled with the Kre33 dimer. Taken together, UTP-C's location could act as suitable place to sense relative conformations of the 5', central and 3' minor domain. This could serve as a checkpoint that can only be overcome if all is primed correctly for the next steps along the maturation route. Moreover, the UTP-C module offers an intriguing connection between ribosome production and global regulatory pathways via the CURI complex (Albert et al., 2016). Phosphorylation activities by the CK2 kinases associated with the UTP-C module offer another possible layer of regulation, albeit this is not well explored and no phosphorylation targets have been identified yet.

3.3 A_1 cleavage is accompanied by crucial structural rearrangements of the 90S pre-ribosome leading to Krr1 release

The base of the 90S pre-ribosome consists of the 5'ETS folded into several helices and what can be referred to as 5'ETS RNP, which mainly includes the structural modules UTP-A and UTP-B as well as the U3 snoRNP (Barandun et al., 2017; Chaker-Margot et al., 2017; Kornprobst et al., 2016). While maturation events lead to an ongoing 90S pre-ribosome compaction, an increased 5'ETS flexibility and/or deconstruction is observed before A_1 cleavage occurs (see Introduction). The dissociation of several AFs (Kre33 module, Krr1, Faf1) accompanies completion of A_1 cleavage as observed in *sc*90S pre-ribosomes in the Post-A_1 state (Figure 3.2) (J. Cheng et al., 2020). Moreover, A_1 cleavage marks the transition of Pno1 from the periphery of the 90S particle to the central domain (Figure 3.3), which pulls H45 to its mature position. Thus, the helix tip is close to the newly recruited Dim1, a dimethyltransferase which adds two methyl groups to highly conserved adenosine

1782 (J. Cheng et al., 2020). This modification is the only one reported to be common to pro- and eukaryotes and Dim1 is one of the AFs having a bacterial counterpart, KsgA (Lafontaine, Delcour, Glasser, Desgres, & Vandenhaute, 1994). The observed relocation marks the first 90S to pre-40S transition step: Pno1's position switches from peripheral 90S factor contributing to Dhr1 activation via Utp14 to pre-40S factor in the body of the 90S recruiting the endonuclease Nob1. Interestingly, during this relocation, Pno1 changes its binding mode to H45. This novel conformation of Pno1 and H45 is stabilized by a C-terminal helix of Utp7, newly constructed from a helix-loop-helix motif in 90S particles before A_1 cleavage has occurred. Notably, this helix-loop-helix motif is engaged in an interaction with Krr1's KH1 domain (Figure 3.3 left panel). This connection is part of an interaction network (Krr1-RpS13-Rrp7-Utp7), which forms a closed circle by Rrp7 interacting with the very C-terminal part of Utp7 (Figure 3.3). The formation of Utp7's extended C-helix appears to be prevented by its interaction with the 5'ETS and Krr1 prior to A_1 cleavage. At the same time, this contact likely contributes to Krr1's incorporation via its KH domains. Moreover, Utp7 seems to have a strategical position in the conformational changes described.

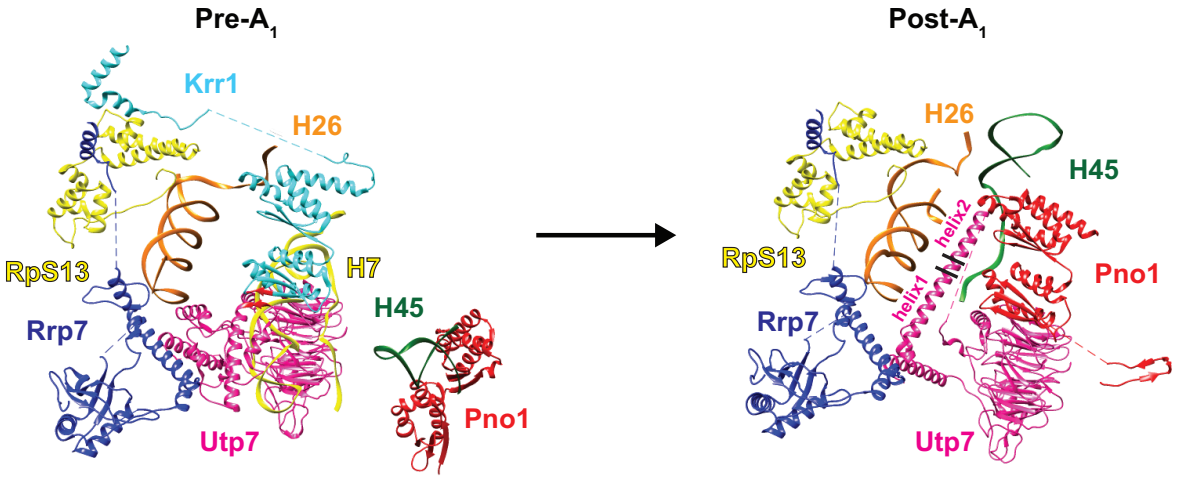


Figure 3.3 Structural rearrangements occurring during and/or after A_1 cleavage. Detailed structural rearrangements occurring from state Pre-A_1 (PDB: 6zqC) to state Post-A_1 (PDB: 6zqD). Krr1 (cyan), RpS13 (yellow), Rrp7 (blue), Utp7 (deep pink), Pno1 (red), Dim1 (salmon), A1 processing site (left panel, black circle) flanked by the 5' domain (purple) and 5'ETS (yellow), H7 (5' ETS, yellow) and H45 (3' minor domain, forest green) including D cleavage site (right panel, black circle). Helix1 and helix2 of the former helix-loop-helix region of Utp7 are indicated in the Post-A_1 state.

Prior to A_1 cleavage, the A_1 processing site is clamped between Utp7 and Sof1, far away from the endonuclease Utp24.In the Post-A_1 state, the newly formed α-helix is

seen to stabilize relocated Pno1-H45 thereby facilitating dimethylation by Dim1 (Figure 3.3). It also shields the D cleavage site, which marks the last 18S pre-rRNA processing step (see also Figure 3J (J. Cheng et al., 2020)). At the same time, Utp14, which interacts with Utp7, covers the protein binding sites of Pno1 for Nob1, the endonuclease acting on cleavage site D. Thus, both proteins contribute to the prevention of premature processing of cleavage site D.

Our mutational analysis shows that *in vivo*, a weakening of the interaction between Utp7 and Krr1 does not impair growth. This suggests that it is redundant with other contact sites, e.g. Utp7's interaction with the 5'ETS. However, the interaction of Utp7 with Krr1's loop region plays a role when Krr1's link to the Kre33 module is affected. One explanation for the observed genetic relationship is that the progression of 90S maturation is dependent on an intact connection between distant regions of the 90S pre-ribosome, and more specifically a completion of 5' domain incorporation. Krr1 could provide this information since its contact sites span from the head of the 90S particle to its base. Moreover, Krr1 integrates the maturation state of the central domain via Krr1's unstructured C-terminus. Coupled with biochemical data showing that 90S maturation and A_1 cleavage are affected in mutant cells and that the Kre33 module is enriched, this points to a specific defect prior to A_1 processing. Currently, it is not known how the Kre33 module and Krr1-Faf1 dissociate form the 90S pre-ribosome and if the release occurs prior or post A_1 cleavage. However, Krr1 could be released as a result of conformational changes such as the deconstruction of the 5'ETS, the construction of the extended C-helix in Utp7, compaction of the 90S particle as a whole or Pno1 competition for the KH domain binding site. Weather and how Krr1's release is coupled with the dissociation of the Kre33 module or how the Krr1-Kre33 connection affects Krr1's link to Utp7 is an interesting question we cannot answer yet. Furthermore, it is not clear weather Pno1 dissociates from the 90S and reassembles once Krr1 leaves the KH domain binding site empty. Pno1's relocation could involve a loose attachment to the 90S particle giving it enough spatial freedom to change its binding mode to H45. Taken together, our data point to a link between the events leading to Kre33 release from the head region and maturation events occurring in the base region of the 90S particle leading to A_1 processing, which ultimately sets off the 90S to pre-40S transition.

3.4 Conclusion and outlook

The major findings described in this work increased our understanding of Krr1's role during ribosome biogenesis as a factor bridging several regions in the extended 90S pre-ribosome structure. As Krr1 is ultimately replaced by Pno1 before the 90S to pre-40S transition occurs, its functional role is to be placed during 90S maturation events. These maturation steps ultimately lead to a successfully rearranged and processed intermediate, which is primed and competent for taking the step of A_1 cleavage and transition into a pre-40S particle. Important events include maturation of the 5' and central domain involving the Kre33 module and Rrp5-Rok1 and UTP-C, as well as interactions in the base domain leading to major rearrangements involving Utp7 and Pno1.

Several questions arise regarding the mechanisms leading to these 90S biogenesis events. Concerning the maturation in the head region, it would be interesting to know where Enp2's C-terminus is located within the 90S architectural framework and how its position leads to the synergistic effects observed in *krr1*ΔC *enp2*ΔC double mutant cells. Moreover, how Kre33's enzymatic activity is integrated within the sequence of maturation events leading up to stable 5' domain incorporation is not known yet. Krr1 is clearly connected to the Kre33 module but ultimately, we cannot say whether this connection serves a monitoring function or as an arm physically transmitting signals. This link between 5' and central domain could lead to the compaction and/or release of the Kre33 module before A_1 cleavage occurs and the 90S pre-ribosome undergoes the transition to the pre-40S particle. The scenarios are not mutually exclusive and it is even possible that Kre33 and Krr1 release are coupled and dependent on the rearrangements occurring in the base region of the 90S particle. Maturation of the 5' domain involves many steps and hence new data on the events and mechanisms leading to Kre33 attachment and release would be an important contribution to understanding 90S maturation as a whole.

A less well understood maturation step concerns the central region of the 90S particle. Clearly, Krr1 is important for proper association of central domain AFs but how this is established remains unclear. The network of AFs involved in this step offers a link to our structure via RpS13 and Rrp7-Utp22, and via Kri1 as an established interaction partner of Krr1. Further studies regarding Krr1 and the afore mentioned AFs promise exciting information on how this set of essential AFs and snoRNPs is entangled in the maturation of the central subdomain, as well as the 90S pre-ribosome

as a whole. Moreover, proteomic analyses of the *krr1*ΔC *utp7*DD double mutant showed that central domain AFs are enriched, supporting the notion that Krr1's involvement in the organization/maturation of the central region precedes steps involving the rearrangements in the base region and its connection to Kre33. It is not known when and how Krr1 enters the 90S pre-ribosome, although it can be speculated that its entry coincides with that of Kri1 and RpS14. Many AFs binding to the central domain are notoriously unresolved in cryo-EM structures, most likely because cryo-EM models represent a static snapshot and dynamic rearrangements can only be visualized within a well resolved series of these snapshots. The combination of improved cryo-EM approaches with a mutational approach and/or split-tag TAP of appropriate AFs might give us the possibility to obtain better resolved cryo-EM maps of 90S pre-ribosome intermediates where central domain AFs can be better discerned.

As detailed as the mechanisms presented in this work and the questions remaining open are, they have a broader, more general implication. As covered in the introduction, ribosome biogenesis is such a burden regarding cellular resources, and hence needs to be tightly regulated and controlled. The better we understand the mechanisms leading to functional ribosomes, the more we have a chance to tackle diseases that are based on faulty processes and mal-regulation of ribosome biogenesis. This not only includes ribosomopathies, but also cancerous cells, which need a highly stimulated ribosome production to meet their demands for faster cell division. The gained knowledge also might open more ways to understand the evolutionary need for a more complex system in eukaryotes. So far, nuclear stages of ribosome biogenesis intermediates have not been obtained from human cells. Many reasons have been speculated to impede the isolation of human nucleolar pre-ribosomes but ultimately, it could boil down to a question of yield. Compared to yeast with its short division cycles and hence unmatchable demand for ribosomes, the absolute amount of newly produced ribosomes is likely to be sobering in human cells. The understanding of human ribosome biogenesis has benefitted from research successes in yeast because many critical players are conserved. However, just as players involved vary between yeast and humans, the approaches to obtain experimental results need to be adjusted to differential physiological needs and settings. Lastly, understanding ribosome biogenesis is a herculean task in itself, with every little detailed information added contributing to the charm of the process as a whole.

4. Materials and Methods

4.1 Molecular biology and genetic methods

4.1.1 Construction of plasmids

Plasmids were generated following standard procedures and are listed in Table 1. DNA fragments were amplified using Phusion High-Fidelity DNA Polymerase (NEB) and restriction digests were performed using enzymes from NEB and Thermo Fischer Scientific. Digested PCR-products were either purified with the GenElute TM PCR Clean-up Kit (SIGMA) or separated by agarose gel electrophoresis with subsequent SERVA DNA Stain G staining (SERVA) and GenElute TM Gel Extraction Kit (SIGMA). Digested DNA fragments were ligated with T4 DNA Ligase (NEB), transformed into chemically competent *E. coli* Dh5α [F– endA1 glnV44 thi-1 recA1 relA1 gyrA96 deoR nupG purB20 φ80dlacZΔM15 Δ(lacZYA-argF)U169, hsdR17(rK–mK+), λ–] (Inoue, Nojima, & Okayama, 1990). The amplified plasmids were isolated with the GenElute TM HP Plasmid Miniprep Kit (SIGMA) and tested by restriction digest for the correct size of the inserted fragment and by DNA sequencing (Eurofins MWG-Operon; Ebersberg, Germany) for the intact DNA sequence of the inserted fragment.

Luria-Bertani (LB) Medium: 0.5% (w/v) yeast extract (MP), 0.5% (w/v) NaCl, 1% (w/v) tryptone (MP), pH 7.2

SOB Medium: 2% (w/v) tryptone (MP), 0.5% (w/v) yeast extract (MP), 10 mM NaCl, 2.5 mM KCl, 10 mM $MgCl_2$, 10 mM $MgSO_4$

TB medium: 10 mM Pipes, 55 mM $MnCl_2$, 15 mM CaCl2, 250 mM KCl (pH 6.7 with KOH prior to $MnCl_2$ addition)

4.1.2 Introduction of point mutations through site-directed mutagenesis

Point mutations of DNA constructs inserted into plasmids were introduced by PCR reactions with primers harboring the desired mutation. Primers were designed to have approximately 25bp downstream and upstream of the mutated nucleotide sequence as well as at least one G/C at either end. Primers were phosphorylated with T4 PN kinase (NEB) according to company's instructions and used for PCR. One PCR reaction contained: 18.5µl H_2O, 10µl 5xHF buffer, 10µl 5mM NAD+ (COMPANY), 8µl

dNTPs, 2.5µl phosphorylated primer from reaction mixture, 1µl plasmid template, 1µl Phusion polymerase, 1µl Taq DNA Ligase (NEB). The PCR program included following steps: 1min at 95˚C, 30 cycles of 1min at 95˚C, 1min at 55˚C, 4min at 65˚C, followed by 10min at 65˚C before cooling to 4˚C. After the PCR reaction was completed, 1µl DpnI (NEB) was added and incubated at 37˚C for at least 3h. Final DNA plasmids were purified using the GenElute TM PCR Clean-up Kit (SIGMA), eluted in 25µl H_2O. 8µl eluate were used for transformation of chemically competent Dh5α cells.

Table 1. Recombinant DNA used in this study. Strains published in (J. Cheng et al., 2019) are marked with *.

Recombinant DNA	Reference	Internal ID
P_{KRR1}-*KRR1*-T_{KRR1}, *URA3*, ARS/CEN, *AmpR*	*	pPV2
P_{BFR2}-*BFR2*-T_{ADH1}, *URA3*, ARS/CEN, *AmpR*	*	
P_{ENP2}-*ENP2*-T_{ADH1}, *URA3*, ARS/CEN, *AmpR*	*	
P_{KRE33}-*KRE33*-T_{ADH1}, *URA3*, ARS/CEN, *AmpR*	*	
P_{UTP7}-*UTP7*-T_{ADH1}, *URA3*, ARS/CEN, *AmpR*	This study	pPV69
P_{KRR1}- *KRR1*-T_{KRR1}, *TRP1*, ARS/CEN, *AmpR*	*	pPV29
P_{KRR1}-*krr1*ΔC-T_{KRR1}, *TRP1*, ARS/CEN, *AmpR*	*	pPV30
P_{KRR1}-*KRR1*-T_{KRR1}, *LEU2*, ARS/CEN, *AmpR*	*	pPV1
P_{KRR1}-*krr1*ΔC-T_{KRR1}, *LEU2*, ARS/CEN, *AmpR*	*	pPV5
P_{BFR2}-*BFR2*-T_{ADH1}, *LEU2*, ARS/CEN, *AmpR*	*	pPV24
P_{BFR2}-*bfr2*ΔN1-T_{ADH1}, *LEU2*, ARS/CEN, *AmpR*	*	pPV384
P_{BFR2}-*bfr2*ΔN2-T_{ADH1}, *LEU2*, ARS/CEN, *AmpR*	*	pPV385
P_{BFR2}-*bfr2*ΔC3-T_{ADH1}, *LEU2*, ARS/CEN, *AmpR*	*	pPV15
P_{BFR2}-*bfr2*ΔC2-T_{ADH1}, *LEU2*, ARS/CEN, *AmpR*	*	pPV16
P_{BFR2}-*bfr2*ΔC1-T_{ADH1}, *LEU2*, ARS/CEN, *AmpR*	*	pPV17
P_{ENP2}-*ENP2*-T_{ADH1}, *TRP1*, ARS/CEN, *AmpR*	*	pPV19
P_{ENP2}- *enp2*ΔC2 -T_{ADH1}, *TRP1*, ARS/CEN, *AmpR*	This study	pPV33
P_{ENP2}- *enp2*ΔC1 -T_{ADH1}, *TRP1*, ARS/CEN, *AmpR*	This study	pPV32
P_{ENP2}- *enp2*ΔC -T_{ADH1}, *TRP1*, ARS/CEN, *AmpR*	*	pPV20
P_{KRE33}-*kre33-1*-T_{ADH1}, *TRP1*, ARS/CEN, *AmpR*	*	pPV22
P_{ENP2}-*ENP2*-Flag-TEV-ProtA-T_{ADH1}, *LEU2*, ARS/CEN, *AmpR*	*	pPV61
P_{ENP2}- *enp2*ΔC -Flag-TEV-ProtA-T_{ADH1}, *LEU2*, ARS/CEN, *AmpR*	*	pPV62
P_{BFR2}-*BFR2*-Flag-TEV-ProtA-T_{ADH1}, *LEU2*, ARS/CEN, *AmpR*	*	pPV63
P_{BFR2}-*bfr2*ΔC2-Flag-TEV-ProtA-T_{ADH1}, *LEU2*, ARS/CEN, *AmpR*	*	pPV64
P_{BFR2}-*KRR1*-Flag-TEV-ProtA-T_{ADH1}, *LEU2*, ARS/CEN, *AmpR*	This study	pPV65
P_{BFR2}-*krr1*ΔC-Flag-TEV-ProtA-T_{ADH1}, *LEU2*, ARS/CEN, *AmpR*	This study	pPV66
P_{KRR1}- *KRR1*-T_{ADH1}, *TRP1*, ARS/CEN, *AmpR*	This study	pPV67
P_{KRR1}-*KRR1*-T_{ADH1}, *LEU2*, ARS/CEN, *AmpR*	This study	pPV68

P_{KRR1}-*krr1*ΔC0-T_{ADH1}, *TRP1*, ARS/CEN, *AmpR*	This study	pPV111
P_{KRR1}-*krr1*ΔEE-T_{ADH1}, *TRP1*, ARS/CEN, *AmpR*	This study	pPV113
P_{KRR1}-*krr1*Δtip-T_{ADH1}, *TRP1*, ARS/CEN, *AmpR*	This study	pPV88
P_{KRR1}-krr1ΔC-T_{ADH1}, *LEU2*, ARS/CEN, *AmpR*	This study	pPV5
P_{KRR1}-*krr1*ΔC2-T_{ADH1}, *TRP1*, ARS/CEN, *AmpR*	This study	pPV395
P_{KRR1}-*krr1*ΔPro-T_{ADH1}, *TRP1*, ARS/CEN, *AmpR*	This study	pPV183
P_{KRR1}-*krr1* DDLΔC-T_{ADH1}, *TRP1*, ARS/CEN, *AmpR*	This study	pPV223
P_{KRR1}-*krr1* LKLΔC-T_{ADH1}, *TRP1*, ARS/CEN, *AmpR*	This study	pPV222
P_{UTP7}-*UTP7*-T_{ADH1}, *LEU2*, ARS/CEN, *AmpR*	This study	pPV71
P_{UTP7}-*utp7*Δh1-T_{ADH1}, *LEU2*, ARS/CEN, *AmpR*	This study	pPV100
P_{UTP7}-*utp7*Δloop-T_{ADH1}, *LEU2*, ARS/CEN, *AmpR*	This study	pPV101
P_{UTP7}-*utp7*Δh2-T_{ADH1}, *LEU2*, ARS/CEN, *AmpR*	This study	pPV170
P_{UTP7}-*utp7* DD-T_{ADH1}, *LEU2*, ARS/CEN, *AmpR*	This study	pPV103

4.1.3 Yeast growth and construction of yeast strains

All yeast strains generated and used during the course of this work are listed in Table 2. Deletion of open reading frames and the introduction of a tag to a gene of interest was performed as described before (Itoh, Fukada, Murata, & Kimura, 1983; Janke et al., 2004; Longtine et al., 1998; Schiestl & Gietz, 1989). Genetic modifications were verified by colony PCR, phenotype selection and/or detection of the successfully introduced protein tag by western blot analysis. Yeast cells were grown under standard laboratory conditions at 30°C unless otherwise indicated. For growth analysis of mutant cells and genetic relationships between two mutant genes, cells were plated in serial dilutions on the respective plates and incubated at either 23°C, 30°C and 37°C for YPD plates or 30°C for selective plates, SDC+5-FOA plates and SGC plates. Unless indicated, cultures used for further experiments were harvested during the logarithmic growth phase ($2 < OD_{600} < 3$).

YPD: 1% (w/v) yeast extract (MP), 2% (w/v) glucose (Merck), 2% (w/v) Bacto TM peptone (BD), pH 5.5

SDC-XY: 2% (w/v) glucose (Merck), 0.67% (w/v) yeast nitrogen base w/o amino acids, complemented with amino acids lacking XY (CSM drop-out, Formedium), pH 5.5

For solid media plates, 22 g/l agar was added.

4.1.4 Generation of yeast double shuffle strains

Shuffle strains for a single gene A were generated as described before. A phenotype inducing variant of gene A encoded on plasmids listed in Table 2 (ts for Kre33, Krr1

and cold-sensitive for Enp2, Bfr2) were introduced into the single shuffle strain and selection on SDC+5-FOA plates ensured that the original URA plasmid encoding the wt version of gene A was lost. Subsequently, a URA plasmid encoding for gene B was transformed into the cells, gene B was deleted genomically by homologous integration and positive clones growing on selection medium were verified by colony PCR. The wt variant of gene A encoded by a URA plasmid was transformed into the cells and selection for cells carrying both URA plasmids was performed at the restrictive temperatures by picking the biggest colonies (37°C for temperature-sensitive phenotypes and 23°C for cold-sensitive phenotypes).

Table 2 Yeast strains used in this study. Strains published in (J. Cheng et al., 2019) are marked with *.

Strains: Saccharomyces cerevisiae	**Source**	**Internal ID**
W303, *krr1::HIS3*, [YCp-*krr1-18*]	(Sasaki et al., 2000)	Y2209
W303, *krr1*::*HIS3*, [pRS316 *KRR1*]	This study	pfY058
W303, *krr1::HIS3*, *enp2*∆*C*::*hphNT1,* [pRS316 *KRR1*]	*	pfY187
W303, *krr1::HIS3*, *UTP10*-FTpA::*natNT2,* [pRS316 *KRR1*]	This study	pfY175
W303, *krr1::HIS3, enp2*∆*C*::*hphNT1*, *UTP10*-FTpA::*natNT2,* [pRS316 *KRR1*]	*	pfY190
W303, *krr1::HIS3, UTP22*-FTpA::*natNT2,* [pRS316 *KRR1*]	This study	pfY247
W303, *krr1::HIS3*, *enp2*∆*C*::*hphNT1*, *UTP22*-FTpA::*natNT2,* [pRS316 *KRR1*]	This study	pfY261
W303, *krr1::HIS3*, *enp2*::*hphNT1, UTP10*-FTpA::kanMX6, [pRS316 *KRR1*, pRS316 *ENP2*]	This study	pfY424
W303, *krr1::HIS3, UTP7*-FTpA*::natNT2*, [pRS316 *KRR1*, pRS316 *ENP2*]	This study	pfY412
W303, *krr1::HIS3, enp2*∆*C*::*hphNT1 UTP7*-FTpA*::kanMX6*, [pRS316 *KRR1*]	This study	pfY414
W303, *krr1::HIS3*, [pRS316 *KRR1*]	This study	pfY647
W303, *krr1::HIS3*, *NOC4*-FTpA[pRS316 *KRR1*]	This study	pfY657
W303, *krr1::HIS3*, *UTP10*-FTpA[pRS316 *KRR1*]	This study	pfY655
W303, *bfr2*::*HIS3*, *ENP2*-FTpA::*natNT2*, [pRS316 *BFR2*, pRS316 *ENP2*]	*	pfY301
W303, *bfr2*::*HIS3*, *UTP10*-FTpA::*natNT2*, [pRS316 *BFR2*, pRS316 *ENP2*]	*	pfY299
W303, *bfr2*::*HIS3*, *ENP1*-FTpA::*natNT2*, [pRS316 *BFR2*, pRS316 *ENP2*]	*	pfY408
W303, *bfr2*::*HIS3*, *UTP22*-FTpA::*natNT2*, [pRS316 *BFR2*, pRS316 *ENP2*]	This study	pfY305
W303, *bfr2*::*HIS3*, *UTP7*-FTpA::*natNT2*, [pRS316 *BFR2*, pRS316 *ENP2*]	This study	pfY418
W303, *krr1*::*HIS3*, *enp2*::*hphNT1,* [pRS316 *KRR1*, pRS316 *ENP2*]	*	pfY241

W303, *krr1*::*HIS3*, *bfr2*::*hphNT1,* [pRS316 *KRR1*, pRS316 *BFR2*]	*	pfY239
W303, *enp2*::*HIS3*, *bfr2*::*hphNT1,* [pRS316 *KRR1*, pRS316 *ENP2*]	*	pfY394
W303, *kre33*::*HIS3*, *krr1*::*hphNT1*, [pRS316 *KRE33*, pRS316 *KRR1*]	*	pfY214
W303, *krr1*::*HIS3*, *utp7*::*hphNT1* [pRS316 *KRR1*, pRS316 *UTP7*]	This study	pfY400
W303, *krr1*::*HIS3*, *utp7*::*hphNT1 UTP10*-FTpA*::kanMX6* [pRS316 *KRR1*, pRS316 *UTP7*]	This study	pfY440
W303, *krr1*::*HIS3*, *utp7*::*hphNT1 NOC4*-FTpA*::natNT2* [pRS316 *KRR1*, pRS316 *UTP7*]	This study	pfY576
W303, *krr1*::*HIS3*, *utp7*::*hphNT1 DHR1*-TpA*::kanMX6 DIM1*-FLAG*::natNT2* [pRS316 *KRR1*, pRS316 *UTP7*]	This study	pfY578

4.1.5 GAL-promoter regulated overexpression of ribosome assembly factors

Yeast cells carrying a plasmid, on which the gene of interest was fused to a galactose inducible promoter, were grown in SDC medium. This selective preculture was used to inoculate 1l of selective SRC medium ON with a start OD_{600}=0.006-0.008. Approximately 16h later the SRC culture reached an OD_{600}=1.0-1.5 and protein expression was induced by adding 1l 2xYPG to a final galactose concentration of 2%. Cells were harvested after 6h of galactose induction.

SRC-XY: 2% (w/v) raffinose (MP), 0.67% (w/v) yeast nitrogen base w/o amino acids, complemented with amino acids lacking XY (CSM drop-out, Formedium), pH 5.5
YPG: 1% (w/v) yeast extract (MP), 2% (w/v) galactose (Sigma), 2% (w/v) Bacto TM peptone (BD), pH 5.5

4.2 Biochemical methods

4.2.1 Tandem-affinity purification of 90S pre-ribosomes

Cell pellets stored at -20°C were resuspended in Lysis Buffer A and disrupted mechanically by glass beads in a bead beater (Fritsch). Yeast cell extract was obtained by clearing the cell lysate by two consecutive centrifugation steps (10 min at 5000 rpm and subsequently 20 min at 17000 rpm, 4°C). The tagged protein was isolated in a first step by incubation of the yeast cell extract with pre-equilibrated immunoglobulin G (IgG) Sepharose 6 Fast Flow beads (GE Healthcare) for at least 2h, washed with at least 15ml Buffer B in at least 3 washing steps before bound proteins were eluted by

TEV cleavage at 16°C for 2h (Parks, Leuther, Howard, Johnston, & Dougherty, 1994).The TEV eluate was then incubated with Flag agarose beads (ANTI-FlagM2 Affinity Gel, Sigma–Aldrich) at 4°C for 2h in a second affinity purification step and the Flag beads were washed once with 5ml Buffer B. Final eluates of bound proteins were obtained by adding buffer supplemented with Flag peptide (concentration 100 µg/ml, 1h, 4°C, Sigma Aldrich) and subsequently analyzed on 4-12% polyacrylamide gels (NUPAGE, Invitrogen) with colloidal Coomassie staining (Roti-Blue, Roth).

Buffer A: 20 mM Hepes, pH 7.5, 150 mM NaCl, 5.5 mM $MgCl_2$, 1 mM dithiothreitol, 5% (v/v) glycerol, 0.1% (v/v) IGEPAL CA-630, SIGMAFAST complete protease inhibitor cocktail (Sigma–Aldrich)

Buffer B: 20 mM Hepes, pH 7.5, 150 mM NaCl, 5.5 mM $MgCl_2$, 1 mM dithiothreitol, 5% (v/v) glycerol, 0.01% (v/v) IGEPAL CA-630

6xSB loading buffer: 350mM Tris-HCl pH 6.8, 60% (v/v) glycerol, 10% (w/v) SDS, 0.6M DTT, 0.02% (w/v) Bromphenol Blue

4.2.2 Protein identification and quantification with mass spectrometry (MALDI and SemiQ-MS)

MALDI: Final TAP-purification eluates were separated on a 4-12% polyacrylamide-SDS gel (NuPAGE, Invitrogen), stained with Coomassie (Roti-Blue, Roth or colloidal Coomassie Brilliant Blue G250, BIORAD), destained and bands were subsequently excised from the gel, digested with trypsin and analyzed with mass spectrometry (in-house BZH mass spectrometry facility, Heidelberg, Germany) as described before (Bassler et al., 2001).
SemiQ-MS: Eluates of TAP-purifications were separated on a 4-12% polyacrylamide-SDS gel (NuPAGE, Invitrogen) for 5min at 185V which were subsequently stained with Coomassie (Roti-Blue, Roth). Fragments below the loading well until the running front were excised and analyzed by FingerPrints proteomics (University of Dundee, UK). Co-precipitating proteins were identified by 1D nLC-ESI-MS-MS.

4.2.3 rRNA extraction and analysis by Northern blot

For TAP-purification of particles subjected to RNA extraction following final Flag elution, 7µl of RiboLock RNase inhibitor (Thermo Fischer Scientific) were added per 2l culture to Buffer A during cell lysis.

RNA from final eluates of the Dhr1/Dim1 split particle (obtained from cells expressing different Krr1 and Utp7 variants) were extracted as described before (Gasse et al., 2015; Kos & Tollervey, 2005). Basically, 400µl Phenol-Chloroform-IAA were added, mixed by shaking for 1min, and centrifuged for 5min at maximum speed. Aqueous phase was added to 500µl chloroform, mixed by shaking and centrifuged for 5min at maximum speed. Aqueous phase was then added to 3 volumes 100% ethanol and 1/10 volume of 3M NaAc pH 5.2 and RNA was precipitated for 2-3h at -20˚C. The precipitated RNA was pelleted by centrifugation for 20min at maximum speed, washed once with 70% ethanol and air dried before resuspension in water.

0.7µg extracted RNA were loaded and resolved on 8% polyacrylamide gel (with 8M urea) after denaturation with formaldehyde. RiboRuler High Range RNA Ladder (Thermo Fischer Scientific) was used as standard. The gel was stained with SYBR® Green II RNA gel stain (Sigma Aldrich), RNA was transferred on positively charged nylon membranes (GE healthcare) and crosslinked with UV. For northern blotting, the following probes (DNA oligonucleotides) were 5'end γ32P-ATP radiolabeled using T4 PNK (NEB): 5′-GTCTTCAACTGCTTTCGCA-3′ (probe c) and 5′-TATTCCCTCTTGCTAGAAG-3′ (probe d) (J. Cheng et al., 2020).

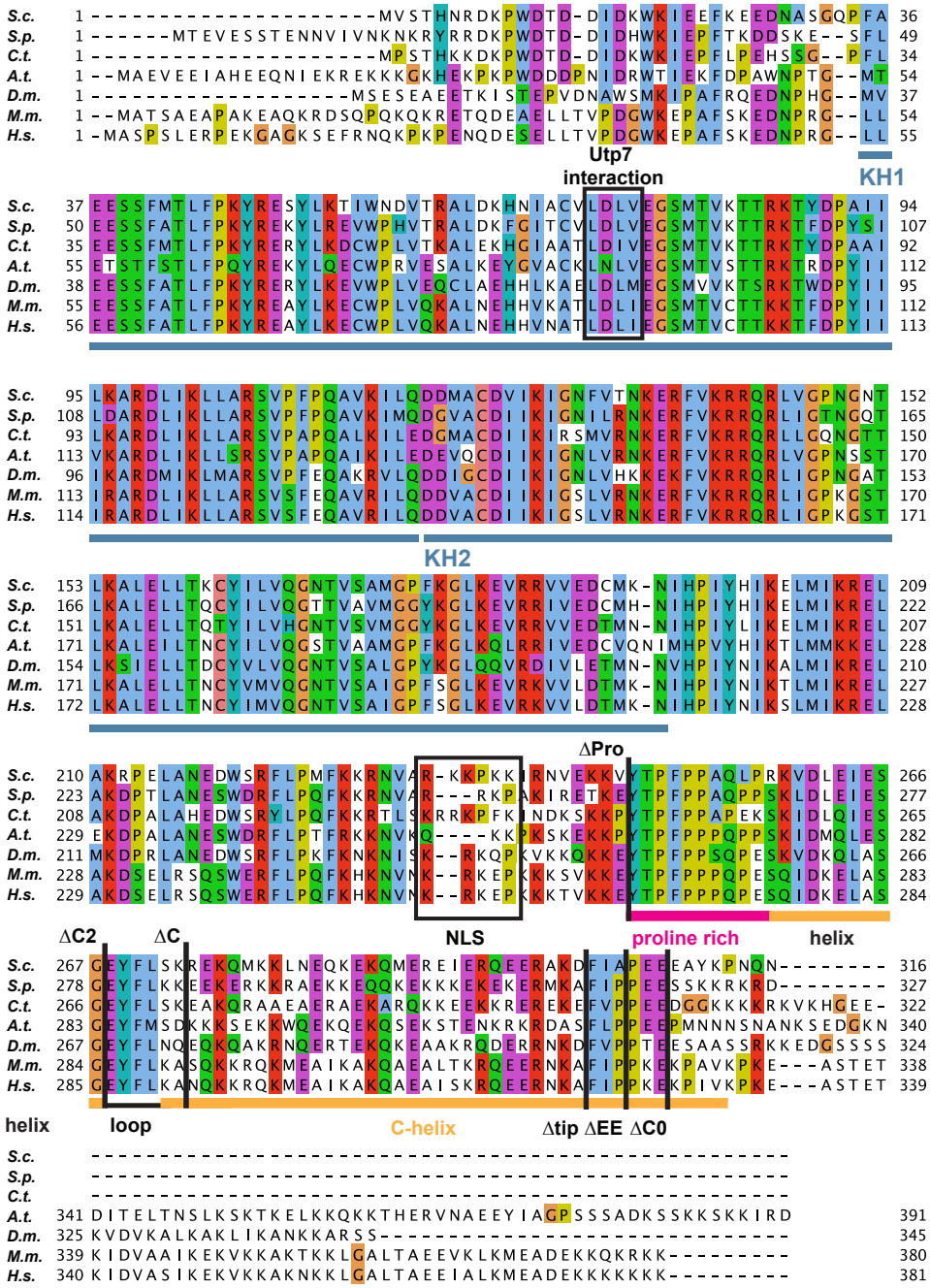
4.3 Computational methods and programs used for *in silico* analysis of proteins, semiQ MS data and cryo-EM maps

Protein homologs from a subset of species were identified using the BLAST algorithm (Altschul, Gish, Miller, Myers, & Lipman, 1990). Sequences were aligned using ClustalW or CustalOmega (Sievers & Higgins, 2014; Thompson, Higgins, & Gibson, 1994) and visualized with Jalview (Thompson et al., 2006; Waterhouse, Procter, Martin, Clamp, & Barton, 2009).

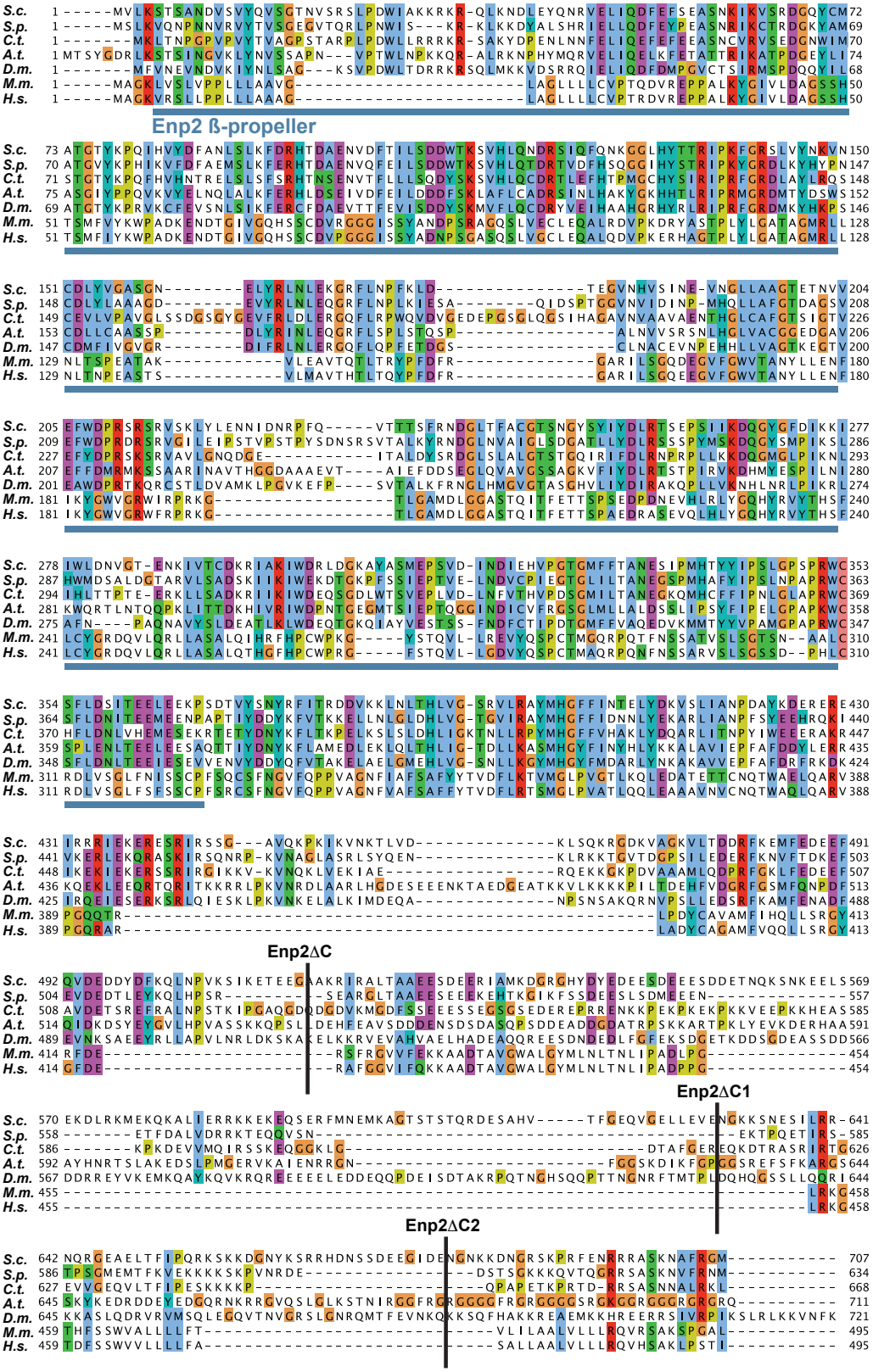
Raw data obtained by FingerPrints proteomics was analyzed using the MaxQuant software (Cox & Mann, 2008). iBAQ values were normalized to the respective bait protein and the log10 value of iBAQ ratios as indicated in the figures are shown.

Cryo-EM maps were visualized using Chimera (Pettersen et al., 2004).

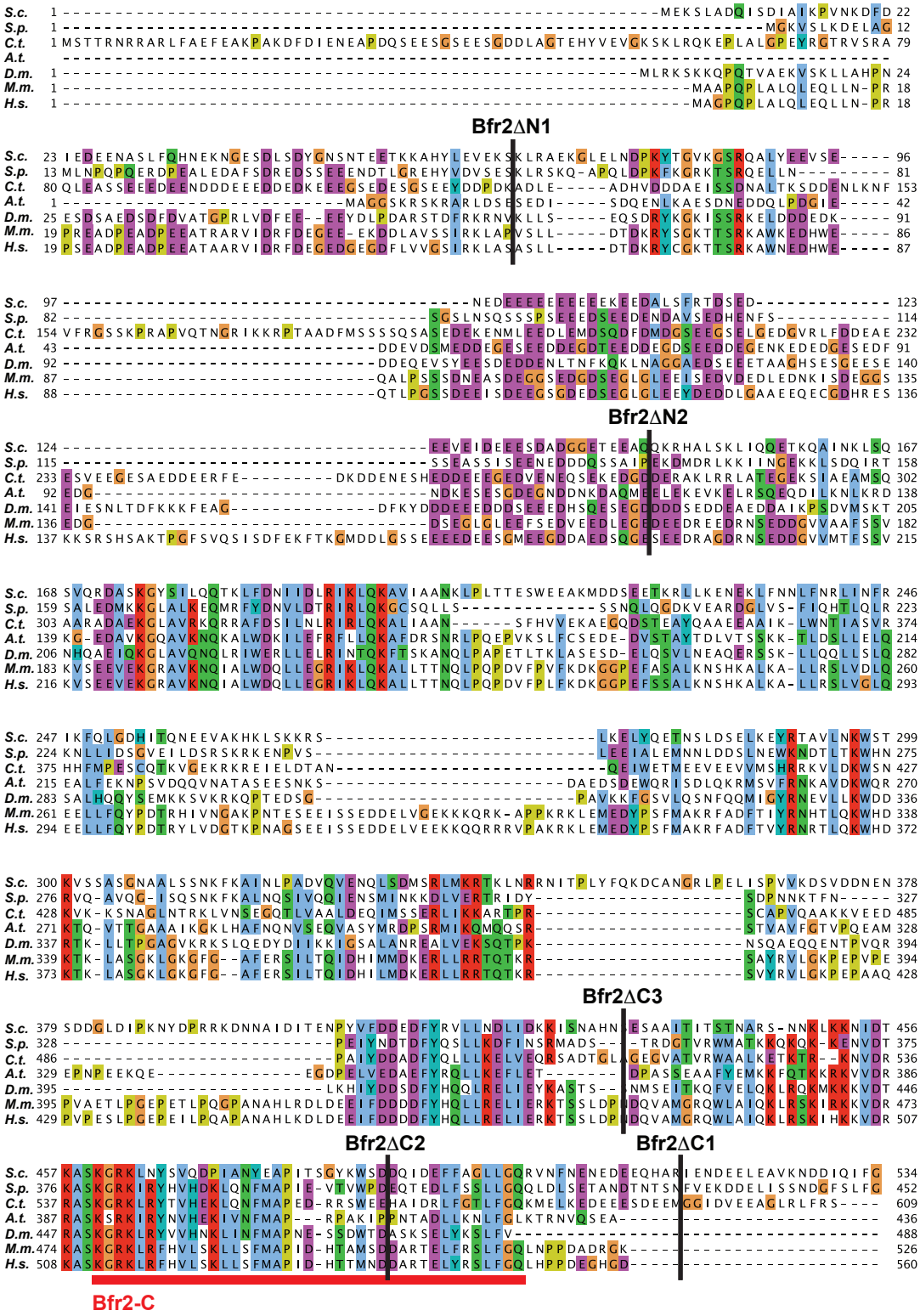
5. Supplemental Information



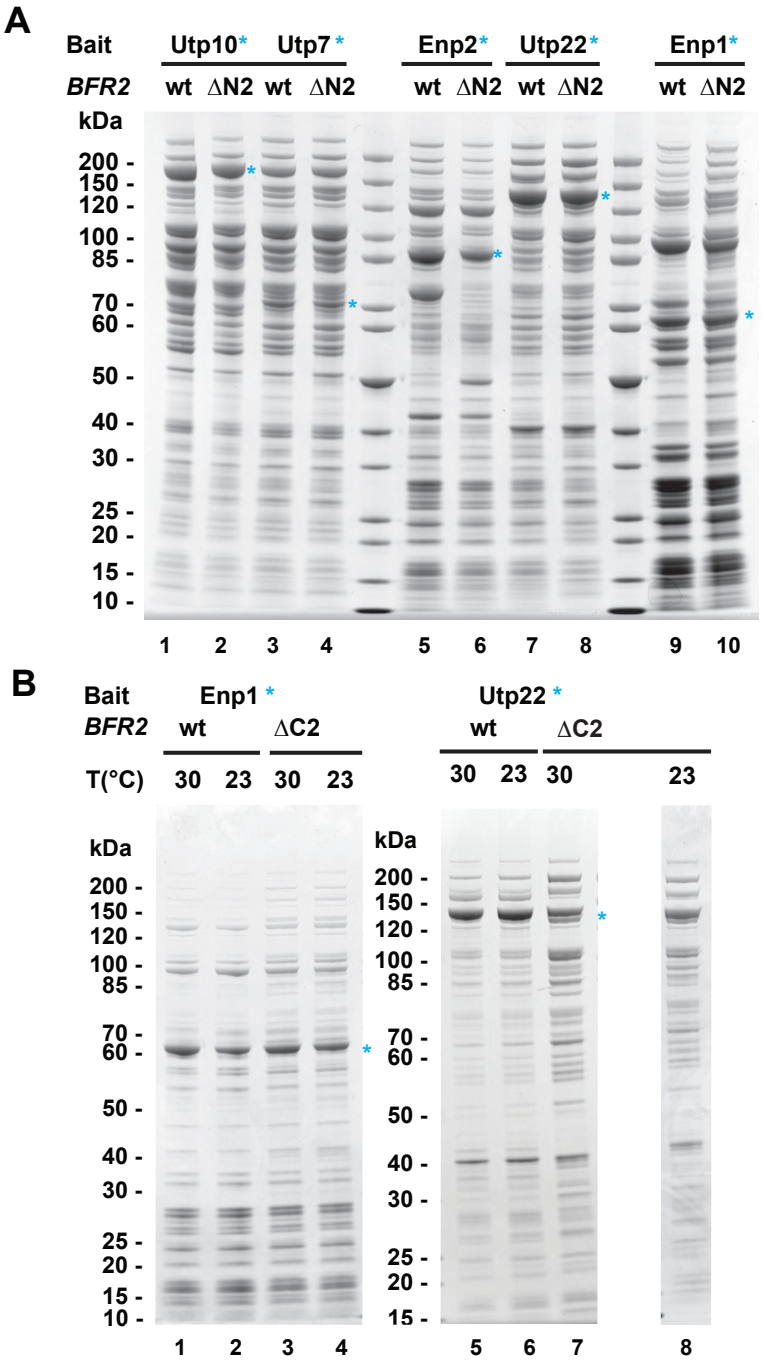
Supplemental Figure 5.1 Multiple sequence alignment of Krr1. Sequences were aligned with ClustalW and alignments visualized with Jalview. C-terminal truncation mutants are indicated as well as the secondary structure elements seen in state B2 from the *ct*90S and *sc*90S Cryo-EM models.*S.c. Saccharomyces cerevisiae, S.p. Schizosaccharomyces pombe, C.t. Chaetomium thermophilum, A.t. Arabidopsis thaliana, D.m. Drosophila melanogaster, M.m. Mus musculus, H.s. Homo sapiens*.



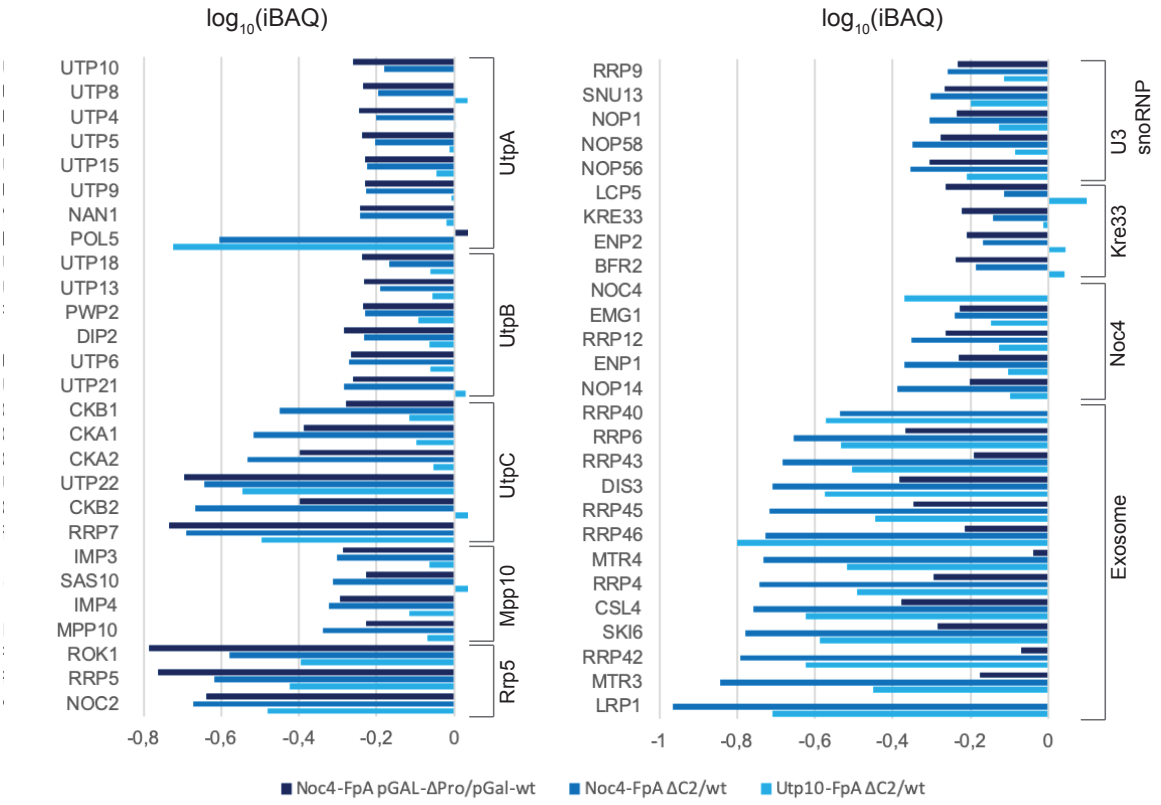
Supplemental Figure 5.2 Multiple sequence alignment of Enp2. Sequences were aligned with ClustalW and alignments visualized with Jalview. C-terminal truncation mutants are indicated as well as the ß-propellar seen in state B2 from the *ct*90S and *sc*90S Cryo-EM models. *S.c. Saccharomyces cerevisiae, S.p. Schizosaccharomyces pombe, C.t. Chaetomium thermophilum, A.t. Arabidopsis thaliana, D.m. Drosophila melanogaster, M.m. Mus musculus, H.s. Homo sapiens*.



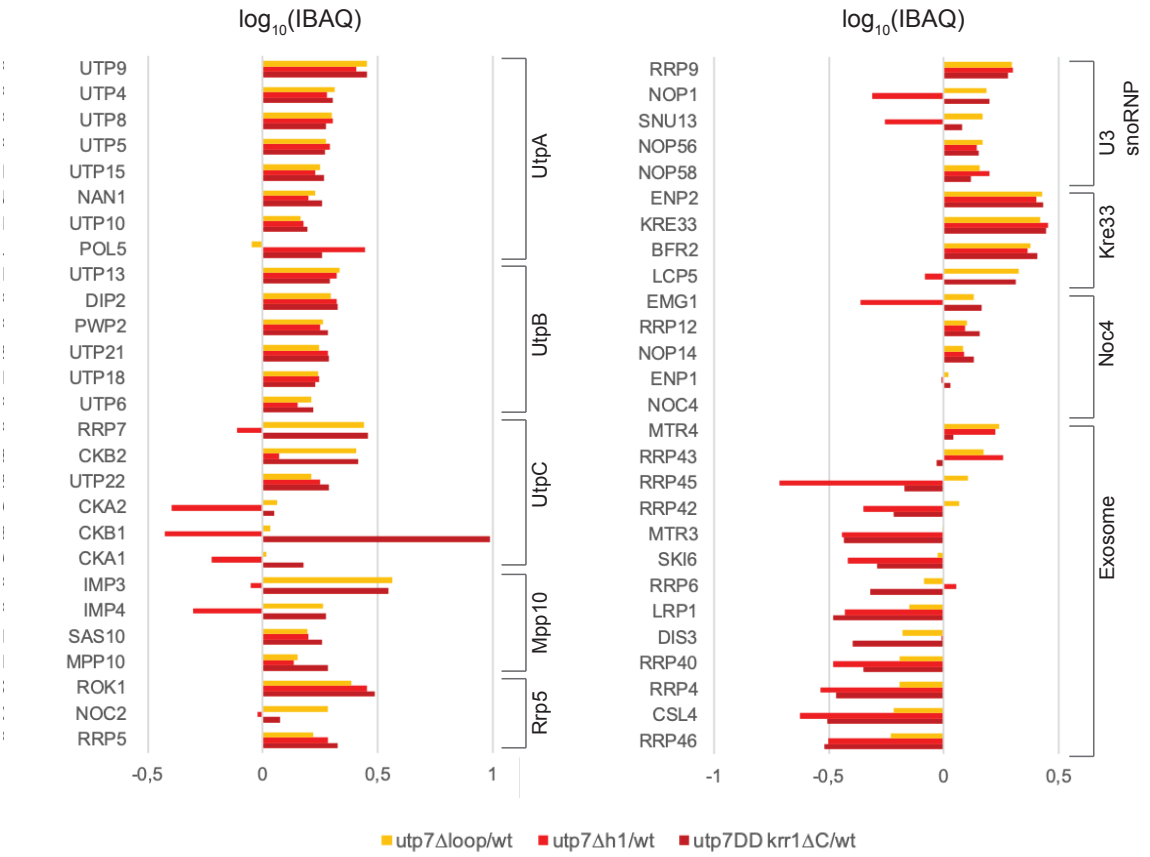
Supplemental Figure 5.3 Multiple sequence alignment of Bfr2. Sequences were aligned with ClustalW and alignments visualized with Jalview. N-terminal and C-terminal truncation mutants are indicated as well as the C-terminal fragment seen in state B2 from the *ct*90S and *sc*90S Cryo-EM models. *S.c. Saccharomyces cerevisiae, S.p. Schizosaccharomyces pombe, C.t. Chaetomium thermophilum, A.t. Arabidopsis thaliana, D.m. Drosophila melanogaster, M.m. Mus musculus, H.s. Homo sapiens*.



Supplemental Figure 5.4 Affinity-purification of pre-ribosomal particles from cells expressing different Bfr2 truncation mutants. (A) Biochemical analysis of proteins associated with different biogenesis factors in *bfr2*ΔN2 cells. Left panel: In the Δ*bfr2* shuffle strain background, the AFs Utp10, Utp7, Enp2, Utp22 and Enp1 were genomically tagged with FLAG-TEV-ProtA at the C-terminus. Bait proteins were purified from *BFR2* or *bfr2*ΔC2 cells. (B): Biochemical analysis of proteins associated with different biogenesis factors in *bfr2*ΔC2 cells. Enp1 and Utp22 were genomically tagged with FLAG-TEV-ProtA at the C-terminus. The bait proteins were purified from *BFR2* or *bfr2*ΔC2 cells. Cell cultures were grown at 30℃ or shifted to 23℃ for 10h. Bait proteins are indicated with an asterisk.



Supplemental Figure 5.5 Semi-quantitative mass spectrometry of 90S particles isolated via different TAP-tagged AFs from cells overexpressing *krr1*ΔPro or expressing *krr1*ΔC2. Intensity-based absolute quantification (iBAQ) values derived from mass spectrometry of final FLAG eluates were normalized to the bait protein. Shown are the log10(iBAQ) values of the ratios of mutant condition to the respective wt condition. Dark blue: Noc4 was C-terminally tagged with a FLAG-TEV-ProtA epitope and *krr1*ΔPro (pGAL-ΔPro) or *KRR1* (pGAL-wt) were overexpressed for 6h by the addition of 2% galactose to the growth medium. Blue: Noc4 was C-terminally tagged with a FLAG-TEV-ProtA epitope in a Δ*krr1* shuffle strain, which was then transformed with pRS314 containing either the wt or mutant *krr1*ΔC2 allele (ΔC2). Transformants were selected on SDC+5-FOA and cultured at 30℃. Cyan: Utp10 was C-terminally tagged with a FLAG-TEV-ProtA epitope in a Δ*krr1* shuffle strain, which was then transformed with pRS314 containing either the wt or mutant *krr1*ΔC2 allele (ΔC2). Transformants were selected on SDC+5-FOA and cultured at 30℃.



Supplemental Figure 5.6 Semi-quantitative mass spectrometry of 90S particles isolated via Noc4-FTpA in cells where the contact site of Krr1 and Utp7 is disturbed. Intensity-based absolute quantification (iBAQ) values derived from mass spectrometry of final FLAG eluates were normalized to the bait protein Noc4. Shown are the log10(iBAQ) values of the ratios of mutant condition to the wt condition. Noc4 was C-terminally tagged with a FLAG-TEV-ProtA epitope in a Δkrr1Δutp7 shuffle strain, which was then transformed with pRS314 containing different combinations of alleles of KRR1 and UTP7 as indicated. Transformants were selected on SDC+5-FOA and cultured at 30℃. Affinity purification was performed from KRR1 utp7Δloop cells (orange), KRR1 utp7Δh1 cells (red) or krr1ΔC utp7DD cells (dark red).

6. Appendix

6.1 List of Abbreviations

°C: degree Celsius

2D: two-dimensional

2µ: two-micron (high copy plasmid)

3D: three-dimensional

5-FOA: 5-fluoroorotic acid

Å: angstrom (10-10 m)

aa: amino acids

AF: assembly factor

Amp: ampicillin

ARS: autonomously replicating sequence

ATP: adenosine triphosphate

bp: basepairs

C-terminus: carboxy-terminus

C.t./Ct: Chaetomium thermophilum

CBP: calmodulin binding protein

cDNA: complementary DNA

CEN: 125bp centromeric DNA sequence

CP: central protuberance

CRAC: UV crosslinking and analysis of cDNA

CURI: CK2-Utp22-Rrp7-Ifh1 (complex)

DFC: dense fibrillar component (nucleolus)

DNA: deoxyribonucleic acid

DTT: dithiothreitol

EM: electron microscopy

ESs: expansion segments (rRNA)

ES6: expansion segment 6 (18S rRNA)

ETS: external transcribed spacer

FC: fibrillar center (nucleolus)

FTpA: Flag-TEV-ProteinA (tag)

GC: granular component (nucleolus)

GDP: guanosine diphosphate

GFP: green flourescent protein

GTP: guanosine triphosphate

HEAT: huntingtin, EF3, PP2A, TOR1 (motif)

His: histidine

iBAQ: intensity-based absolute quantification (mass spectrometry)

ITS: internal transcribed spacer

Kan: kanamycin

kDa: kilo-Dalton (10^3 Da)

KH: K-homology (domain)

LB: lysogeny broth (Escherichia coli medium)

Leu: leucine

LSU: large subunit (ribosome)

M: molar concentration (1 M = 1 mol/l)

MDa: mega-Dalton (10^6 Da)

mRNA: messenger RNA

MS: mass spectrometry

N-terminus: amino-terminus

NLS: nuclear localization sequence

nm: nanometer (10^{-9} m)

ns-EM: negative-stain EM

nt: nucleotides

ORF: open reading frame

ProtA: protein A

PCR: polymerase chain reaction

PDB: protein data bank

pGAL: galactose inducible promoter (yeast)

PIN: PilT N-terminus (domain)

Pol I: RNA polymerase I

PPI: protein-protein interaction

PTC: peptidyl transferase center

RecA: recombinase A-like

rDNA: ribosomal DNA/chromatin

RNA: ribonucleic acid

RNP: ribonucleoprotein particle

RPLs: ribosomal proteins of the large subunit

rpm: rounds per minute

R-proteins: ribosomal proteins

RPSs: ribosomal proteins of the small subunit

rRNA: ribosomal RNA

S: Svedberg unit (sedimentation rate)

S.c./Sc: Saccharomyces cerevisiae

SDC: synthetic yeast growth media (synthetic dextrose complete)

SDS-PAGE: sodium dodecyl sulfate polyacrylamide gel electrophoresis

Sec: second

snoRNA: small nucleolar RNA

SSU: small subunit(ribosome)

TAP: tandem-affinity purification

TAP-Flag: proteinA-TEV-CBP-Flag (tag)

TCA: trichloroacetic acid

TEV: tobacco etch virus (protease or cleavage site)

TORC1: target of rapamycin 1

tRNA: transfer RNA

Trp: tryptophan

Ura: uracil

Utp: U three protein

UV: ultraviolet

WD40: tryptophan-aspartic acid (W-D) motif

X-link: crosslink

xg: standard gravity (9.81 m/s2)

YPD: complete yeast growth media (yeast extract, peptone, dextrose)

YPG: complete yeast growth media (yeast extract, peptone, galactose)

6.2 List of Figures

Figure 1.1 Structural comparison of ribosomal subunits from a prokaryote and eukaryote…… ……..2

Figure 1.2 Overview of the ribosome biogenesis in eukaryotic cells ……..8

Figure 1.3 Visualization of pre-ribosomal 90S particles over the course of half a century ……..……..11

Figure 1.4 rRNA processing and folding during ribosome biogenesis in yeast ……..14

Figure 1.5 Structural depiction of ribosomal biogenesis in yeast ……..18

Figure 1.6 snoRNPs catalyze chemical modifications on pre-rRNA molecules……21

Figure 1.7 The 90S particle is mainly shaped by modules chaperoning the rRNA …..30

Figure 1.8 Major structural rearrangements of 18S pre-rRNA domain on the route from 90S pre-ribosomes to cytoplasmic pre-40S particles……34

Figure 2.1 Krr1 spans the 90S from head to toe…….……37

Figure 2.2 Structure based mutations of Krr1 show that its proline-rich region is essential……..39

Figure 2.3 C-terminal truncation mutants of Enp2 are viable and enp2ΔC cells exhibit a cold sensitive phenotype……41

Figure 2.4 Structure based mutations of Bfr2 show importance of wedge helix for Kre33 module assembly……43

Figure 2.5 Genetic interactions show link of Krr1 to head region via the C-terminus of Enp2……45

Figure 2.6 Enp2 C-terminus is linked to Krr1 via Krr1's helix tip which points to the interface between the C-terminus of Bfr2 and Enp2's ß-propeller……..47

Figure 2.7 Deletion of the C-terminus of Krr1 and Enp2 has an effect on 90S formation and maturation……49

Figure 2.8 Region between Krr1's KH1 domain and its C-helix is important for stabilization of the central platform domain……51

Figure 2.9 Mutations of Krr1 within the region contacting the central domain lead to depletion of Rrp5 and Utp22……52

Figure 2.10 Krr1 C-helix is genetically linked to Utp7 via a loop-loop interaction site..54

Figure 2.11 Mutations in the Krr1-Utp7 contact site cause defects in the progression of 90S maturation in *krr1*ΔC background……56

Figure 2.12 Mutations in the Krr1-Utp7 contact site lead to defects in A_1 processing of the 35S pre-rRNA in *krr1*ΔC background……58

Figure 3.1 Model highlighting the role of Krr1 in 90S biogenesis ……60

Figure 3.2 Sequential stable integration of the 5' domain and compaction of the 90S pre-ribosome visualized by a series of yeast cryo-EM models……..……..….62

Figure 3.3 Structural rearrangements occurring during and/or after A_1 cleavage…..67

Supplemental Figure 5.1 Multiple sequence alignment of Krr1……83

Supplemental Figure 5.2 Multiple sequence alignment of Enp2……..84

Supplemental Figure 5.3 Multiple sequence alignment of Bfr2……85

Supplemental Figure 5.4 Affinity-purified pre-ribosomal particles from cells expressing different Bfr2 truncation mutants……86

Supplemental Figure 5.5 Semi-quantitative mass spectrometry of 90S particles isolated via different TAP-tagged AFs from cells overexpressing *krr1*ΔPro or expressing *krr1*ΔC2……87

Supplemental Figure 5.6 Semi-quantitative mass spectrometry of 90S particles isolated via Noc4-FTpA in cells where the contact site of Krr1 and Utp7 is disturbed……88

6.3 Own Publications

1. **Fischer, P.***, Cheng, J.*, Baßler, J. *, Lau B., Kellner, N., Kunze, R., Griesel, S., Kallas, M., Berninghausen, O., Strauss, D., Beckmann, R., Hurt, E. Mol Cell 75, 1256-1269. doi: 10.1016/j.molcel.2019.06.032

**Co-sharing first authorships*.

7. References

Ahmad, Y., Boisvert, F. M., Gregor, P., Cobley, A., & Lamond, A. I. (2009). NOPdb: Nucleolar Proteome Database--2008 update. *Nucleic Acids Res, 37*(Database issue), D181-184. doi:10.1093/nar/gkn804

Albert, B., Knight, B., Merwin, J., Martin, V., Ottoz, D., Gloor, Y., . . . Shore, D. (2016). A Molecular Titration System Coordinates Ribosomal Protein Gene Transcription with Ribosomal RNA Synthesis. *Mol Cell, 64*(4), 720-733. doi:10.1016/j.molcel.2016.10.003

Albert, B., Kos-Braun, I. C., Henras, A. K., Dez, C., Rueda, M. P., Zhang, X., . . . Shore, D. (2019). A ribosome assembly stress response regulates transcription to maintain proteome homeostasis. *Elife, 8*. doi:ARTN e45002

10.7554/eLife.45002

Allmang, C., Kufel, J., Chanfreau, G., Mitchell, P., Petfalski, E., & Tollervey, D. (1999). Functions of the exosome in rRNA, snoRNA and snRNA synthesis. *EMBO J., 18*(19), 5399-5410.

Allmang, C., Mitchell, P., Petfalski, E., & Tollervey, D. (2000). Degradation of ribosomal RNA precursors by the exosome. *Nucl. Acid Res., 28*, 1648-1691.

Altschul, S. F., Gish, W., Miller, W., Myers, E. W., & Lipman, D. J. (1990). Basic local alignment search tool. *J Mol Biol, 215*(3), 403-410. doi:10.1016/S0022-2836(05)80360-2

Balakin, A. G., Smith, L., & Fournier, M. J. (1996). The RNA world of the nucleolus: Two major families of small RNAs defined by different box elements with related functions. *Cell, 86*, 823-834.

Bally, M., Hughes, J., & Cesareni, G. (1988). SnR30: a new, essential small nuclear RNA from Saccharomyces cerevisiae. *Nucleic Acids Res, 16*(12), 5291-5303. Retrieved from https://www.ncbi.nlm.nih.gov/pubmed/2898766

Bammert, L., Jonas, S., Ungricht, R., & Kutay, U. (2016). Human AATF/Che-1 forms a nucleolar protein complex with NGDN and NOL10 required for 40S ribosomal subunit synthesis. *Nucleic Acids Res, 44*(20), 9803-9820. doi:10.1093/nar/gkw790

Barandun, J., Chaker-Margot, M., Hunziker, M., Molloy, K. R., Chait, B. T., & Klinge, S. (2017). The complete structure of the small-subunit processome. *Nat Struct Mol Biol, 24*(11), 944-953. doi:10.1038/nsmb.3472

Bassler, J., Ahmed, Y. L., Kallas, M., Kornprobst, M., Calvino, F. R., Gnadig, M., . . . Hurt, E. (2017). Interaction network of the ribosome assembly machinery from a eukaryotic thermophile. *Protein science : a publication of the Protein Society, 26*(2), 327-342. doi:10.1002/pro.3085

Bassler, J., Grandi, P., Gadal, O., Leßmann, T., Tollervey, D., Lechner, J., & Hurt, E. C. (2001). Identification of a 60S pre-ribosomal particle that is closely linked to nuclear export. *Mol. Cell, 8*, 517-529.

Bassler, J., & Hurt, E. (2018). Eukaryotic Ribosome Assembly. *Annu Rev Biochem*. doi:10.1146/annurev-biochem-013118-110817

Belhabich-Baumas, K., Joret, C., Jady, B. E., Plisson-Chastang, C., Shayan, R., Klopp, C., . . . Mougin, A. (2017). The Rio1p ATPase hinders premature entry into translation of late pre-40S pre-ribosomal particles. *Nucleic Acids Res, 45*(18), 10824-10836. doi:10.1093/nar/gkx734

Bellodi, C., Kopmar, N., & Ruggero, D. (2010). Deregulation of oncogene-induced senescence and p53 translational control in X-linked dyskeratosis congenita. *EMBO J, 29*(11), 1865-1876. doi:10.1038/emboj.2010.83

Bellodi, C., Krasnykh, O., Haynes, N., Theodoropoulou, M., Peng, G., Montanaro, L., & Ruggero, D. (2010). Loss of function of the tumor suppressor DKC1 perturbs p27 translation control and contributes to pituitary tumorigenesis. *Cancer Res, 70*(14), 6026-6035. doi:10.1158/0008-5472.CAN-09-4730

Beltrame, M., Henry, Y., & Tollervey, D. (1994). Mutational analysis of an essential binding site for the U3 snoRNA in the 5' external transcribed spacer of yeast pre-rRNA. *Nucleic Acids Res., 22*, 5139-5147.

Beltrame, M., & Tollervey, D. (1992). Identification and functional analysis of two U3 binding sites on yeast pre-ribosomal RNA. *EMBO J, 11*(4), 1531-1542. Retrieved from https://www.ncbi.nlm.nih.gov/pubmed/1563354

Ben-Shem, A., Garreau de Loubresse, N., Melnikov, S., Jenner, L., Yusupova, G., & Yusupov, M. (2011). The structure of the eukaryotic ribosome at 3.0 A resolution. *Science, 334*(6062), 1524-1529. doi:10.1126/science.1212642

Ben-Shem, A., Jenner, L., Yusupova, G., & Yusupov, M. (2010). Crystal structure of the eukaryotic ribosome. *Science, 330*(6008), 1203-1209. doi:10.1126/science.1194294

Bernstein, K. A., Gallagher, J. E., Mitchell, B. M., Granneman, S., & Baserga, S. J. (2004). The small-subunit processome is a ribosome assembly intermediate. *Eukaryot Cell, 3*(6), 1619-1626. doi:3/6/1619 [pii]

10.1128/EC.3.6.1619-1626.2004

Bernstein, K. A., Granneman, S., Lee, A. V., Manickam, S., & Baserga, S. J. (2006). Comprehensive mutational analysis of yeast DEXD/H box RNA helicases involved in large ribosomal subunit biogenesis. *Mol Cell Biol, 26*(4), 1195-1208. doi:26/4/1195 [pii]

10.1128/MCB.26.4.1195-1208.2006

Berto, G., Ferreira-Cerca, S., & De Wulf, P. (2019). The Rio1 protein kinases/ATPases: conserved regulators of growth, division, and genomic stability. *Curr Genet, 65*(2), 457-466. doi:10.1007/s00294-018-0912-y

Bleichert, F., Granneman, S., Osheim, Y. N., Beyer, A. L., & Baserga, S. J. (2006). The PINc domain protein Utp24, a putative nuclease, is required for the early cleavage steps in 18S rRNA maturation. *Proc Natl Acad Sci U S A, 103*(25), 9464-9469. doi:10.1073/pnas.0603673103

Bohnsack, M. T., Kos, M., & Tollervey, D. (2008). Quantitative analysis of snoRNA association with pre-ribosomes and release of snR30 by Rok1 helicase. *EMBO Rep, 9*(12), 1230-1236. doi:embor2008184 [pii]

10.1038/embor.2008.184

Bohnsack, M. T., Martin, R., Granneman, S., Ruprecht, M., Schleiff, E., & Tollervey, D. (2009). Prp43 bound at different sites on the Pre-rRNA performs distinct functions in ribosome synthesis. *Mol Cell, 36*(4), 583-592. doi:S1097-2765(09)00699-6 [pii]

10.1016/j.molcel.2009.09.039

Bond, A. T., Mangus, D. A., He, F., & Jacobson, A. (2001). Absence of Dbp2p alters both nonsense-mediated mRNA decay and rRNA processing. *Mol Cell Biol, 21*(21), 7366-7379. doi:10.1128/MCB.21.21.7366-7379.2001

Bowman, J. C., Petrov, A. S., Frenkel-Pinter, M., Penev, P. I., & Williams, L. D. (2020). Root of the Tree: The Significance, Evolution, and Origins of the Ribosome. *Chemical Reviews, 120*(11), 4848-4878. doi:10.1021/acs.chemrev.9b00742

Braun, C. M., Hackert, P., Schmid, C. E., Bohnsack, M. T., Bohnsack, K. E., & Perez-Fernandez, J. (2020). Pol5 is required for recycling of small subunit biogenesis factors and for

formation of the peptide exit tunnel of the large ribosomal subunit. *Nucleic Acids Res, 48*(1), 405-420. doi:10.1093/nar/gkz1079

Briggs, M. W., Burkard, K. T. D., & Butler, J. S. (1998). Rrp6p, the yeast homologue of the human PM-Scl 100-kDa autoantigen, is essential for efficient 5.8 S rRNA 3 ' end formation. *Journal of Biological Chemistry, 273*(21), 13255-13263. doi:DOI 10.1074/jbc.273.21.13255

Britton, R. A. (2009). Role of GTPases in bacterial ribosome assembly. *Annu Rev Microbiol, 63*, 155-176. doi:10.1146/annurev.micro.091208.073225

Brown, E. D. (2005). Conserved P-loop GTPases of unknown function in bacteria: an emerging and vital ensemble in bacterial physiology. *Biochem Cell Biol, 83*(6), 738-746. doi:10.1139/o05-162

Burger, F., Daugeron, M. C., & Linder, P. (2000). Dbp10p, a putative RNA helicase from Saccharomyces cerevisiae, is required for ribosome biogenesis. *Nucleic Acids Res., 28*(12), 2315-2323.

Calvino, F. R., Kharde, S., Ori, A., Hendricks, A., Wild, K., Kressler, D., . . . Sinning, I. (2015). Symportin 1 chaperones 5S RNP assembly during ribosome biogenesis by occupying an essential rRNA-binding site. *Nat Commun, 6*, 6510. doi:10.1038/ncomms7510

Chaker-Margot, M., Barandun, J., Hunziker, M., & Klinge, S. (2017). Architecture of the yeast small subunit processome. *Science, 355*(6321). doi:10.1126/science.aal1880

Chaker-Margot, M., Hunziker, M., Barandun, J., Dill, B. D., & Klinge, S. (2015). Stage-specific assembly events of the 6-MDa small-subunit processome initiate eukaryotic ribosome biogenesis. *Nat Struct Mol Biol, 22*(11), 920-923. doi:10.1038/nsmb.3111

Chamberlain, J. R., Lee, Y., Lane, W. S., & Engelke, D. R. (1998). Purification and characterization of the nuclear RNase P holoenzyme complex reveals extensive subunit overlap with RNase MRP. *Genes Dev, 12*(11), 1678-1690. doi:10.1101/gad.12.11.1678

Champion, E. A., Lane, B. H., Jackrel, M. E., Regan, L., & Baserga, S. J. (2008). A direct interaction between the Utp6 half-a-tetratricopeptide repeat domain and a specific peptide in Utp21 is essential for efficient pre-rRNA processing. *Mol Cell Biol, 28*(21), 6547-6556. doi:10.1128/MCB.00906-08

Champney, W. S. (1977). Kinetics of ribosome synthesis during a nutritional shift-up in Escherischia coli K-12. *Mol Gen Genet, 152*(3), 259-266. doi:10.1007/BF00693079

Charette, J. M., & Baserga, S. J. (2010). The DEAD-box RNA helicase-like Utp25 is an SSU processome component. *RNA, 16*(11), 2156-2169. doi:10.1261/rna.2359810

Cheng, J., Bassler, J., Fischer, P., Lau, B., Kellner, N., Kunze, R., . . . Hurt, E. (2019). Thermophile 90S Pre-ribosome Structures Reveal the Reverse Order of Co-transcriptional 18S rRNA Subdomain Integration. *Mol Cell, 75*(6), 1256-1269 e1257. doi:10.1016/j.molcel.2019.06.032

Cheng, J., Lau, B., La Venuta, G., Ameismeier, M., Berninghausen, O., Hurt, E., & Beckmann, R. (2020). 90S pre-ribosome transformation into the primordial 40S subunit. *Science, 369*(6510), 1470-1476. doi:10.1126/science.abb4119

Cheng, Y. F. (2015). Single-Particle Cryo-EM at Crystallographic Resolution. *Cell, 161*(3), 450-457. doi:10.1016/j.cell.2015.03.049

Cheutin, T., O'Donohue, M. F., Beorchia, A., Vandelaer, M., Kaplan, H., Defever, B., . . . Thiry, M. (2002). Three-dimensional organization of active rRNA genes within the nucleolus. *J Cell Sci, 115*(Pt 16), 3297-3307. Retrieved from https://www.ncbi.nlm.nih.gov/pubmed/12140261

Chimnaronk, S., Suzuki, T., Manita, T., Ikeuchi, Y., Yao, M., Suzuki, T., & Tanaka, I. (2009). RNA helicase module in an acetyltransferase that modifies a specific tRNA anticodon. *EMBO J, 28*(9), 1362-1373. doi:10.1038/emboj.2009.69

Choque, E., Marcellin, M., Burlet-Schiltz, O., Gadal, O., & Dez, C. (2011). The nucleolar protein Nop19p interacts preferentially with Utp25p and Dhr2p and is essential for the production of the 40S ribosomal subunit in Saccharomyces cerevisiae. *RNA Biol, 8*(6), 1158-1172. doi:10.4161/rna.8.6.17699

Choque, E., Schneider, C., Gadal, O., & Dez, C. (2018). Turnover of aberrant pre-40S pre-ribosomal particles is initiated by a novel endonucleolytic decay pathway. *Nucleic Acids Res, 46*(9), 4699-4714. doi:10.1093/nar/gky116

Combs, D. J., Nagel, R. J., Ares, M., Jr., & Stevens, S. W. (2006). Prp43p is a DEAH-box spliceosome disassembly factor essential for ribosome biogenesis. *Mol Cell Biol, 26*(2), 523-534. doi:26/2/523 [pii]

10.1128/MCB.26.2.523-534.2006

Connolly, K., & Culver, G. (2009). Deconstructing ribosome construction. *Trends Biochem Sci, 34*(5), 256-263. doi:10.1016/j.tibs.2009.01.011

Correll, C. C., Bartek, J., & Dundr, M. (2019). The Nucleolus: A Multiphase Condensate Balancing Ribosome Synthesis and Translational Capacity in Health, Aging and Ribosomopathies. *Cells, 8*(8). doi:10.3390/cells8080869

Cote, C. A., Greer, C. L., & Peculis, B. A. (2002). Dynamic conformational model for the role of ITS2 in pre-rRNA processing in yeast. *RNA, 8*, 786-797.

Cox, J., & Mann, M. (2008). MaxQuant enables high peptide identification rates, individualized p.p.b.-range mass accuracies and proteome-wide protein quantification. *Nat Biotechnol, 26*(12), 1367-1372. doi:10.1038/nbt.1511

Davis, J. H., & Williamson, J. R. (2017). Structure and dynamics of bacterial ribosome biogenesis. *Philosophical Transactions of the Royal Society B-Biological Sciences, 372*(1716). doi:ARTN 20160181

10.1098/rstb.2016.0181

de la Cruz, J., Gomez-Herreros, F., Rodriguez-Galan, O., Begley, V., de la Cruz Munoz-Centeno, M., & Chavez, S. (2018). Feedback regulation of ribosome assembly. *Curr Genet, 64*(2), 393-404. doi:10.1007/s00294-017-0764-x

De la Cruz, J., Kressler, D., Rojo, M., Tollervey, D., & Linder, P. (1998). Spb4p, an essential putative RNA helicase, is required for a late step in the assembly of 60S ribosomal subunits in Saccharomyces cerevisiae. *RNA, 4*(10), 1268-1281. Retrieved from http://www.ncbi.nlm.nih.gov/entrez/query.fcgi?cmd=Retrieve&db=PubMed&dopt=Citation&list_uids=9769101

De Zoysa, M. D., & Yu, Y. T. (2017). Posttranscriptional RNA Pseudouridylation. *Enzymes, 41*, 151-167. doi:10.1016/bs.enz.2017.02.001

Decatur, W. A., & Fournier, M. J. (2002). rRNA modifications and ribosome function. *Trends Biochem Sci, 27*(7), 344-351. doi:10.1016/s0968-0004(02)02109-6

Decatur, W. A., Liang, X. H., Piekna-Przybylska, D., & Fournier, M. J. (2007). Identifying effects of snoRNA-guided modifications on the synthesis and function of the yeast ribosome. *Rna Modification, 425*, 283-+. doi:10.1016/S0076-6879(07)25013-X

Dechampesme, A. M., Koroleva, O., Leger-Silvestre, I., Gas, N., & Camier, S. (1999). Assembly of 5S ribosomal RNA is required at a specific step of the pre-rRNA processing pathway. *J.Cell Biol., 145*(7), 1369-1380.

Dennis, P. P., Ehrenberg, M., & Bremer, H. (2004). Control of rRNA synthesis in Escherichia coli: a systems biology approach. *Microbiol Mol Biol Rev, 68*(4), 639-668. doi:10.1128/MMBR.68.4.639-668.2004

Deshmukh, M., Stark, J., Yeh, L. C., Lee, J. C., & Woolford, J. L., Jr. (1995). Multiple regions of yeast ribosomal protein L1 are important for its interaction with 5 S rRNA and assembly into ribosomes. *J Biol Chem, 270*(50), 30148-30156. Retrieved from http://www.ncbi.nlm.nih.gov/entrez/query.fcgi?cmd=Retrieve&db=PubMed&dopt=Citation&list_uids=8530422

Deshmukh, M., Tsay, Y. F., Paulovich, A. G., & Woolford, J. L., Jr. (1993). Yeast ribosomal protein L1 is required for the stability of newly synthesized 5S rRNA and the assembly of 60S ribosomal subunits. *Mol Cell Biol, 13*(5), 2835-2845. doi:10.1128/mcb.13.5.2835

Dosil, M., & Bustelo, X. R. (2004). Functional characterization of Pwp2, a WD family protein essential for the assembly of the 90 S pre-ribosomal particle. *J Biol Chem, 279*(36), 37385-37397. doi:10.1074/jbc.M404909200

Dragon, F., Gallagher, J. E., Compagnone-Post, P. A., Mitchell, B. M., Porwancher, K. A., Wehner, K. A., . . . Baserga, S. J. (2002). A large nucleolar U3 ribonucleoprotein required for 18S ribosomal RNA biogenesis. *Nature, 417*, 967-970. Retrieved from 0

Drygin, D., Rice, W. G., & Grummt, I. (2010). The RNA polymerase I transcription machinery: an emerging target for the treatment of cancer. *Annu Rev Pharmacol Toxicol, 50*, 131-156. doi:10.1146/annurev.pharmtox.010909.105844

Dunbar, D. A., Wormsley, S., Agentis, T. M., & Baserga, S. J. (1997). Mpp10p, a U3 small nucleolar ribonucleoprotein component required for pre-18S rRNA processing in yeast. *Mol.Cell.Biol., 17*, 5803-5812.

Ebersberger, I., Simm, S., Leisegang, M. S., Schmitzberger, P., Mirus, O., von Haeseler, A., . . . Schleiff, E. (2014). The evolution of the ribosome biogenesis pathway from a yeast perspective. *Nucleic Acids Res, 42*(3), 1509-1523. doi:10.1093/nar/gkt1137

El Hage, A., Koper, M., Kufel, J., & Tollervey, D. (2008). Efficient termination of transcription by RNA polymerase I requires the 5 ' exonuclease Rat1 in yeast. *Genes & Development, 22*(8), 1069-1081. doi:10.1101/gad.463708

Emery, B., De la Cruz, J., Rocak, S., Deloche, O., & Linder, P. (2004). Has1p, a member of the DEAD-box family, is required for 40S ribosomal subunit biogenesis in Saccharomyces cerevisiae. *Mol Microbiol, 52*(1), 141-158. doi:10.1111/j.1365-2958.2003.03973.x
MMI3973 [pii]

Esguerra, J., Warringer, J., & Blomberg, A. (2008). Functional importance of individual rRNA 2'-O-ribose methylations revealed by high-resolution phenotyping. *RNA, 14*(4), 649-656. doi:10.1261/rna.845808

Espinar-Marchena, F. J., Babiano, R., & Cruz, J. (2017). Placeholder factors in ribosome biogenesis: please, pave my way. *Microb Cell, 4*(5), 144-168. doi:10.15698/mic2017.05.572

Faber, A. W., Van Dijk, M., Raue, H. A., & Vos, J. C. (2002). Ng12p is a Ccr4p-like RNA nuclease essential for the final step in 3'-end processing of 5.8S rRNA in Saccharomyces cerevisiae. *RNA, 8*(9), 1095-1101. doi:10.1017/S1355838202021027

Fatica, A., Oeffinger, M., Dlakic, M., & Tollervey, D. (2003). Nob1p is required for cleavage of the 3' end of 18S rRNA. *Mol Cell Biol, 23*(5), 1798-1807. Retrieved from http://www.ncbi.nlm.nih.gov/entrez/query.fcgi?cmd=Retrieve&db=PubMed&dopt=Citation&list_uids=12588997

Fayet-Lebaron, E., Atzorn, V., Henry, Y., & Kiss, T. (2009). 18S rRNA processing requires base pairings of snR30 H/ACA snoRNA to eukaryote-specific 18S sequences. *EMBO J, 28*(9), 1260-1270. doi:10.1038/emboj.2009.79

Ferreira-Cerca, S., Kiburu, I., Thomson, E., LaRonde, N., & Hurt, E. (2014). Dominant Rio1 kinase/ATPase catalytic mutant induces trapping of late pre-40S biogenesis factors in 80S-like ribosomes. *Nucleic Acids Res, 42*(13), 8635-8647. doi:10.1093/nar/gku542

Ferreira-Cerca, S., Poll, G., Gleizes, P. E., Tschochner, H., & Milkereit, P. (2005). Roles of Eukaryotic Ribosomal Proteins in Maturation and Transport of Pre-18S rRNA and Ribosome Function. *Mol Cell, 20*(2), 263-275. Retrieved from http://www.ncbi.nlm.nih.gov/entrez/query.fcgi?cmd=Retrieve&db=PubMed&dopt=Citation&list_uids=16246728

Ferreira-Cerca, S., Poll, G., Kuhn, H., Neueder, A., Jakob, S., Tschochner, H., & Milkereit, P. (2007). Analysis of the in vivo assembly pathway of eukaryotic 40S ribosomal proteins. *Molecular Cell, 28*(3), 446-457. doi:10.1016/j.molcel.2007.09.029

Fischer, N., Neumann, P., Konevega, A. L., Bock, L. V., Ficner, R., Rodnina, M. V., & Stark, H. (2015). Structure of the E. coli ribosome-EF-Tu complex at <3 A resolution by Cs-corrected cryo-EM. *Nature, 520*(7548), 567-570. doi:10.1038/nature14275

Fischer, U., Schauble, N., Schutz, S., Altvater, M., Chang, Y., Faza, M. B., & Panse, V. G. (2015). A non-canonical mechanism for Crm1-export cargo complex assembly. *Elife, 4*. doi:10.7554/eLife.05745

Fox, G. E. (2010). Origin and Evolution of the Ribosome. *Cold Spring Harbor Perspectives in Biology, 2*(9). doi:ARTN a003483

10.1101/cshperspect.a003483

Gallagher, J. E., Dunbar, D. A., Granneman, S., Mitchell, B. M., Osheim, Y., Beyer, A. L., & Baserga, S. J. (2004). RNA polymerase I transcription and pre-rRNA processing are linked by specific SSU processome components. *Genes Dev, 18*(20), 2506-2517. doi:18/20/2506 [pii]

10.1101/gad.1226604

Gallagher, J. E. G. (2019). Proteins and RNA sequences required for the transition of the t-Utp complex into the SSU processome. *FEMS Yeast Res, 19*(1). doi:10.1093/femsyr/foy120

Gallesio, J. D., Hackert, P., Bohnsack, K. E., & Bohnsack, M. T. (2020). Sgd1 is an MIF4G domain-containing cofactor of the RNA helicase Fal1 and associates with the 5' domain of the 18S rRNA sequence. *RNA Biol, 17*(4), 539-553. doi:10.1080/15476286.2020.1716540

Gamalinda, M., Ohmayer, U., Jakovljevic, J., Kumcuoglu, B., Woolford, J., Mbom, B., . . . Woolford, J. L., Jr. (2014). A hierarchical model for assembly of eukaryotic 60S ribosomal subunit domains. *Genes Dev, 28*(2), 198-210. doi:10.1101/gad.228825.113

Gasse, L., Flemming, D., & Hurt, E. (2015). Coordinated Ribosomal ITS2 RNA Processing by the Las1 Complex Integrating Endonuclease, Polynucleotide Kinase, and Exonuclease Activities. *Mol Cell, 60*(5), 808-815. doi:10.1016/j.molcel.2015.10.021

Gaviraghi, M., Vivori, C., & Tonon, G. (2019). How Cancer Exploits Ribosomal RNA Biogenesis: A Journey beyond the Boundaries of rRNA Transcription. *Cells, 8*(9). doi:10.3390/cells8091098

Gelperin, D., Horton, L., Beckman, J., Hensold, J., & Lemmon, S. K. (2001). Bms1p, a novel GTP-binding protein, and the related Tsr1p are required for distinct steps of 40S ribosome biogenesis in yeast. *RNA, 7*, 1268-1283.

Gerczei, T., & Correll, C. C. (2004). Imp3p and Imp4p mediate formation of essential U3-precursor rRNA (pre-rRNA) duplexes, possibly to recruit the small subunit processome to the pre-rRNA. *Proceedings of the National Academy of Sciences of the United States of America, 101*(43), 15301-15306. doi:10.1073/pnas.0406819101

Gerczei, T., Shah, B. N., Manzo, A. J., Walter, N. G., & Correll, C. C. (2009). RNA chaperones stimulate formation and yield of the U3 snoRNA-Pre-rRNA duplexes needed for eukaryotic ribosome biogenesis. *Journal of molecular biology, 390*(5), 991-1006. doi:10.1016/j.jmb.2009.05.072

Golomb, L., Volarevic, S., & Oren, M. (2014). p53 and ribosome biogenesis stress: the essentials. *FEBS Lett, 588*(16), 2571-2579. doi:10.1016/j.febslet.2014.04.014

Grandi, P., Rybin, V., Bassler, J., Petfalski, E., Strauss, D., Marzioch, M., . . . Hurt, E. (2002). 90S pre-ribosomes include the 35S pre-rRNA, the U3 snoRNP, and 40S subunit processing factors but predominantly lack 60S synthesis factors. *Mol. Cell, 10*, 105-115.

Granneman, S., & Baserga, S. J. (2004). Ribosome biogenesis: of knobs and RNA processing. *Exp Cell Res, 296*(1), 43-50. Retrieved from http://www.ncbi.nlm.nih.gov/entrez/query.fcgi?cmd=Retrieve&db=PubMed&dopt=Citation&list_uids=15120992

Granneman, S., & Baserga, S. J. (2005). Crosstalk in gene expression: coupling and co-regulation of rDNA transcription, pre-ribosome assembly and pre-rRNA processing. *Curr Opin Cell Biol, 17*(3), 281-286. Retrieved from http://www.ncbi.nlm.nih.gov/entrez/query.fcgi?cmd=Retrieve&db=PubMed&dopt=Citation&list_uids=15901498

Granneman, S., Lin, C., Champion, E. A., Nandineni, M. R., Zorca, C., & Baserga, S. J. (2006). The nucleolar protein Esf2 interacts directly with the DExD/H box RNA helicase, Dbp8, to stimulate ATP hydrolysis. *Nucleic Acids Res, 34*(10), 3189-3199. doi:34/10/3189 [pii]

10.1093/nar/gkl419

Granneman, S., Petfalski, E., & Tollervey, D. (2011). A cluster of ribosome synthesis factors regulate pre-rRNA folding and 5.8S rRNA maturation by the Rat1 exonuclease. *The EMBO journal, 30*(19), 4006-4019. doi:10.1038/emboj.2011.256

Harnpicharnchai, P., Jakovljevic, J., Horsey, E., Miles, T., Roman, J., Rout, M., . . . Woolford, J. L. (2001). Composition and functional characterization of yeast 66s ribosome assembly intermediates. *Mol. Cell, 8*, 505-515.

Held, W. A., Mizushima, S., & Nomura, M. (1973). Reconstitution of Escherichia-Coli 30 S Ribosomal-Subunits from Purified Molecular Components. *Journal of Biological Chemistry, 248*(16), 5720-5730. Retrieved from <Go to ISI>://WOS:A1973Q550400025

Henras, A. K., Bertrand, E., & Chanfreau, G. (2004). A cotranscriptional model for 3 '-end processing of the Saccharomyces cerevisiae pre-ribosomal RNA precursor. *RNA, 10*(10), 1572-1585. doi:10.1261/rna.7750804

Henry, Y., Wood, H., Morrissey, J. P., Petfalski, E., Kearsey, S., & Tollervey, D. (1994). The 5' end of yeast 5.8S rRNA is generated by exonucleases from an upstream cleavage site. *EMBO J., 13*, 2452-2463.

Heuer, A., Thomson, E., Schmidt, C., Berninghausen, O., Becker, T., Hurt, E., & Beckmann, R. (2017). Cryo-EM structure of a late pre-40S ribosomal subunit from Saccharomyces cerevisiae. *Elife, 6*. doi:10.7554/eLife.30189

Hierlmeier, T., Merl, J., Sauert, M., Perez-Fernandez, J., Schultz, P., Bruckmann, A., . . . Tschochner, H. (2013). Rrp5p, Noc1p and Noc2p form a protein module which is part of early large ribosomal subunit precursors in S. cerevisiae. *Nucleic Acids Res, 41*(2), 1191-1210. doi:10.1093/nar/gks1056

Hilbert, M., Karow, A. R., & Klostermeier, D. (2009). The mechanism of ATP-dependent RNA unwinding by DEAD box proteins. *Biol Chem, 390*(12), 1237-1250. doi:10.1515/BC.2009.135

Hoang, T., Peng, W. T., Vanrobays, E., Krogan, N., Hiley, S., Beyer, A. L., . . . Lafontaine, D. L. (2005). Esf2p, a U3-associated factor required for small-subunit processome assembly and compaction. *Mol Cell Biol, 25*(13), 5523-5534. doi:25/13/5523 [pii]
10.1128/MCB.25.13.5523-5534.2005

Hodnett, J. L., & Busch, H. (1968). Isolation and characterization of uridylic acid-rich 7 S ribonucleic acid of rat liver nuclei. *J Biol Chem, 243*(24), 6334-6342. Retrieved from https://www.ncbi.nlm.nih.gov/pubmed/5726890

Horn, D. M., Mason, S. L., & Karbstein, K. (2011). Rcl1 protein, a novel nuclease for 18 S ribosomal RNA production. *J Biol Chem, 286*(39), 34082-34087. doi:10.1074/jbc.M111.268649

Houseley, J., & Tollervey, D. (2006). Yeast Trf5p is a nuclear poly(A) polymerase. *EMBO Rep, 7*(2), 205-211. doi:7400612 [pii]
10.1038/sj.embor.7400612

Hughes, J. M., & Ares, M., Jr. (1991). Depletion of U3 small nucleolar RNA inhibits cleavage in the 5' external transcribed spacer of yeast pre-ribosomal RNA and impairs formation of 18S ribosomal RNA. *EMBO J, 10*(13), 4231-4239. Retrieved from https://www.ncbi.nlm.nih.gov/pubmed/1756730

Hughes, J. M. X. (1996). Functional base-pairing interaction between highly conserved elements of U3 small nucleolar RNA and the small ribosomal subunit RNA. *Journal of Molecular Biology, 259*(4), 645-654. doi:DOI 10.1006/jmbi.1996.0346

Hunziker, M., Barandun, J., Buzovetsky, O., Steckler, C., Molina, H., & Klinge, S. (2019). Conformational switches control early maturation of the eukaryotic small ribosomal subunit. *Elife, 8*. doi:ARTN e45185
10.7554/eLife.45185

Hunziker, M., Barandun, J., Petfalski, E., Tan, D., Delan-Forino, C., Molloy, K. R., . . . Klinge, S. (2016). UtpA and UtpB chaperone nascent pre-ribosomal RNA and U3 snoRNA to initiate eukaryotic ribosome assembly. *Nat Commun, 7*, 12090. doi:10.1038/ncomms12090

Inoue, H., Nojima, H., & Okayama, H. (1990). High-Efficiency Transformation of Escherichia-Coli with Plasmids. *Gene, 96*(1), 23-28. doi:Doi 10.1016/0378-1119(90)90336-P

Itoh, H., Fukada, Y., Murata, K., & Kimura, A. (1983). Transformation of intact cells with alkali cations. *J.Bacteriol., 153*, 163-168.

Jakob, S., Ohmayer, U., Neueder, A., Hierlmeier, T., Perez-Fernandez, J., Hochmuth, E., . . . Milkereit, P. (2012). Interrelationships between yeast ribosomal protein assembly events and transient ribosome biogenesis factors interactions in early pre-ribosomes. *PLoS One, 7*(3), e32552. doi:10.1371/journal.pone.0032552

James, A., Wang, Y., Raje, H., Rosby, R., & DiMario, P. (2014). Nucleolar stress with and without p53. *Nucleus, 5*(5), 402-426. doi:10.4161/nucl.32235

Janke, C., Magiera, M. M., Rathfelder, N., Taxis, C., Reber, S., Maekawa, H., . . . Knop, M. (2004). A versatile toolbox for PCR-based tagging of yeast genes: new fluorescent proteins, more markers and promoter substitution cassettes. *Yeast, 21*(11), 947-962.

Retrieved from http://www.ncbi.nlm.nih.gov/entrez/query.fcgi?cmd=Retrieve&db=PubMed&dopt=Citation&list_uids=15334558

Jankowsky, E. (2011). RNA helicases at work: binding and rearranging. *Trends in Biochemical Sciences, 36*(1), 19-29. doi:DOI 10.1016/j.tibs.2010.07.008

Jenner, L., Melnikov, S., Garreau de Loubresse, N., Ben-Shem, A., Iskakova, M., Urzhumtsev, A., . . . Yusupov, M. (2012). Crystal structure of the 80S yeast ribosome. *Curr Opin Struct Biol, 22*(6), 759-767. doi:10.1016/j.sbi.2012.07.013

Johnson, M. C., Ghalei, H., Doxtader, K. A., Karbstein, K., & Stroupe, M. E. (2017). Structural Heterogeneity in Pre-40S Ribosomes. *Structure, 25*(2), 329-340. doi:10.1016/j.str.2016.12.011

Kaczanowska, M., & Ryden-Aulin, M. (2007). Ribosome biogenesis and the translation process in Escherichia coli. *Microbiol Mol Biol Rev, 71*(3), 477-494. doi:10.1128/MMBR.00013-07

Kafri, M., Metzl-Raz, E., Jona, G., & Barkai, N. (2016). The Cost of Protein Production. *Cell Rep, 14*(1), 22-31. doi:10.1016/j.celrep.2015.12.015

Karbstein, K. (2007). Role of GTPases in ribosome assembly. *Biopolymers, 87*(1), 1-11. doi:10.1002/bip.20762

Karbstein, K., & Doudna, J. A. (2006). GTP-dependent formation of a ribonucleoprotein subcomplex required for ribosome biogenesis. *J Mol Biol, 356*(2), 432-443. doi:S0022-2836(05)01456-7 [pii]
10.1016/j.jmb.2005.11.052

Karbstein, K., Jonas, S., & Doudna, J. A. (2005). An essential GTPase promotes assembly of preribosomal RNA processing complexes. *Mol Cell, 20*(4), 633-643. doi:S1097-2765(05)01638-2 [pii]
10.1016/j.molcel.2005.09.017

Karkusiewicz, I., Rempola, B., Gromadka, R., Grynberg, M., & Rytka, J. (2004). Functional and physical interactions of Faf1p, a Saccharomyces cerevisiae nucleolar protein. *Biochemical and biophysical research communications, 319*(2), 349-357. doi:10.1016/j.bbrc.2004.05.012

Kass, S., & Sollner-Webb, B. (1990). The first pre-rRNA-processing event occurs in a large complex: analysis by gel retardation, sedimentation and UV cross-linking. *Molec.Cell.Biol., 10*, 4920-4931.

Kass, S., Tyc, K., Steitz, J. A., & Sollner-Webb, B. (1990). The U3 small nucleolar ribonucleoprotein functions in the first step of preribosomal RNA processing. *Cell, 60*, 897-908.

Kater, L., Thoms, M., Barrio-Garcia, C., Cheng, J., Ismail, S., Ahmed, Y. L., . . . Beckmann, R. (2017). Visualizing the Assembly Pathway of Nucleolar Pre-60S Ribosomes. *Cell, 171*(7), 1599-1610 e1514. doi:10.1016/j.cell.2017.11.039

Khatter, H., Myasnikov, A. G., Natchiar, S. K., & Klaholz, B. P. (2015). Structure of the human 80S ribosome. *Nature, 520*(7549), 640-645. doi:10.1038/nature14427

Khoshnevis, S., Askenasy, I., Johnson, M. C., Dattolo, M. D., Young-Erdos, C. L., Stroupe, M. E., & Karbstein, K. (2016). The DEAD-box Protein Rok1 Orchestrates 40S and 60S Ribosome Assembly by Promoting the Release of Rrp5 from Pre-40S Ribosomes to Allow for 60S Maturation. *PLoS biology, 14*(6), e1002480. doi:10.1371/journal.pbio.1002480

King, T. H., Liu, B., McCully, R. R., & Fournier, M. J. (2003). Ribosome structure and activity are altered in cells lacking snoRNPs that form pseudouridines in the peptidyl

transferase center. *Molecular Cell, 11*(2), 425-435. doi:Doi 10.1016/S1097-2765(03)00040-6

Klinge, S., Voigts-Hoffmann, F., Leibundgut, M., & Ban, N. (2012). Atomic structures of the eukaryotic ribosome. *Trends Biochem Sci, 37*(5), 189-198. doi:10.1016/j.tibs.2012.02.007

Klinge, S., & Woolford, J. L., Jr. (2018). Ribosome assembly coming into focus. *Nat Rev Mol Cell Biol*. doi:10.1038/s41580-018-0078-y

Kornprobst, M., Turk, M., Kellner, N., Cheng, J., Flemming, D., Kos-Braun, I., . . . Hurt, E. (2016). Architecture of the 90S Pre-ribosome: A Structural View on the Birth of the Eukaryotic Ribosome. *Cell, 166*(2), 380-393. doi:10.1016/j.cell.2016.06.014

Kos, M., & Tollervey, D. (2005). The Putative RNA Helicase Dbp4p Is Required for Release of the U14 snoRNA from Preribosomes in Saccharomyces cerevisiae. *Mol Cell, 20*(1), 53-64. Retrieved from http://www.ncbi.nlm.nih.gov/entrez/query.fcgi?cmd=Retrieve&db=PubMed&dopt=Citation&list_uids=16209945

Kos, M., & Tollervey, D. (2010). Yeast pre-rRNA processing and modification occur cotranscriptionally. *Mol Cell, 37*(6), 809-820. doi:S1097-2765(10)00206-6 [pii]
10.1016/j.molcel.2010.02.024

Kos-Braun, I. C., Jung, I., & Kos, M. (2017). Tor1 and CK2 kinases control a switch between alternative ribosome biogenesis pathways in a growth-dependent manner. *PLoS biology, 15*(3). doi:ARTN e2000245
10.1371/journal.pbio.2000245

Kressler, D., Bange, G., Ogawa, Y., Stjepanovic, G., Bradatsch, B., Pratte, D., . . . Hurt, E. (2012). Synchronizing nuclear import of ribosomal proteins with ribosome assembly. *Science, 338*(6107), 666-671. doi:10.1126/science.1226960

Kressler, D., De la Cruz, J., Rojo, M., & Linder, P. (1997). Fal1p is an essential DEAD-box protein involved in 40S-ribosomal-subunit biogenesis in Saccharomyces cerevisiae. *Mol.Cell.Biol., 17*, 7283-7294.

Kressler, D., Hurt, E., Bergler, H., & Bassler, J. (2012). The power of AAA-ATPases on the road of pre-60S ribosome maturation--molecular machines that strip pre-ribosomal particles. *Biochim Biophys Acta, 1823*(1), 92-100. doi:10.1016/j.bbamcr.2011.06.017

Kressler, D., Linder, P., & De La Cruz, J. (1999). Protein trans-acting factors involved in ribosome biogenesis in Saccharomyces cerevisiae. *Mol. Cell. Biol., 19*, 7897-7912.

Krogan, N. J., Peng, W. T., Cagney, G., Robinson, M. D., Haw, R., Zhong, G., . . . Greenblatt, J. F. (2004). High-definition macromolecular composition of yeast RNA-processing complexes. *Mol Cell, 13*(2), 225-239. Retrieved from http://www.ncbi.nlm.nih.gov/entrez/query.fcgi?cmd=Retrieve&db=PubMed&dopt=Citation&list_uids=14759368

Kufel, J., Dichtl, B., & Tollervey, D. (1999). Yeast Rnt1p is required for cleavage of the pre-ribosomal RNA in the 3' ETS but not the 5' ETS. *RNA, 5*(7), 909-917. doi:10.1017/s135583829999026x

Kuhn, H., Hierlmeier, T., Merl, J., Jakob, S., Aguissa-Toure, A. H., Milkereit, P., & Tschochner, H. (2009). The Noc-domain containing C-terminus of Noc4p mediates both formation of the Noc4p-Nop14p submodule and its incorporation into the SSU processome. *PLoS One, 4*(12), e8370. doi:10.1371/journal.pone.0008370

Kumar, A., & Warner, J. R. (1972). Characterization of ribosomal precursor particles from HeLa cell nucleoli. *J Mol Biol, 63*(2), 233-246. doi:10.1016/0022-2836(72)90372-5

Laferte, A., Favry, E., Sentenac, A., Riva, M., Carles, C., & Chedin, S. (2006). The transcriptional activity of RNA polymerase I is a key determinant for the level of all ribosome components. *Genes Dev, 20*(15), 2030-2040. doi:10.1101/gad.386106

Lafontaine, D., Delcour, J., Glasser, A. L., Desgres, J., & Vandenhaute, J. (1994). The DIM1 gene responsible for the conserved m6(2)Am6(2)A dimethylation in the 3'-terminal loop of 18 S rRNA is essential in yeast. *J Mol Biol, 241*(3), 492-497. doi:10.1006/jmbi.1994.1525

Lamanna, A. C., & Karbstein, K. (2011). An RNA conformational switch regulates pre-18S rRNA cleavage. *J Mol Biol, 405*(1), 3-17. doi:10.1016/j.jmb.2010.09.064

Lamaye, F., Galliot, S., Alibardi, L., Lafontaine, D. L., & Thiry, M. (2011). Nucleolar structure across evolution: the transition between bi- and tri-compartmentalized nucleoli lies within the class Reptilia. *Journal of structural biology, 174*(2), 352-359. doi:10.1016/j.jsb.2011.02.003

Lan, P., Zhou, B., Tan, M., Li, S., Cao, M., Wu, J., & Lei, M. (2020). Structural insight into precursor ribosomal RNA processing by ribonuclease MRP. *Science, 369*(6504), 656-663. doi:10.1126/science.abc0149

Lau, B., Cheng, J., Flemming, D., La Venuta, G., Berninghausen, O., Beckmann, R., & Hurt, E. (2021). Structure of the Maturing 90S Pre-ribosome in Association with the RNA Exosome. *Mol Cell, 81*(2), 293-303 e294. doi:10.1016/j.molcel.2020.11.009

Lebaron, S., Froment, C., Fromont-Racine, M., Rain, J. C., Monsarrat, B., Caizergues-Ferrer, M., & Henry, Y. (2005). The splicing ATPase Prp43p is a component of multiple preribosomal particles. *Mol Cell Biol, 25*(21), 9269-9282. doi:25/21/9269 [pii]
10.1128/MCB.25.21.9269-9282.2005

Lebaron, S., Papin, C., Capeyrou, R., Chen, Y. L., Froment, C., Monsarrat, B., . . . Henry, Y. (2009). The ATPase and helicase activities of Prp43p are stimulated by the G-patch protein Pfa1p during yeast ribosome biogenesis. *EMBO J, 28*(24), 3808-3819. doi:10.1038/emboj.2009.335

Lebaron, S., Schneider, C., van Nues, R. W., Swiatkowska, A., Walsh, D., Bottcher, B., . . . Tollervey, D. (2012). Proofreading of pre-40S ribosome maturation by a translation initiation factor and 60S subunits. *Nature structural & molecular biology, 19*(8), 744-753. doi:10.1038/nsmb.2308

Lebaron, S., Segerstolpe, A., French, S. L., Dudnakova, T., de Lima Alves, F., Granneman, S., . . . Tollervey, D. (2013). Rrp5 binding at multiple sites coordinates pre-rRNA processing and assembly. *Mol Cell, 52*(5), 707-719. doi:10.1016/j.molcel.2013.10.017

Lecompte, O., Ripp, R., Thierry, J. C., Moras, D., & Poch, O. (2002). Comparative analysis of ribosomal proteins in complete genomes: an example of reductive evolution at the domain scale. *Nucleic Acids Research, 30*(24), 5382-5390. doi:DOI 10.1093/nar/gkf693

Lee, S. J., & Baserga, S. J. (1999). Imp3p and Imp4p, two specific components of the U3 small nucleolar ribonucleoprotein that are essential for pre-18S rRNA processing. *Molecular and cellular biology, 19*(8), 5441-5452. Retrieved from http://www.ncbi.nlm.nih.gov/pubmed/10409734

Lee, Y., & Nazar, R. N. (1997). Ribosomal 5 S rRNA maturation in Saccharomyces cerevisiae. *J Biol Chem, 272*(24), 15206-15212. doi:10.1074/jbc.272.24.15206

Leeds, N. B., Small, E. C., Hiley, S. L., Hughes, T. R., & Staley, J. P. (2006). The splicing factor Prp43p, a DEAH box ATPase, functions in ribosome biogenesis. *Mol Cell Biol, 26*(2), 513-522. doi:26/2/513 [pii]
10.1128/MCB.26.2.513-522.2006

Lemay, V., Hossain, A., Osheim, Y. N., Beyer, A. L., & Dragon, F. (2011). Identification of novel proteins associated with yeast snR30 small nucleolar RNA. *Nucleic Acids Res, 39*(22), 9659-9670. doi:10.1093/nar/gkr659

Li, G. W., Burkhardt, D., Gross, C., & Weissman, J. S. (2014). Quantifying absolute protein synthesis rates reveals principles underlying allocation of cellular resources. *Cell, 157*(3), 624-635. doi:10.1016/j.cell.2014.02.033

Li, H. V., Zagorski, J., & Fournier, M. J. (1990). Depletion of U14 small nuclear RNA (snR128) disrupts production of 18S rRNA in Saccharomyces cerevisiae. *Molec.Cell.Biol., 10*, 1145-1152.

Liang, W. Q., & Fournier, M. J. (1995). U14 base-pairs with 18S rRNA: a novel snoRNA interaction required for rRNA processing. *Genes Dev, 9*(19), 2433-2443. doi:10.1101/gad.9.19.2433

Liang, X. H., & Fournier, M. J. (2006). The helicase Has1p is required for snoRNA release from pre-rRNA. *Mol Cell Biol, 26*(20), 7437-7450. doi:MCB.00664-06 [pii]
10.1128/MCB.00664-06

Lin, J., Lu, J., Feng, Y., Sun, M., & Ye, K. (2013). An RNA-binding complex involved in ribosome biogenesis contains a protein with homology to tRNA CCA-adding enzyme. *PLoS biology, 11*(10), e1001669. doi:10.1371/journal.pbio.1001669

Liu, F., Putnam, A., & Jankowsky, E. (2008). ATP hydrolysis is required for DEAD-box protein recycling but not for duplex unwinding. *Proc Natl Acad Sci U S A, 105*(51), 20209-20214. doi:0811115106 [pii]
10.1073/pnas.0811115106

Loc'h, J., Blaud, M., Rety, S., Lebaron, S., Deschamps, P., Bareille, J., . . . Leulliot, N. (2014). RNA mimicry by the fap7 adenylate kinase in ribosome biogenesis. *PLoS biology, 12*(5), e1001860. doi:10.1371/journal.pbio.1001860

Longtine, M. S., McKenzie, A., Demarini, D. J., Shah, N. G., Wach, A., Brachat, A., . . . Pringle, J. R. (1998). Additional modules for versatile and economical PCR-based gene deletion and modification in Saccharomyces cerevisiae. *Yeast, 10*(14), 953-961.

Lübben, B., Fabrizio, P., Kastner, B., & Lührmann, R. (1995). Isolation and characterization of the small nucleolar ribonucleoprotein particle snR30 from Saccharomyces cerevisiae. *J.Biol.Chem., 270*, 11549-11554.

Lygerou, Z., Allmang, C., Tollervey, D., & Seraphin, B. (1996). Accurate processing of a eukaryotic precursor ribosomal RNA by ribonuclease MRP in vitro. *Science, 272*(5259), 268-270. Retrieved from https://www.ncbi.nlm.nih.gov/pubmed/8602511

Martin, R., Hackert, P., Ruprecht, M., Simm, S., Bruning, L., Mirus, O., . . . Bohnsack, M. T. (2014). A pre-ribosomal RNA interaction network involving snoRNAs and the Rok1 helicase. *RNA, 20*(8), 1173-1182. doi:10.1261/rna.044669.114

Martin, R., Straub, A. U., Doebele, C., & Bohnsack, M. T. (2013). DExD/H-box RNA helicases in ribosome biogenesis. *RNA Biol, 10*(1), 4-18. doi:10.4161/rna.21879

Marz, M., & Stadler, P. F. (2009). Comparative analysis of eukaryotic U3 snoRNA. *RNA Biol, 6*(5), 503-507. doi:10.4161/rna.6.5.9607

McCaughan, U. M., Jayachandran, U., Shchepachev, V., Chen, Z. A., Rappsilber, J., Tollervey, D., & Cook, A. G. (2016). Pre-40S ribosome biogenesis factor Tsr1 is an inactive structural mimic of translational GTPases. *Nat Commun, 7*, 11789. doi:10.1038/ncomms11789

Miles, T. D., Jakovljevic, J., Horsey, E. W., Harnpicharnchai, P., Tang, L., & Woolford, J. L., Jr. (2005). Ytm1, Nop7, and Erb1 form a complex necessary for maturation of yeast 66S

preribosomes. *Mol Cell Biol, 25*(23), 10419-10432. Retrieved from http://www.ncbi.nlm.nih.gov/entrez/query.fcgi?cmd=Retrieve&db=PubMed&dopt=Citation&list_uids=16287855

Milkereit, P., Gadal, O., Podtelejnikov, A., Trumtel, S., Gas, N., Petfalski, E., . . . Tschochner, H. (2001). Maturation of Pre-Ribosomes Requires Noc-Proteins and is Coupled to Transport from the Nucleolus to the Nucleoplasm. *Cell, 105*, 499-509.

Milkereit, P., Strauss, D., Bassler, J., Gadal, O., Kühn, H., Schütz, S., . . . Tschochner.H. (2003). A Noc-complex specifically involved in the formation and nuclear export of ribosomal 40S subunits. *J. Biol. Chem., 278*, 4072-4081.

Miller, O. L., & Beatty, B. R. (1969). Visualization of nucleolar genes. *Science, 164*, 955-957.

Mills, E. W., & Green, R. (2017). Ribosomopathies: There's strength in numbers. *Science, 358*(6363). doi:10.1126/science.aan2755

Montanaro, L., Calienni, M., Bertoni, S., Rocchi, L., Sansone, P., Storci, G., . . . Derenzini, M. (2010). Novel dyskerin-mediated mechanism of p53 inactivation through defective mRNA translation. *Cancer Res, 70*(11), 4767-4777. doi:10.1158/0008-5472.CAN-09-4024

Moriggi, G., Nieto, B., & Dosil, M. (2014). Rrp12 and the Exportin Crm1 participate in late assembly events in the nucleolus during 40S ribosomal subunit biogenesis. *PLoS Genet, 10*(12), e1004836. doi:10.1371/journal.pgen.1004836

Morrissey, J. P., & Tollervey, D. (1993). Yeast snR30 is a small nucleolar RNA required for 18S rRNA synthesis. *Mol.Cell.Biol., 13*, 2469-2477.

Moss, T., Langlois, F., Gagnon-Kugler, T., & Stefanovsky, V. (2007). A housekeeper with power of attorney: the rRNA genes in ribosome biogenesis. *Cell Mol Life Sci, 64*(1), 29-49. doi:10.1007/s00018-006-6278-1

Mougey, E. B., O'Reilly, M., Osheim, Y., Miller, O. L. J., Beyer, A., & Sollner-Webb, B. (1993). The terminal balls characteristic of eukaryotic rRNA transcription units in chromatin spreads are rRNA processing complexes. *Genes Dev., 7*, 1609-1619.

Nierhaus, K. H. (2014). Mg2+, K+, and the ribosome. *J Bacteriol, 196*(22), 3817-3819. doi:10.1128/JB.02297-14

Nierhaus, K. H., & Dohme, F. (1974). Ribosomal-Proteins .100. Total Reconstitution of Functionally Active 50s Ribosomal-Subunits from Escherichia-Coli. *Proceedings of the National Academy of Sciences of the United States of America, 71*(12), 4713-4717. doi:DOI 10.1073/pnas.71.12.4713

Nogales, E. (2016). The development of cryo-EM into a mainstream structural biology technique. *Nature methods, 13*(1), 24-27. doi:10.1038/nmeth.3694

O'Donohue, M. F., Choesmel, V., Faubladier, M., Fichant, G., & Gleizes, P. E. (2010). Functional dichotomy of ribosomal proteins during the synthesis of mammalian 40S ribosomal subunits. *Journal of Cell Biology, 190*(5), 853-866. doi:10.1083/jcb.201005117

Oeffinger, M., Zenklusen, D., Ferguson, A., Wei, K. E., El Hage, A., Tollervey, D., . . . Rout, M. P. (2009). Rrp17p is a eukaryotic exonuclease required for 5' end processing of Pre-60S ribosomal RNA. *Mol Cell, 36*(5), 768-781. doi:10.1016/j.molcel.2009.11.011

Ojha, S., Malla, S., & Lyons, S. M. (2020). snoRNPs: Functions in Ribosome Biogenesis. *Biomolecules, 10*(5). doi:ARTN 783

10.3390/biom10050783

Osheim, Y. N., French, S. L., Keck, K. M., Champion, E. A., Spasov, K., Dragon, F., . . . Beyer, A. L. (2004). Pre-18S ribosomal RNA is structurally compacted into the SSU processome

prior to being cleaved from nascent transcripts in Saccharomyces cerevisiae. *Mol Cell, 16*(6), 943-954. doi:S1097276504007233 [pii]
10.1016/j.molcel.2004.11.031
Palade, G. E. (1955). A small particulate component of the cytoplasm. *J Biophys Biochem Cytol, 1*(1), 59-68. doi:10.1083/jcb.1.1.59
Parker, M. D., Collins, J. C., Korona, B., Ghalei, H., & Karbstein, K. (2019). A kinase-dependent checkpoint prevents escape of immature ribosomes into the translating pool. *PLoS biology, 17*(12), e3000329. doi:10.1371/journal.pbio.3000329
Parks, T. D., Leuther, K. K., Howard, E. D., Johnston, S. A., & Dougherty, W. G. (1994). Release of Proteins and Peptides from Fusion Proteins Using a Recombinant Plant-Virus Proteinase. *Analytical Biochemistry, 216*(2), 413-417. doi:DOI 10.1006/abio.1994.1060
Pena, C., Schutz, S., Fischer, U., Chang, Y., & Panse, V. G. (2016). Prefabrication of a ribosomal protein subcomplex essential for eukaryotic ribosome formation. *Elife, 5*. doi:10.7554/eLife.21755
Penzo, M., Rocchi, L., Brugiere, S., Carnicelli, D., Onofrillo, C., Coute, Y., . . . Montanaro, L. (2015). Human ribosomes from cells with reduced dyskerin levels are intrinsically altered in translation. *FASEB J, 29*(8), 3472-3482. doi:10.1096/fj.15-270991
Perez-Fernandez, J., Martin-Marcos, P., & Dosil, M. (2011). Elucidation of the assembly events required for the recruitment of Utp20, Imp4 and Bms1 onto nascent pre-ribosomes. *Nucleic Acids Res, 39*(18), 8105-8121. doi:10.1093/nar/gkr508
Perez-Fernandez, J., Roman, A., De Las Rivas, J., Bustelo, X. R., & Dosil, M. (2007). The 90S preribosome is a multimodular structure that is assembled through a hierarchical mechanism. *Mol Cell Biol, 27*(15), 5414-5429. doi:MCB.00380-07 [pii]
10.1128/MCB.00380-07
Pertschy, B., Schneider, C., Gnädig, M., Schäfer, T., Tollervey, D., & Hurt, E. (2009). RNA helicase Prp43 and its co-factor Pfa1 promote 20S to 18S rRNA processing catalyzed by the endonuclease Nob1. *J Biol Chem, 284*(50), 35079-35091. doi:M109.040774 [pii]
10.1074/jbc.M109.040774
Pestova, T. V., Lomakin, I. B., Lee, J. H., Choi, S. K., Dever, T. E., & Hellen, C. U. T. (2000). The joining of ribosomal subunits in eukaryotes requires eIF5B. *Nature, 403*(6767), 332-335.
Pettersen, E. F., Goddard, T. D., Huang, C. C., Couch, G. S., Greenblatt, D. M., Meng, E. C., & Ferrin, T. E. (2004). UCSF Chimera--a visualization system for exploratory research and analysis. *J Comput Chem, 25*(13), 1605-1612. Retrieved from http://www.ncbi.nlm.nih.gov/entrez/query.fcgi?cmd=Retrieve&db=PubMed&dopt=Citation&list_uids=15264254
Phipps, K. R., Charette, J., & Baserga, S. J. (2011). The small subunit processome in ribosome biogenesis-progress and prospects. *Wiley Interdiscip Rev RNA, 2*(1), 1-21. doi:10.1002/wrna.57
Pillet, B., Mitterer, V., Kressler, D., & Pertschy, B. (2017). Hold on to your friends: Dedicated chaperones of ribosomal proteins: Dedicated chaperones mediate the safe transfer of ribosomal proteins to their site of pre-ribosome incorporation. *Bioessays, 39*(1), 1-12. doi:10.1002/bies.201600153
Pillon, M. C., Sobhany, M., Borgnia, M. J., Williams, J. G., & Stanley, R. E. (2017). Grc3 programs the essential endoribonuclease Las1 for specific RNA cleavage. *Proc Natl Acad Sci U S A, 114*(28), E5530-E5538. doi:10.1073/pnas.1703133114

Pöll, G., Li, S., Ohmayer, U., Hierlmeier, T., Milkereit, P., & Perez-Fernandez, J. (2014). In vitro reconstitution of yeast tUTP/UTP A and UTP B subcomplexes provides new insights into their modular architecture. *PLoS One, 9*(12), e114898. doi:10.1371/journal.pone.0114898

Prestayko, A. W., Tonato, M., & Busch, H. (1970). Low molecular weight RNA associated with 28 s nucleolar RNA. *J Mol Biol, 47*(3), 505-515. Retrieved from https://www.ncbi.nlm.nih.gov/pubmed/5418169

Preti, M., O'Donohue, M. F., Montel-Lehry, N., Bortolin-Cavaille, M. L., Choesmel, V., & Gleizes, P. E. (2013). Gradual processing of the ITS1 from the nucleolus to the cytoplasm during synthesis of the human 18S rRNA. *Nucleic Acids Research, 41*(8), 4709-4723. doi:10.1093/nar/gkt160

Puig, O., Caspary, F., Rigaut, G., Rutz, B., Bouveret, E., Bragado-Nilsson, E., . . . Seraphin, B. (2001). The tandem affinity purification (TAP) method: a general procedure of protein complex purification. *Methods, 24*(3), 218-229. Retrieved from http://www.ncbi.nlm.nih.gov/entrez/query.fcgi?cmd=Retrieve&db=PubMed&dopt=Citation&list_uids=11403571

Richard, P., & Manley, J. L. (2009). Transcription termination by nuclear RNA polymerases. *Genes & Development, 23*(11), 1247-1269. doi:10.1101/gad.1792809

Ripmaster, T. L., Vaughn, G. P., & Woolford, J. L., Jr. (1992). A putative ATP-dependent RNA helicase involved in Saccharomyces cerevisiae ribosome assembly. *Proc.Natl.Acad.Sci.USA, 89*, 11131-11135.

Rocchi, L., Pacilli, A., Sethi, R., Penzo, M., Schneider, R. J., Trere, D., . . . Montanaro, L. (2013). Dyskerin depletion increases VEGF mRNA internal ribosome entry site-mediated translation. *Nucleic Acids Res, 41*(17), 8308-8318. doi:10.1093/nar/gkt587

Rodriguez-Galan, O., Garcia-Gomez, J. J., & de la Cruz, J. (2013). Yeast and human RNA helicases involved in ribosome biogenesis: current status and perspectives. *Biochim Biophys Acta, 1829*(8), 775-790. doi:10.1016/j.bbagrm.2013.01.007

Rohl, R., & Nierhaus, K. H. (1982). Assembly map of the large subunit (50S) of Escherichia coli ribosomes. *Proc Natl Acad Sci U S A, 79*(3), 729-733. doi:10.1073/pnas.79.3.729

Root-Bernstein, M., & Root-Bernstein, R. (2015). The ribosome as a missing link in the evolution of life. *Journal of Theoretical Biology, 367*, 130-158. doi:10.1016/j.jtbi.2014.11.025

Rudra, D., Mallick, J., Zhao, Y., & Warner, J. R. (2007). Potential interface between ribosomal protein production and pre-rRNA processing. *Mol Cell Biol, 27*(13), 4815-4824. doi:10.1128/MCB.02062-06

Rudra, D., Zhao, Y., & Warner, J. R. (2005). Central role of Ifh1p-Fhl1p interaction in the synthesis of yeast ribosomal proteins. *EMBO J, 24*(3), 533-542. doi:10.1038/sj.emboj.7600553

Russell, J. B., & Cook, G. M. (1995). Energetics of bacterial growth: balance of anabolic and catabolic reactions. *Microbiol Rev, 59*(1), 48-62. Retrieved from https://www.ncbi.nlm.nih.gov/pubmed/7708012

Samarsky, D. A., & Fournier, M. J. (1999). A comprehensive database for the small nucleolar RNAs from Saccharomyces cerevisiae. *Nucleic Acids Res, 27*(1), 161-164. doi:10.1093/nar/27.1.161

Sardana, R., Liu, X., Granneman, S., Zhu, J., Gill, M., Papoulas, O., . . . Johnson, A. W. (2015). The DEAH-box helicase Dhr1 dissociates U3 from the pre-rRNA to promote formation of the central pseudoknot. *PLoS biology, 13*(2), e1002083. doi:10.1371/journal.pbio.1002083

Sasaki, T., Toh-E, A., & Kikuchi, Y. (2000). Yeast Krr1p physically and functionally interacts with a novel essential Kri1p, and both proteins are required for 40S ribosome biogenesis in the nucleolus. *Mol. Cell. Biol., 20*, 7971-7979.

Scaiola, A., Pena, C., Weisser, M., Bohringer, D., Leibundgut, M., Klingauf-Nerurkar, P., . . . Ban, N. (2018). Structure of a eukaryotic cytoplasmic pre-40S ribosomal subunit. *EMBO J, 37*(7). doi:10.15252/embj.201798499

Schäfer, T., Maco, B., Petfalski, E., Tollervey, D., Bottcher, B., Aebi, U., & Hurt, E. (2006). Hrr25-dependent phosphorylation state regulates organization of the pre-40S subunit. *Nature, 441*(7093), 651-655. Retrieved from http://www.ncbi.nlm.nih.gov/entrez/query.fcgi?cmd=Retrieve&db=PubMed&dopt=Citation&list_uids=16738661

Schafer, T., Strauss, D., Petfalski, E., Tollervey, D., & Hurt, E. (2003). The path from nucleolar 90S to cytoplasmic 40S pre-ribosomes. *EMBO J, 22*(6), 1370-1380. doi:10.1093/emboj/cdg121

Schattner, P., Decatur, W. A., Davis, C. A., Ares, M., Jr., Fournier, M. J., & Lowe, T. M. (2004). Genome-wide searching for pseudouridylation guide snoRNAs: analysis of the Saccharomyces cerevisiae genome. *Nucleic Acids Res, 32*(14), 4281-4296. doi:10.1093/nar/gkh768

Schawalder, S. B., Kabani, M., Howald, I., Choudhury, U., Werner, M., & Shore, D. (2004). Growth-regulated recruitment of the essential yeast ribosomal protein gene activator Ifh1. *Nature, 432*(7020), 1058-1061. doi:10.1038/nature03200

Scherrer, K., Latham, H., & Darnell, J. E. (1963). Demonstration of an unstable RNA and of a precursor to ribosomal RNA in HeLa cells. *Proc Natl Acad Sci U S A, 49*, 240-248. Retrieved from https://www.ncbi.nlm.nih.gov/pubmed/13991616

Schiestl, R. H., & Gietz, R. D. (1989). High efficiency transformation of intact yeast cells using single stranded nucleic acid as carrier. *Curr.Genet., 16*, 339-346.

Schillewaert, S., Wacheul, L., Lhomme, F., & Lafontaine, D. L. (2012). The evolutionarily conserved protein Las1 is required for pre-rRNA processing at both ends of ITS2. *Mol Cell Biol, 32*(2), 430-444. doi:10.1128/MCB.06019-11

Schmitt, M. E., & Clayton, D. A. (1992). Yeast Site-Specific Ribonucleoprotein Endoribonuclease Mrp Contains an Rna Component Homologous to Mammalian Rnase Mrp Rna and Essential for Cell Viability. *Genes & Development, 6*(10), 1975-1985. doi:DOI 10.1101/gad.6.10.1975

Schmitt, M. E., & Clayton, D. A. (1993). Nuclear RNase MRP is required for correct processing of pre-5.8S rRNA in Saccharomyces cerevisiae. *Mol.Cell.Biol., 13*, 7935-7941.

Schneider, D. A., Michel, A., Sikes, M. L., Vu, L., Dodd, J. A., Salgia, S., . . . Nomura, M. (2007). Transcription elongation by RNA polymerase I is linked to efficient rRNA processing and ribosome assembly. *Mol Cell, 26*(2), 217-229. doi:10.1016/j.molcel.2007.04.007

Schuwirth, B. S., Borovinskaya, M. A., Hau, C. W., Zhang, W., Vila-Sanjurjo, A., Holton, J. M., & Cate, J. H. (2005). Structures of the bacterial ribosome at 3.5 A resolution. *Science, 310*(5749), 827-834. doi:10.1126/science.1117230

Schwanhausser, B., Busse, D., Li, N., Dittmar, G., Schuchhardt, J., Wolf, J., . . . Selbach, M. (2011). Global quantification of mammalian gene expression control. *Nature, 473*(7347), 337-342. doi:10.1038/nature10098

Scott, D. D., Trahan, C., Zindy, P. J., Aguilar, L. C., Delubac, M. Y., Van Nostrand, E. L., . . . Oeffinger, M. (2017). Nol12 is a multifunctional RNA binding protein at the nexus of RNA and DNA metabolism. *Nucleic Acids Research, 45*(21), 12509-12528. doi:10.1093/nar/gkx963

Shah, B. N., Liu, X., & Correll, C. C. (2013). Imp3 unfolds stem structures in pre-rRNA and U3 snoRNA to form a duplex essential for small subunit processing. *RNA, 19*(10), 1372-1383. doi:10.1261/rna.039511.113

Shah, P., Ding, Y., Niemczyk, M., Kudla, G., & Plotkin, J. B. (2013). Rate-limiting steps in yeast protein translation. *Cell, 153*(7), 1589-1601. doi:10.1016/j.cell.2013.05.049

Shajani, Z., Sykes, M. T., & Williamson, J. R. (2011). Assembly of bacterial ribosomes. *Annu Rev Biochem, 80*, 501-526. doi:10.1146/annurev-biochem-062608-160432

Sharma, K., & Tollervey, D. (1999). Base pairing between U3 small nucleolar RNA and the 5' end of 18S rRNA is required for pre-rRNA processing. *Mol. Cell. Biol., 19*, 6012-6019.

Sharma, S., Langhendries, J. L., Watzinger, P., Kotter, P., Entian, K. D., & Lafontaine, D. L. (2015). Yeast Kre33 and human NAT10 are conserved 18S rRNA cytosine acetyltransferases that modify tRNAs assisted by the adaptor Tan1/THUMPD1. *Nucleic Acids Res, 43*(4), 2242-2258. doi:10.1093/nar/gkv075

Shu, S., & Ye, K. (2018). Structural and functional analysis of ribosome assembly factor Efg1. *Nucleic Acids Res, 46*(4), 2096-2106. doi:10.1093/nar/gky011

Shuai, K., & Warner, J. R. (1991). A temperature sensitive mutant of Saccharomyces cerevisiae defective in pre-rRNA processing. *Nucleic Acids Res., 19*(18), 5059-5064.

Sievers, F., & Higgins, D. G. (2014). Clustal omega. *Curr Protoc Bioinformatics, 48*, 3 13 11-16. doi:10.1002/0471250953.bi0313s48

Sloan, K. E., Mattijssen, S., Lebaron, S., Tollervey, D., Pruijn, G. J., & Watkins, N. J. (2013). Both endonucleolytic and exonucleolytic cleavage mediate ITS1 removal during human ribosomal RNA processing. *J Cell Biol, 200*(5), 577-588. doi:10.1083/jcb.201207131

Soltanieh, S., Lapensee, M., & Dragon, F. (2014). Nucleolar proteins Bfr2 and Enp2 interact with DEAD-box RNA helicase Dbp4 in two different complexes. *Nucleic Acids Res, 42*(5), 3194-3206. doi:10.1093/nar/gkt1293

Soltanieh, S., Osheim, Y. N., Spasov, K., Trahan, C., Beyer, A. L., & Dragon, F. (2015). DEAD-box RNA helicase Dbp4 is required for small-subunit processome formation and function. *Mol Cell Biol, 35*(5), 816-830. doi:10.1128/MCB.01348-14

Strom, A. R., & Brangwynne, C. P. (2019). The liquid nucleome - phase transitions in the nucleus at a glance. *J Cell Sci, 132*(22). doi:10.1242/jcs.235093

Strunk, B., Loucks, C., Su, M., Vashisth, H., Cheng, S., Schilling, J., . . . Skiniotis, G. (2011). Ribosome assembly factors prevent premature translation initiation by 40S assembly intermediates. *Science, 333*(6048), 1449-1502. doi:10.1126/science.1208245

Strunk, B. S., Novak, M. N., Young, C. L., & Karbstein, K. (2012). A Translation-Like Cycle Is a Quality Control Checkpoint for Maturing 40S Ribosome Subunits. *Cell, 150*(1), 111-121. doi:10.1016/j.cell.2012.04.044

Sturm, M., Cheng, J., Bassler, J., Beckmann, R., & Hurt, E. (2017). Interdependent action of KH domain proteins Krr1 and Dim2 drive the 40S platform assembly. *Nat Commun, 8*(1), 2213. doi:10.1038/s41467-017-02199-4

Sun, Q., Zhu, X., Qi, J., An, W., Lan, P., Tan, D., . . . Ye, K. (2017). Molecular architecture of the 90S small subunit pre-ribosome. *Elife, 6*. doi:10.7554/eLife.22086

Sung, M. K., Porras-Yakushi, T. R., Reitsma, J. M., Huber, F. M., Sweredoski, M. J., Hoelz, A., . . . Deshaies, R. J. (2016). A conserved quality-control pathway that mediates degradation of unassembled ribosomal proteins. *Elife, 5*, e19105. doi:10.7554/eLife.19105

Suzuki, S., Kanno, M., Fujiwara, T., Sugiyama, H., Yokoyama, A., Takahashi, H., & Tanaka, J. (2006). Molecular cloning and characterization of Nop25, a novel nucleolar RNA

binding protein, highly conserved in vertebrate species. *Exp Cell Res, 312*(7), 1031-1041. doi:10.1016/j.yexcr.2005.12.017

Talkish, J., Biedka, S., Jakovljevic, J., Zhang, J., Tang, L., Strahler, J. R., . . . Woolford, J. L., Jr. (2016). Disruption of ribosome assembly in yeast blocks cotranscriptional pre-rRNA processing and affects the global hierarchy of ribosome biogenesis. *RNA, 22*(6), 852-866. doi:10.1261/rna.055780.115

Tamaoki, T. (1966). The particulate fraction containing 45 s RNA in L cell nuclei. *J Mol Biol, 15*(2), 624-639. Retrieved from https://www.ncbi.nlm.nih.gov/pubmed/5915185

Tang, L., Sahasranaman, A., Jakovljevic, J., Schleifman, E., & Woolford, J. L., Jr. (2008). Interactions among Ytm1, Erb1, and Nop7 required for assembly of the Nop7-subcomplex in yeast preribosomes. *Mol Biol Cell, 19*(7), 2844-2856. doi:E07-12-1281 [pii]

10.1091/mbc.E07-12-1281

Thiry, M., & Lafontaine, D. L. (2005). Birth of a nucleolus: the evolution of nucleolar compartments. *Trends Cell Biol, 15*(4), 194-199. doi:10.1016/j.tcb.2005.02.007

Thompson, J. D., Higgins, D. G., & Gibson, T. J. (1994). CLUSTAL W: improving the sensitivity of progressive multiple sequence alignment through sequence weighting, position-specific gap penalties and weight matrix choice. *Nucleic Acids Res, 22*(22), 4673-4680. doi:10.1093/nar/22.22.4673

Thompson, J. D., Muller, A., Waterhouse, A., Procter, J., Barton, G. J., Plewniak, F., & Poch, O. (2006). MACSIMS: multiple alignment of complete sequences information management system. *BMC Bioinformatics, 7*, 318. doi:10.1186/1471-2105-7-318

Thoms, M., Thomson, E., Bassler, J., Gnadig, M., Griesel, S., & Hurt, E. (2015). The Exosome Is Recruited to RNA Substrates through Specific Adaptor Proteins. *Cell, 162*(5), 1029-1038. doi:10.1016/j.cell.2015.07.060

Thomson, E., Ferreira-Cerca, S., & Hurt, E. (2013). Eukaryotic ribosome biogenesis at a glance. *J Cell Sci, 126*(Pt 21), 4815-4821. doi:10.1242/jcs.111948

Tollervey, D. (1987). A yeast small nuclear RNA is required for normal processing of pre-ribosomal RNA. *EMBO J., 6*, 4169-4175.

Tollervey, D., & Guthrie, C. (1985). Deletion of a yeast small nuclear RNA gene impairs growth. *EMBO J, 4*(13B), 3873-3878. Retrieved from https://www.ncbi.nlm.nih.gov/pubmed/3004976

Tollervey, D., Lehtonen, H., Jansen, R., Kern, H., & Hurt, E. C. (1993). Temperature-sensitive mutations demonstrate roles for yeast fibrillarin in pre-rRNA processing, pre-rRNA methylation, and ribosome assembly. *Cell, 72*(3), 443-457. doi:10.1016/0092-8674(93)90120-f

Tomecki, R., Sikorski, P. J., & Zakrzewska-Placzek, M. (2017). Comparison of preribosomal RNA processing pathways in yeast, plant and human cells - focus on coordinated action of endo- and exoribonucleases. *FEBS Lett, 591*(13), 1801-1850. doi:10.1002/1873-3468.12682

Toussaint, M., Levasseur, G., Tremblay, M., Paquette, M., & Conconi, A. (2005). Psoralen photocrosslinking, a tool to study the chromatin structure of RNA polymerase I--transcribed ribosomal genes. *Biochem Cell Biol, 83*(4), 449-459. doi:10.1139/o05-141

Trapman, J., Planta, R. J., & Raue, H. A. (1976). Maturation of ribosomes in yeast. II. Position of the low molecular weight rRNA species in the maturation process. *Biochim Biophys Acta, 442*(3), 275-284. doi:10.1016/0005-2787(76)90302-6

Trapman, J., Retèl, J., & Planta, R. J. (1975). Ribosomal precursor particles from yeast. *Exp.Cell Res., 90*, 95-104.

Traub, P., & Nomura, M. (1969). Studies on the assembly of ribosomes in vitro. *Cold Spring Harb Symp Quant Biol, 34*, 63-67. doi:10.1101/sqb.1969.034.01.010

Turowski, T. W., Lebaron, S., Zhang, E., Peil, L., Dudnakova, T., Petfalski, E., . . . Tollervey, D. (2014). Rio1 mediates ATP-dependent final maturation of 40S ribosomal subunits. *Nucleic Acids Res, 42*(19), 12189-12199. doi:10.1093/nar/gku878

van Hoof, A., Lennertz, P., & Parker, R. (2000). Three conserved members of the RNase D family have unique and overlapping functions in the processing of 5S, 5.8S, U4, U5, RNase MRP and RNase P RNAs in yeast. *Embo Journal, 19*(6), 1357-1365. doi:DOI 10.1093/emboj/19.6.1357

van Nues, R. W., Rientjes, J. M., Morre, S. A., Mollee, E., Planta, R. J., Venema, J., & Raue, H. A. (1995). Evolutionarily conserved structural elements are critical for processing of Internal Transcribed Spacer 2 from Saccharomyces cerevisiae precursor ribosomal RNA. *J Mol Biol, 250*(1), 24-36. doi:10.1006/jmbi.1995.0355

Van Nues, R. W., Rientjes, J. M. J., Van der Sande, C. A. F. M., Zerp, S. F., Sluiter, C., Venema, J., . . . Raué, H. A. (1994). Separate structural elements within internal transcribed spacer 1 of Saccharomyces cerevisiae precursor ribosomal RNA direct the formation of 17S and 26S rRNA. *Nucleic Acids Res., 22*, 912-919.

van Nues, R. W., Venema, J., Rientjes, J. M., Dirks-Mulder, A., & Raue, H. A. (1995). Processing of eukaryotic pre-rRNA: the role of the transcribed spacers. *Biochem Cell Biol, 73*(11-12), 789-801. doi:10.1139/o95-087

Vanrobays, E., Gleizes, P. E., Bousquet-Antonelli, C., Noaillac-Depeyre, J., Caizergues-Ferrer, M., & Gelugne, J. P. (2001). Processing of 20S pre-rRNA to 18S ribosomal RNA in yeast requires Rrp10p, an essential non-ribosomal cytoplasmic protein. *EMBO J., 20*(15. 15), 4204-4213.

Venema, J., & Tollervey, D. (1999). Ribosome synthesis in Saccharomyces cerevisiae. *Annu.Rev.Genet., 33*, 261-311.

Vogel, C., Abreu Rde, S., Ko, D., Le, S. Y., Shapiro, B. A., Burns, S. C., . . . Penalva, L. O. (2010). Sequence signatures and mRNA concentration can explain two-thirds of protein abundance variation in a human cell line. *Mol Syst Biol, 6*, 400. doi:10.1038/msb.2010.59

Vos, H. R., Bax, R., Faber, A. W., Vos, J. C., & Raue, H. A. (2004). U3 snoRNP and Rrp5p associate independently with Saccharomyces cerevisiae 35S pre-rRNA, but Rrp5p is essential for association of Rok1p. *Nucleic Acids Res, 32*(19), 5827-5833. doi:32/19/5827 [pii]
10.1093/nar/gkh904

Warburg, O., Wind, F., & Negelein, E. (1927). The Metabolism of Tumors in the Body. *J Gen Physiol, 8*(6), 519-530. doi:10.1085/jgp.8.6.519

Warner, J. R. (1999). The economics of ribosome biosynthesis in yeast. *Trends Biochem.Sci., 24*(11), 437-440.

Warner, J. R., & Soeiro, R. (1967). Nascent ribosomes from HeLa cells. *Proc Natl Acad Sci U S A, 58*(5), 1984-1990. Retrieved from https://www.ncbi.nlm.nih.gov/pubmed/5237493

Waterhouse, A. M., Procter, J. B., Martin, D. M., Clamp, M., & Barton, G. J. (2009). Jalview Version 2--a multiple sequence alignment editor and analysis workbench. *Bioinformatics, 25*(9), 1189-1191. www.jalview.org. doi:btp033 [pii]
10.1093/bioinformatics/btp033

Watkins, N. J., & Bohnsack, M. T. (2012). The box C/D and H/ACA snoRNPs: key players in the modification, processing and the dynamic folding of ribosomal RNA. *Wiley Interdiscip Rev RNA, 3*(3), 397-414. doi:10.1002/wrna.117

Weaver, P. L., Sun, C., & Chang, T. H. (1997). Dbp3p, a putative RNA helicase in Saccharomyces cerevisiae, is required for efficient pre-rRNA processing predominantly at site A3. *Mol Cell Biol, 17*(3), 1354-1365. Retrieved from http://www.ncbi.nlm.nih.gov/entrez/query.fcgi?cmd=Retrieve&db=PubMed&dopt=Citation&list_uids=9032262

Wegierski, T., Billy, E., Nasr, F., & Filipowicz, W. (2001). Bms1p, a G-domain-containing protein, associates with Rcl1p and is required for 18S rRNA biogenesis in yeast. *RNA, 7*(9), 1254-1267. Retrieved from http://www.ncbi.nlm.nih.gov/entrez/query.fcgi?cmd=Retrieve&db=PubMed&dopt=Citation&list_uids=11565748

Wehner, K. A., Gallagher, J. E., & Baserga, S. J. (2002). Components of an interdependent unit within the SSU processome regulate and mediate its activity. *Mol. Cell Biol., 22*, 7258-7267.

Weinberg, R. A., & Penman, S. (1968). Small molecular weight monodisperse nuclear RNA. *J Mol Biol, 38*(3), 289-304. doi:10.1016/0022-2836(68)90387-2

Wells, G. R., Weichmann, F., Colvin, D., Sloan, K. E., Kudla, G., Tollervey, D., . . . Schneider, C. (2016). The PIN domain endonuclease Utp24 cleaves pre-ribosomal RNA at two coupled sites in yeast and humans. *Nucleic Acids Res, 44*(18), 9016. doi:10.1093/nar/gkw645

Wells, G. R., Weichmann, F., Sloan, K. E., Colvin, D., Watkins, N. J., & Schneider, C. (2017). The ribosome biogenesis factor yUtp23/hUTP23 coordinates key interactions in the yeast and human pre-40S particle and hUTP23 contains an essential PIN domain. *Nucleic Acids Res, 45*(8), 4796-4809. doi:10.1093/nar/gkw1344

Wojda, I., Cytrynska, M., Frajnt, M., & Jakubowicz, T. (2002). Protein kinases CKI and CKII are implicated in modification of ribosomal proteins of the yeast Trichosporon cutaneum. *Acta Biochim Pol, 49*(4), 947-957. doi:024904947

Woodson, S. A. (2011). RNA folding pathways and the self-assembly of ribosomes. *Acc Chem Res, 44*(12), 1312-1319. doi:10.1021/ar2000474

Woolford, J. L., Jr., & Baserga, S. J. (2013). Ribosome biogenesis in the yeast Saccharomyces cerevisiae. *Genetics, 195*(3), 643-681. doi:10.1534/genetics.113.153197

Wormsley, S., Samarsky, D. A., Fournier, M. J., & Baserga, S. J. (2001). An unexpected, conserved element of the U3 snoRNA is required for Mpp10p association. *RNA, 7*(6), 904-919. doi:10.1017/s1355838201010238

Yang, K., Yang, J., & Yi, J. (2018). Nucleolar Stress: hallmarks, sensing mechanism and diseases. *Cell Stress, 2*(6), 125-140. doi:10.15698/cst2018.06.139

Yoshihama, M., Uechi, T., Asakawa, S., Kawasaki, K., Kato, S., Higa, S., . . . Kenmochi, N. (2002). The human ribosomal protein genes: sequencing and comparative analysis of 73 genes. *Genome Res, 12*(3), 379-390. doi:10.1101/gr.214202

Young, C. L., Khoshnevis, S., & Karbstein, K. (2013). Cofactor-dependent specificity of a DEAD-box protein. *Proceedings of the National Academy of Sciences of the United States of America, 110*(29), E2668-E2676. doi:10.1073/pnas.1302577110

Zakrzewska-Placzek, M., Souret, F. F., Sobczyk, G. J., Green, P. J., & Kufel, J. (2010). Arabidopsis thaliana XRN2 is required for primary cleavage in the pre-ribosomal RNA. *Nucleic Acids Research, 38*(13), 4487-4502. doi:10.1093/nar/gkq172

Zebarjadian, Y., King, T., Fournier, M. J., Clarke, L., & Carbon, J. (1999). Point mutations in yeast CBF5 can abolish in vivo pseudouridylation of rRNA. *Molecular and Cellular Biology, 19*(11), 7461-7472. Retrieved from <Go to ISI>://WOS:000083203100017

Zhang, C., Lin, J., Liu, W., Chen, X., Chen, R., & Ye, K. (2014). Structure of Utp21 tandem WD domain provides insight into the organization of the UTPB complex involved in ribosome synthesis. *PLoS One, 9*(1), e86540. doi:10.1371/journal.pone.0086540

Zhang, J., Harnpicharnchai, P., Jakovljevic, J., Tang, L., Guo, Y., Oeffinger, M., . . . Woolford, J. L., Jr. (2007). Assembly factors Rpf2 and Rrs1 recruit 5S rRNA and ribosomal proteins rpL5 and rpL11 into nascent ribosomes. *Genes Dev, 21*(20), 2580-2592. doi:21/20/2580 [pii]

10.1101/gad.1569307

Zhang, L., Wu, C., Cai, G., Chen, S., & Ye, K. (2016). Stepwise and dynamic assembly of the earliest precursors of small ribosomal subunits in yeast. *Genes Dev, 30*(6), 718-732. doi:10.1101/gad.274688.115

Zheng, S., Lan, P., Liu, X., & Ye, K. (2014). Interaction between ribosome assembly factors Krr1 and Faf1 is essential for formation of small ribosomal subunit in yeast. *J Biol Chem, 289*(33), 22692-22703. doi:10.1074/jbc.M114.584490

Zhu, J., Liu, X., Anjos, M., Correll, C. C., & Johnson, A. W. (2016). Utp14 Recruits and Activates the RNA Helicase Dhr1 To Undock U3 snoRNA from the Preribosome. *Mol Cell Biol, 36*(6), 965-978. doi:10.1128/MCB.00773-15